POLITECNICO DI TORINO

Department of Mechanical and Aerospace Engineering

MSc Thesis
in Automotive Engineering

Human Body Model and Passive Safety in Autonomous Vehicles: Far Side Impact

Tutors

Prof. Eng. Alessandro Scattina

Prof. Eng. Giovanni Belingardi

Candidate

Pietro Assandri

March 2021

INDEX

List of Figures

List of Tables

Abstract

Beginning in 1996 the European New Car Assessment Program (EuroNCAP), continuously evolved its test methodology to better reflect the European road environment and to better inform the customers on the safety of the vehicles they drive. To this end, a new assessment test was developed and introduced as part of the final vehicle safety rating in 2020 with the aim of evaluating the protection provided to the occupants positioned on the far-side of the vehicle respect to the impact location. The purpose of this thesis is to replicate the new assessment methodology by studying the behaviour of a detailed Human Body Model (HBM) positioned and belted inside a Finite Element (FE) model of a representative automobile. Starting from a full-scale vehicle model, a simplified system was developed. The model, consisting of the vehicle Body-In-White (BIW) and the interiors, represents a deceleration-based sled which reproduces the kinematic of the complete model following the rules laid down by the EuroNCAP protocol. The sled model has been validated by comparison with the complete system to verify that the modifications required would not significantly affect the behaviour. The results obtained, show a realistic behaviour of the sled model in representing its kinematics and the HBM motion. The methodology used in this work represents a powerful tool towards an accurate prediction of possible injuries due to the high fidelity provided by the THUMS with the potential to be the ideal platform for evaluating far-side active safety devices.

Chapter 1:   Preface

1.1 Thesis Introduction

With the increase focus of the public towards safer vehicles in recent years, multiple authors highlighted the role that far-side impacts have and the harshness of the possible injuries. Following a research effort lasted for several years, an assessment test has been introduced in 2020 as part of the EuroNCAP adult occupant score to evaluate the safety provided in the eventuality of a far-side impact.

The aim of this thesis is to develop a Finite Element model able to replicate the newly implemented EuroNCAP protocol and to evaluate the behaviour of a detailed Human Body Model in that environment. The starting model is an FE model of a 2012 Toyota Camry representative of a mid-size sedan. From this, a simplified model has been obtained to replicate the interior environment of the car, to adhere to the far-side assessment protocol and to reduce the computing resources required. The complete vehicle model, subjected to an oblique side impact against a rigid pole, has been used for validating the simplified model and to provide the kinematic input required to properly describe the sled movement. An instrumented HBM has been positioned in the driver position to replicate the WorldSID dummy used in the real-world test setup. The monitored parameters required to provide a complete assessment include the head acceleration, the neck loads, the thorax displacement, the abdomen displacement and the pelvis loads. The level of detail provided by the THUMS adopted, allows for also evaluating aspects difficult to analyse otherwise: internal organ volume and spine deformation represent two examples.

The numerical simulations presented in this work have been developed using LS-DYNA explicit code.

1.2 Work Roadmap

The main steps developed in this work are represented in Figure 1.1.
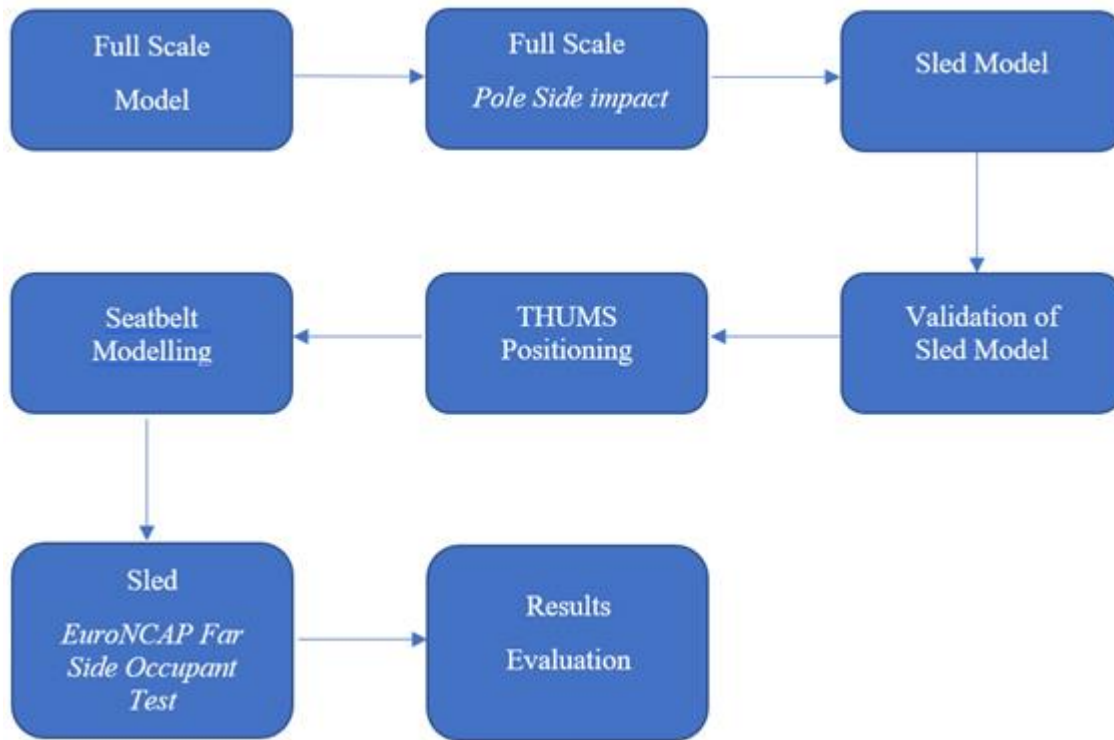
Figure 1.1: Thesis Work Roadmap

At the beginning of the thesis work, a thorough research on the literature available on the far-side impact, the dynamic at play, the crucial parameters and the test methodology has been carried out With the fundamentals solidified, the models adopted are considered. Three models are considered in Chapter 4: the HBM model described in its details and with highlight on the sensors installed; the Full-scale Camry Model representative of the full vehicle; the Sled model, how it was obtained and what the necessary modifications were in order to have a functioning model.

Two different validation tests are performed to ensure that the simplified model obtained, would behave as desired and can be representative of the full-scale impact.

At this point, the different steps needed to properly position the THUMS inside the environment are described. A sitting simulation was needed to pre-deform the driver's seat and, using the PIPER tool software the body was positioned in a standard driving position. Then, to properly secure the occupant inside the vehicle, a seatbelt system equipped with a single stage pretensioner has been modelled and fitted to the body. With the THUMS in position, the final simulation can be carried on and its result evaluated and compared to be within the EuroNCAP guidelines.

Chapter 2:   Literature Review

2.1 Introduction

During the last decades, significant steps forwards towards having safer roads and vehicles have been carried out by car manufacturers, led in this direction by legislators, independent organisations, and the common sentiment towards having safer vehicles for everyone. New Car Assessment Programmes (NCAPs) critically worked towards increasing consumer awareness and their demand for safer vehicle as highlighted by the Global Status Report on Road Safety redacted by the World Health Organisation in 2015 [33]. Side impacts consequences have been a major topic of research and development in the car industry since the mid to late 70's but only in the last two decades a lot more interest was dedicated towards improving our understanding of what occurs during a far-side impact to the vehicle and to the occupants. In Europe, the EuroNCAP represents the major promoter of increased awareness towards demanding higher safety in our everyday vehicles and to this end, a new assessment test has become part in 2020 of the overall safety rating, with the aim of evaluating the vehicle's capability of reducing the injury risk as aftermath of a far side impact. This new protocol comes as the combined result of multiple studies conducted in the last two decades on this matter with two different objectives: evaluate the occupants protection in this type of accident and limiting the increased test cost both for the EuroNCAP and the car manufacturer. The first objective can be achieved by incorporating a non-destructive test inside the safety evaluation protocol where only the Body In White (BIW) of the vehicle is subjected to the same acceleration experienced during a representative full scale crash test. The second objective can be satisfied by integrating Finite Element (FE) simulations inside the development process of the vehicle in order to evaluate the crash worthiness of the vehicle and the biomechanical parameter of a virtual human subject in a variety of configurations. The development of detailed Human Body Models (HBM), increased the level of prediction of the movement of the occupants inside the vehicle and the injuries that would be the outcome of that movement. The virtual environment in which these simulations are developed, does not take place of the real assessment, but it is a fundamental tool in the development phase and for the different research groups investigating the phenomenon.

2.2   EuroNCAP

The European New Car Assessment Program (EuroNCAP) represent a non-profit assessment project devoted towards car safety. It was founded in 1996 but extends it roots to 1979 when the United Stated National Highway Traffic Safety Administration (NHTSA) created the New Car Assessment Program in order to encourage car manufacturers to build safer vehicles for the consumers [33]. As the slogan *"For Safer Cars"* says, this has always been the objective of the EuroNCAP, and towards this goal, since the year 2000 multiple revisions of the side impact test protocol have been brought forwards. In that same year, the perpendicular pole impact test was added to the standard side impact test. In 2003, the dummy and the barrier used were updated and in 2015 updated again while the perpendicular pole test was replaced with a more significant oblique one. To that date, the focus of the crash tests, was on the near-side occupant in the driving position while no evaluation was carried on for the far-side occupant.

To find a remedy to this issue, in that same year, 2015, the EuroNCAP Board of Directors agreed to the need of improving the relevance of the safety rating provided to the consumers and issued the EuroNCAP Side Impact Working Group (SIWG) with the task of developing an assessment protocol able to properly evaluate the far-side vehicle safety. The new procedure developed is performed by installing the vehicle's BIW on a rear-firing sled with the aim to reduce the cost and time burden of a full-scale side impact test. This methodology allows for implementing a wide variety of real-world scenarios and furthermore provides a versatile platform to the car manufacturers to work on efficient countermeasures. The work by the SIWG was concluded in June 2019 and it was introduced as part of the final vehicle safety rating in 2020 [10].

In the latest update to the EuroNCAP protocols, the final rating is composed by four different aspects concerning the vehicle safety:

- *Adult Occupant Protection:* In this category multiple crash tests are needed for evaluating the occupant protection provided by the vehicle. The tests requires two different frontal impacts against a rigid wall and a Mobile Progressive Deformable Barrier (MPDB); two different lateral impacts against a rigid pole and a Mobile Deformable Barrier (MDB) and three sled tests: two dedicated towards evaluating the whiplash for the front and rear seats and one dedicated towards evaluating the far-side occupant behaviour. An evaluation concerning the rescue and extraction of the occupants in the aftermath of an accident also incorporates the final score.
- *Child Occupant Protection:* In this category the protection provided to the child occupant is evaluated in frontal and side crash tests and the capability of the

vehicle to accommodate different child ages and the required Child Retention Systems (CRS).

- *Vulnerable Road User (VRU) Protection:* In this category it is evaluated how the vehicle can guarantee a reasonable level of protection provided to the VRU with which the vehicle may collide. To this end a series of tests take place where the impact between the vehicle and surrogates of different body parts (Head, Upper and Lower Leg) is evaluated. Furthermore, the behaviour of the Automated Emergency Braking (AEB) system is evaluated under different scenarios such as potential impacts against pedestrians and cyclists.

- *Safety Assist:* In this category different active safety systems installed on the vehicle are evaluated. The systems considered are: Occupant Status Monitoring, Speed Assistance Systems, Lane Support Systems and the AEB under potential impacts against other vehicles.

Each one of these categories is evaluated independently and their single scores are combined to provide a final rating. To better visualize the overall vehicle score and how it compare with other similar vehicle, the score is presented as a number of stars between 0 and 5 where 0 corresponds to a vehicle that satisfies the legal requirements but lacks any critical modern safety technology and 5 corresponds to an excellent performance and represents a vehicle equipped with comprehensive and robust safety technology. In Figure 2.1 the EuroNCAP rating system with the general guidelines that are to use to understand the star rating system.

5 star safety: Overall excellent performance in crash protection and well equipped with comprehensive and robust crash avoidance technology

4 star safety: Overall good performance in crash protection and all round; additional crash avoidance technology may be present

3 star safety: At least average occupant protection but not always equipped with the latest crash avoidance features

2 star safety: Nominal crash protection but lacking crash avoidance technology

1 star safety: Marginal crash protection and little in the way of crash avoidance technology

0 star safety: Meeting type-approval standards so can legally be sold but lacking critical modern safety technology

Figure 2.1: Star Rating System (EuroNCAP, 2020)

2.2.1 Far Side Assessment Test [10]

This test is an acceleration-sled based test which involves the bare structure of the vehicle Body-In-White (BIW) and the necessary equipment. The sled is programmed in order to reproduce the accelerations experienced by the vehicle during two separate full-scale crash tests: a 60km/h AE-MDB side impact and a 32km/h oblique pole side impact. In addition to the standard interiors and the seats, foam spacers are required to be fitted on the sides of the passenger seat to simulate the intrusion of the pole inside the vehicle and the following transmission of forces between the different parts. A WorldSID 50th percentile male dummy is installed in the driver's seat in a standard driving position. If the vehicle is equipped with countermeasures designed to provide additional protection from occupant interaction, such as central airbags, a second WorldSID dummy may be seated in the passenger position.
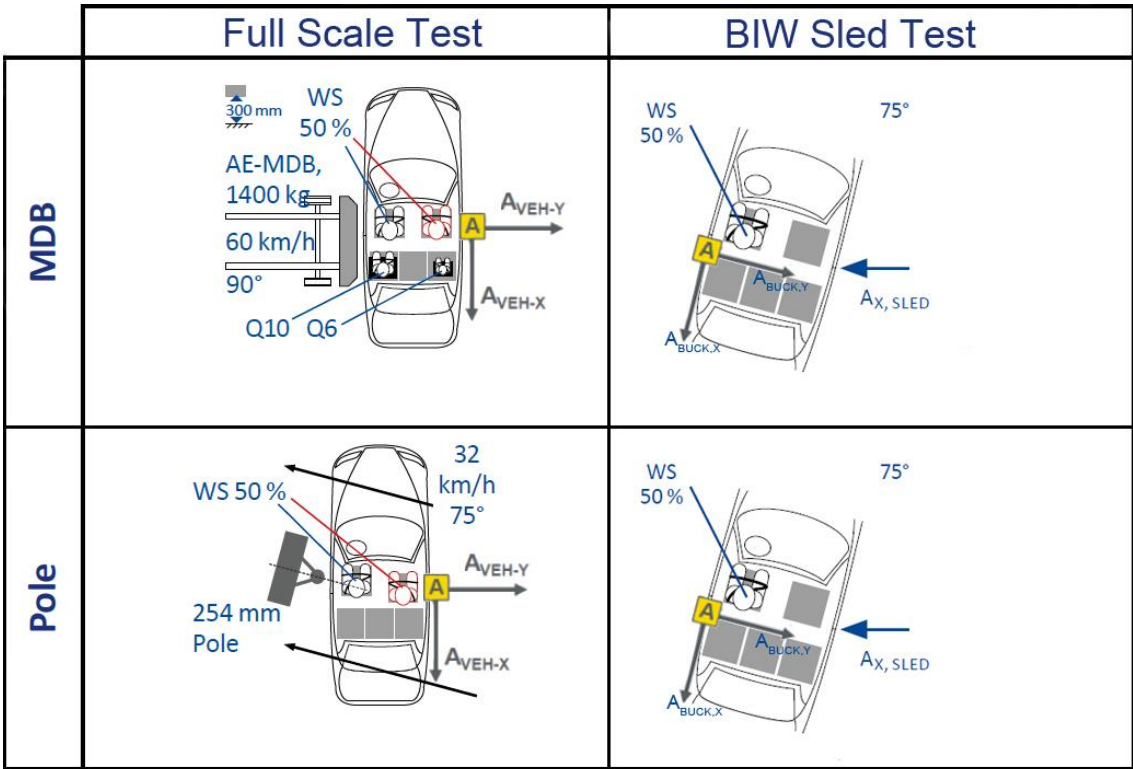
Figure 2.2: Far-Side assessment tests (EuroNCAP, 2020)

The safety score awarded is based on the dummy displacement. On the passenger side, as it can be seen in Figure 2.3 four vertical lines are applied to the vehicle body and they are used for evaluating the kinematic excursion of the dummy in the opposite impact direction.
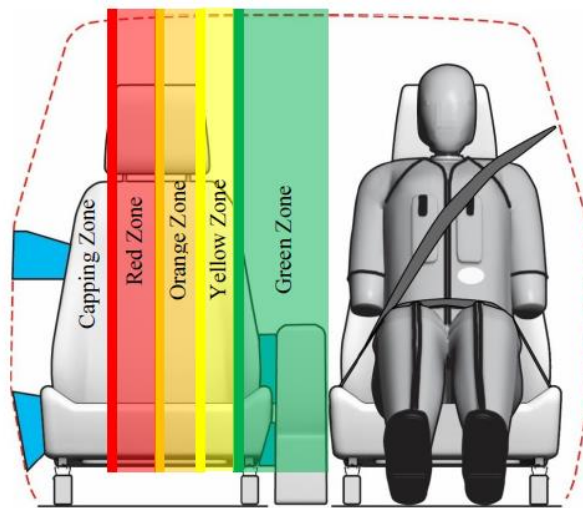
Figure 2.3: Head excursion zones (EuroNCAP, 2020)

The lines are colour coded as it follows:

- *Red Line:* This line defines the maximum intrusion measured during the two full scale crash tests
- *Orange Line:* This line is defined as the centre line of the passenger seat pre-test. It is used for defining a head excursion performance limit.
- *Yellow Line:* This line is defined as a parallel line to the orange one, inboard of 125mm. It is used for defining a head excursion performance limit.
- *Green Line:* This line is defined as a parallel line to the yellow one, inboard of 125mm. It is used for defining a head excursion performance limit.

These lines define between them different assessment zones where the maximum excursion of head, neck and chest is evaluated by assigning a point score to each body part.

In addition to the kinematic evaluation, the WorldSID is equipped with a series of sensors with the aim of capturing the most significant parameters of this test. The acceleration of the head is measured, load cells able to measure forces and moments are positioned in the upper neck and lower neck while the chest and abdomen compression in the lateral direction are recorded. For each parameter, two values are given: a higher performance limit and a lower performance limit. These values are used in order to weigh the results obtained by analysing the dummy lateral excursion. A result below the higher performance limit means full points, a result above the lower performance limit means no points. Between the two limits an interpolated score is assigned. Load sensors are also positioned in the pelvis and lumbar areas, exceeding one of the performance

limits assigned to these areas will result in a negative factor in the final safety rating. A summary of the rating system is reported in Table 1.

Head Excursion without far-side countermeasure					
	Capping Zone	*Red Zone*	*Orange Zone*	*Yellow Zone*	*Green Zone*
Head Score	0	0	1	2	4
Neck Score	0	1	1	2	4
Chest Score	0	0	1	2	4
MAX Score	0	1	3	6	12

Dummy Criteria				
	Criteria	*Performance Limits*		
		High	*Low*	*Cap*
Head	HIC15	500	700	700
	3ms Acceleration	72g	80g	80g
Upper Neck	Tension Fz		3.74 kN	
	Lateral Moment Mx	162 Nm	248 Nm	
	Forward Moment My		50 Nm	
Lower Neck	Tension Fz		3.74 kN	
	Lateral Moment Mx	162 Nm	248 Nm	
	Forward Moment My		100 Nm	
Chest & Abdomen	Chest lateral compression	28 mm	50 mm	50 mm
	Abdomen lateral compression	47mm	65 mm	65 mm

Pelvis & Lumbar Criteria		
Criteria	*Performance Limits*	*Modifier*
Pubic Symphysis	2.8 kN	
Lumbar Fy	2.0 kN	-4 points
Lumbar Fz	3.5 kN	
Lumbar Mx	120 Nm	

Table 1:EuroNCAP far-side assessment tables (EuroNCAP, 2020)

2.2.2 Oblique Pole Side Test [11]

It is relevant to report a brief description of the Oblique Pole Side Test since it is one of the starting points for the Far-Side impact assessment test. In this test the vehicle is subjected to a lateral-oblique impact against a fixed rigid pole. The car is positioned at an angle of 75° on a moving platform and it is set to impact the pole at a velocity of 32 km/h. The friction between the surface of the platform and the vehicle needs to be minimized as much as possible and for this reason, sheets of PTFE are positioned between the tires and the ground. The platform does not impact the rigid pole and a minimum distance of 102mm in the Z direction between the platform surface and the pole needs to be guaranteed. A WorldSID 50th percentile male dummy is installed in the driver's seat in a standardized position and, in the case the vehicle is fitted with a far-side designed countermeasure, then a second dummy is positioned in the front passenger seat for evaluating the interaction between the front row occupants. Once the driver dummy has been seated in the proper position, the vehicle is positioned on the platform such that the centre of gravity of the WorldSID head, is aligned with the fixed pole as shown in Figure 2.4. Multiple sensors are installed both on the dummy and the vehicle for evaluating the crash test performance. What it is relevant to this thesis work is the inclusion of an accelerometer in the area of the unstruck B-Pillar. The output from this sensor is fundamental for reproducing the movement of the full-vehicle on the accelerated-sled.
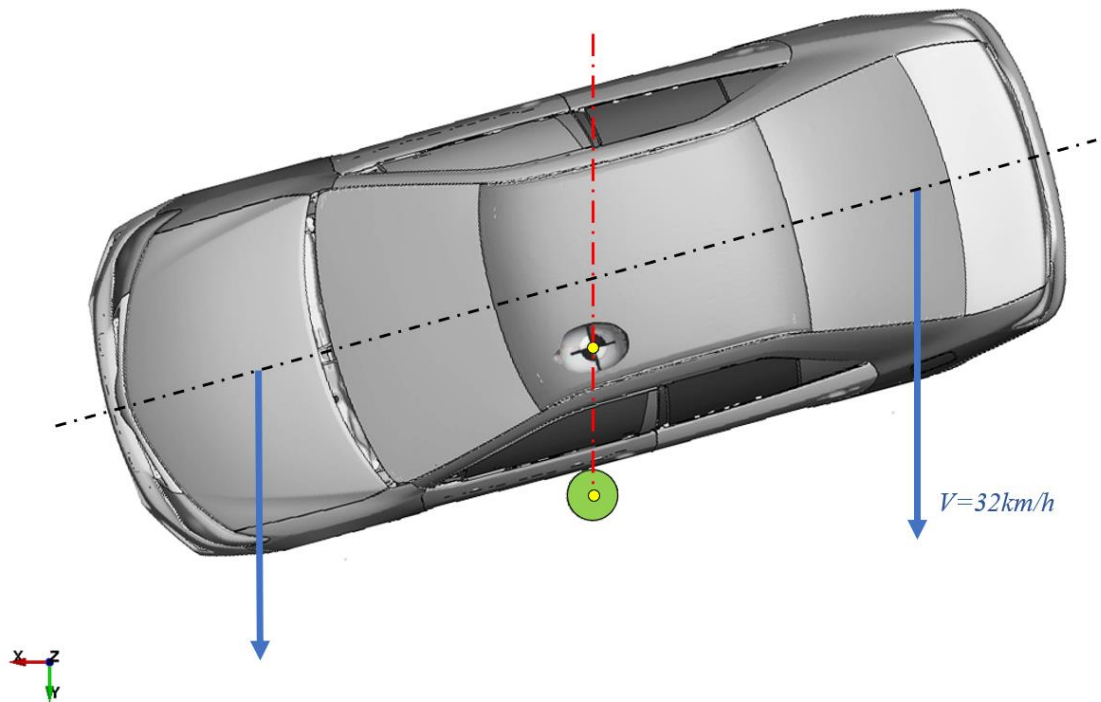
Figure 2.4: Oblique Pole Side Test

2.3 Mechanic of the impact

During a lateral far side impact, the vehicle crashes against an obstacle, being it a fixed pole or a mobile deformable barrier, at a considerable high speed. In this scenario the lateral excursion of the occupant positioned towards the unstruck side of the vehicle is significant and can lead to major injuries. A study conducted in 2005 [15] analysed the National Automotive Sampling System (NASS) database and identified that 43% of far-side crashes in a period between 1993 and 2002 resulted in AIS3+ injuries for the occupants, of these, injuries to the head and the chest accounted for more than 50% of the total. Multiple factors are considered by different authors to critically influence the severity of these injuries. One of the most comprehensive studies on the matter, conducted by Forman et al. [13] on Post-Mortem Huma Subjects evaluated the influence on the outcome of the impact direction, of the seatbelt pretensioning and of the D-Ring position. In a more recent study of 2018 by Umale et al. [31], those parameters were considered using a GHBMC[1] HBM on a rigid buck in a simulated environment. In the same work, also the influence of the friction between the body and the seatbelt was considered and regarded as influential in increasing the occupant retention during the crash. In these studies, the engagement between the occupant torso and shoulder with the seatbelt has been considered critical towards limiting the lateral acceleration and excursion of the head, the chest compression and the number of fractured ribs.

Figure 2.5: Far-Side impact test

---

[1] Global Human Body Models Consortium

Chapter 3: Methods

In this work, multiple Finite Element Models (FEM) have been used. A FEM model of a 2012 Toyota Camry has been used for simulating a full-scale crash test, while a simplified model was obtained from the previous one and is referenced in this work as Sled Model. For representing the human body in the simulation environment, the Total HUman Model for Safety (THUMS) version 4 was used in the current study. In the following, a detailed description of the different models, the modifications that they required and how they have been implemented in our simulations is provided.

3.1 HBM

3.1.1 Introduction

The process that led to safer vehicles on the road went through multiple stages. The technology changed significantly since when the necessity for evaluating the effectiveness of the automobiles to protect the passengers from injuries was first established. From analysing the damage sustained by animals, Post-Mortem Human Subjects (PMHS) and human volunteers to studying the outcome of an accident through the use of human surrogate more and more complex and representative of the body of the occupants of the vehicle. Different crash dummies, so they are called, have been developed for different scenarios and according to different standards. Despite their high level of biofidelity that these proxies represent, they are expensive tools that require expensive maintenance due to the cost of replacement parts and the tight temperature control required, while still not being completely representative of the human body. For these reasons, the industry moved towards using more complex and complete Finite Element (FE) simulations able to faithfully reproduce different impacts and able describe in detail how the occupants would behave in such scenarios, in this environment detailed Human Body Models (HBM) were developed and introduced. The HBMs have been designed to replicate the human body behaviour for what concerns its kinematics and biomechanics, and for these reason the models include detailed descriptions of tissues, bones, internal organs and major veins with accurate material descriptions representative of how the real counterpart would behave. The very-high detail with which these HBMs are modelled, allows for acquiring accelerations and stresses developed during a crash scenario, evaluating internal injuries and fracture locations. The adaptability of these models allows for describing female and male occupants of different ages and sizes. In this thesis the HBM developed by Toyota, the THUMS was adopted for representing a 50th percentile male occupant in a far-side scenario.

3.1.2 THUMSv4 Model [30]

Total Human Model for Safety (THUMS) is a human FE model jointly developed by Toyota Motor Corporation and Toyota Central R&D Labd., Inc. The model aims to simulate human body kinematics and injury response in car crashes. The geometries of the human body parts are represented by FE meshes and their material properties are defined assuming constitutive laws. In this work it has been used an average size adult male (AM50%ile) model which has a height of 175 cm and a weight of 77 kg. The model provided is in a sitting position close to the actual driving position, but it has been modified in order to properly fit the simulation environment (Sitting Simulation §7.2).

Figure 3.1: THUMSv4 Initial Sitting Position

The first version of the THUMS was developed in the year 2000 and went through multiple revisions to include more details of the human body representation. In this thesis the Version 4 of this project has been used. High-resolution CT scans were needed in order to obtain precise geometry details of the internal organs, their layout and their connecting structures. Each organ was modelled reflecting of the physical properties of its tissues according to the latest research. This work allowed to accurately simulate internal organ and brain injuries. The final model contains approximately 2 million elements. The THUMS v4 has been validated for the use in far side impact by a study conducted by Toyota [21].

In Figure 3.2, the most important modelled parts of the head are highlighted. This model includes the epidermis, skull, mandible, eyeballs, teeth, meninges, cerebrum, cerebellum, brainstem, cerebrospinal fluid (CSF), grey and white matter. The neck muscles are modelled through 1D elements which attachment points to bony parts correspond to the actual insertion points.
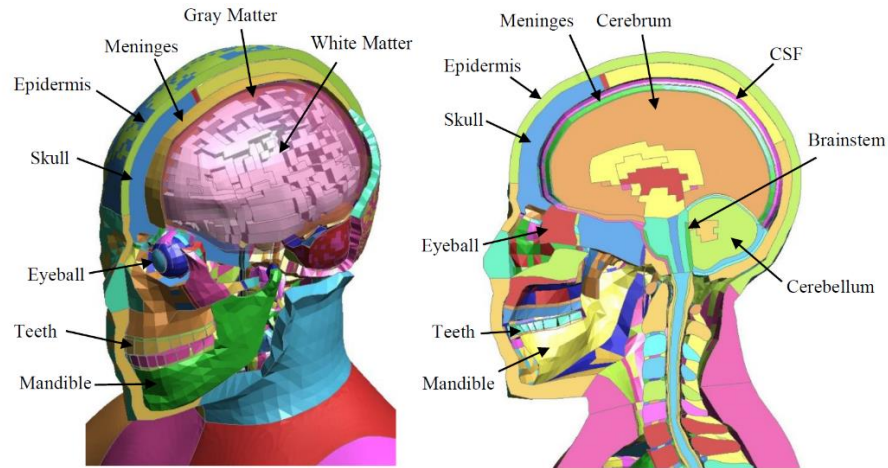
Figure 3.2: THUMS Head Model

All the skeletal parts and the major soft tissues are included in the model. Both hard tissues such as the different bones and the connective tissues are modelled. Shell elements and solid elements are used for describing these body parts. Figure 3.3 highlights the details of the skeletal structure.
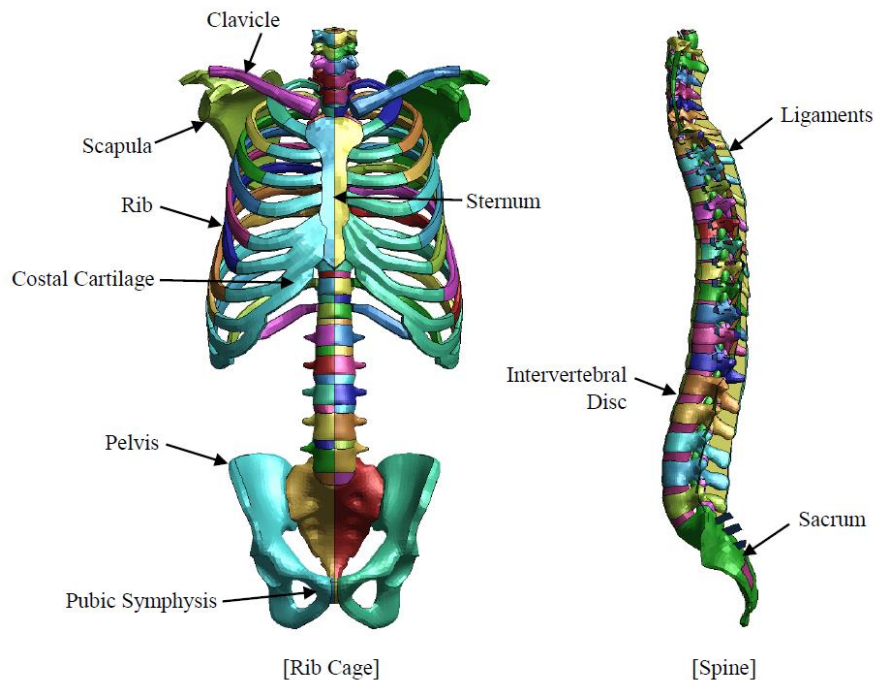
Figure 3.3: THUMS - Skeletal parts in Torso and Neck model

In the Version 4 of the THUMS, all the internal organs are present. The internal organs included in the model are: heart, lungs, liver, kidneys, spleen, pancreas, gall bladder, bladder, oesophagus,

stomach, duodenum, small and large intestines. Solid elements and 1D elements have been used respectively for describing thicker and thinner muscles. In Figure 3.4, a visual identification of the different parts is provided.

[Bones, Muscles and Fat]   [Internal Organs]
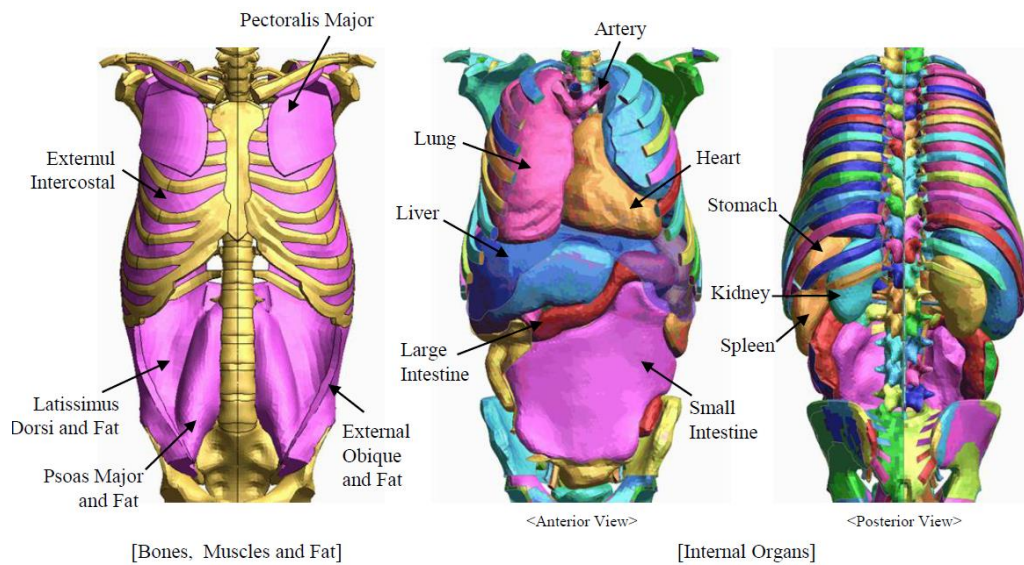
Figure 3.4: THUMS - Soft tissue parts in torso model

The limbs are described similarly by representing the bones with solid elements and surrounding the skeletal parts with flesh parts for modelling the muscles. These muscles can be roughly divided between flexor and extensor muscles. Shell elements are then used for describing the skin which covers the entirety of the body.

Upper Extremity   Thigh   Lower Leg
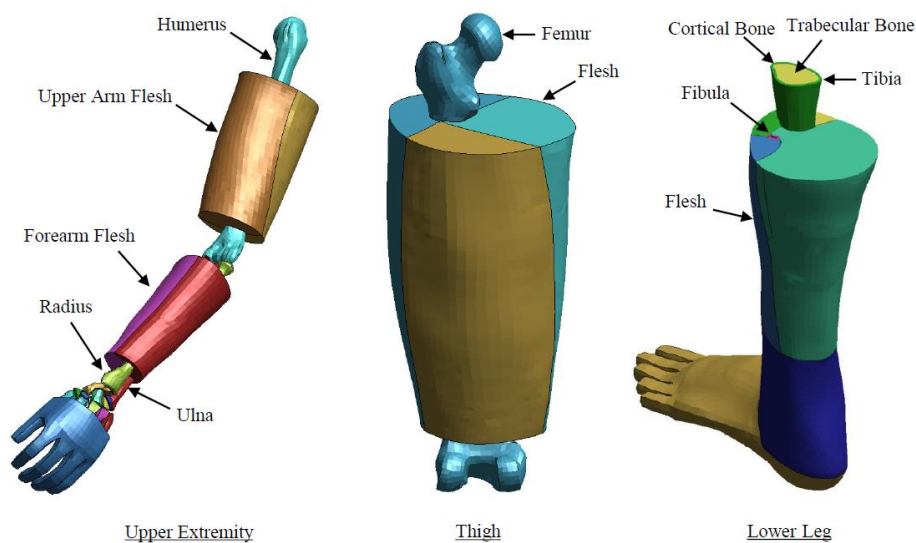
Figure 3.5: THUMS - Extremety Models

3.1.3 Instrumentation

In order to properly analyse the behaviour of the THUMS, it is required to process the accelerations and loads through which it undergoes and for this reason, a system of sensors it is required. The model published by Toyota, does not come with a pre-installed array of sensors as it states: *"The THUMS models do not include database definitions. Users need to specify the entities for output such as nodes, elements, materials and cross sections in order to output the resultant data such as acceleration, velocity, displacement, force, stress, strain and energy. It is suggested to specify multiple points for nodal output not to overestimate resultant values due to local deformation or singularity in the model."*.

In this work, an existing example of sensors system, realized for previous activities by Germanetti [17] has been used. Some modifications have been implemented in order to better comply with the EuroNCAP requirements for the dummy outputs. The additional components are needed to register the loading during the far-side impact in specific areas such as: shoulder, upper neck, lower neck and pelvis. In Figure 3.6, the complete set of accelerometers and load sensors is shown, the data measured are:

- Linear Acceleration of the Head in X, Y, Z direction
- Angular Velocity of the Head around X, Y, Z axis
- Force and Moment on the Upper Neck at the height of the C1 Vertebrae
- Force and Moment on the Lower Neck at the height of the C7 Vertebrae
- Force and Moment on the Spine at the height of the T12 Vertebrae
- Force and Moment on the Spine at the height of the L5 Vertebrae
- Load on the Pelvis transmitted at the Symphysis
- Load on the Shoulder Joints transmitted between clavicles
- Load on the Shoulder Joints transmitted between rotator cuffs
- Displacement and Rotation of the Shoulder Ribs
- Displacement and Rotation of the Thorax Upper Ribs
- Displacement and Rotation of the Thorax Middle Ribs
- Displacement and Rotation of the Thorax Lower Ribs
- Displacement and Rotation of the Abdomen Upper Ribs
- Displacement and Rotation of the Abdomen Lower Ribs
- Spine Deformation
- Volume of Internal Organs
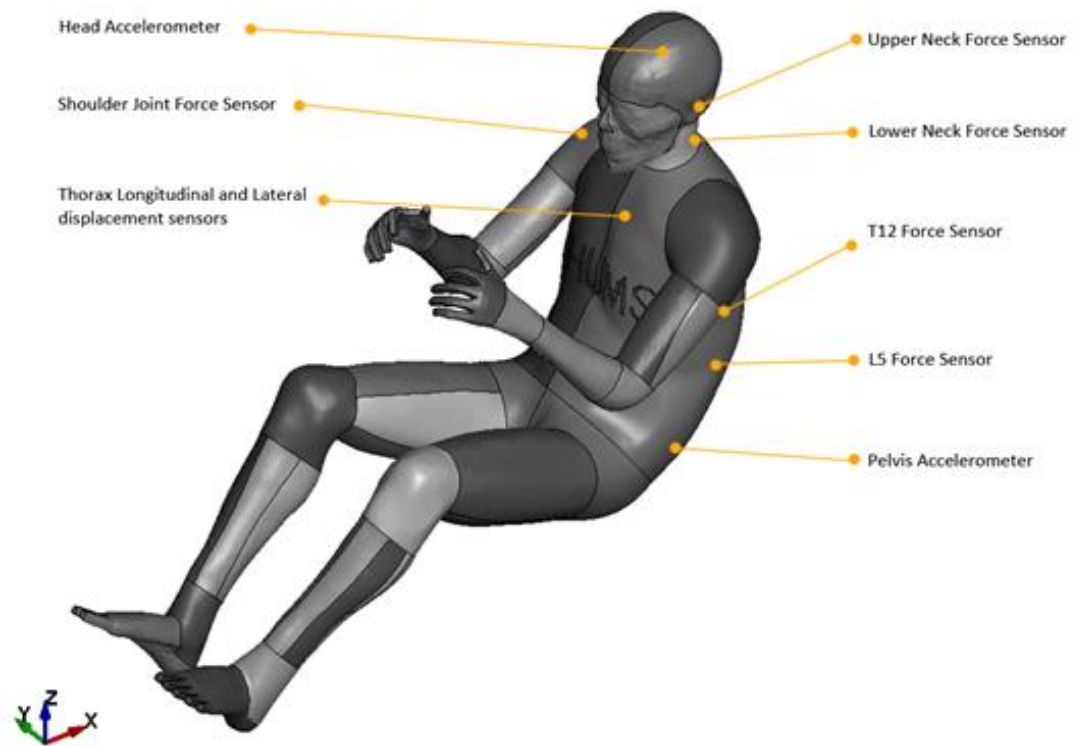
Figure 3.6: THUMS Sensors System

The model is equipped with an accelerometer sensor able to record the head movement in the three direction of space. For a proper implementation inside the THUMS, a small part of the brain visible in Figure 3.7, the *third ventricle left*, has been converted to rigid and used as an accelerometer. This operation is important in order to obtain cleaner and more stable results from the accelerometer defined on those elements. In LS-DYNA the sensor is modelled through the *ELEMENT_SEATBELT_ACCELEROMETER keyword.
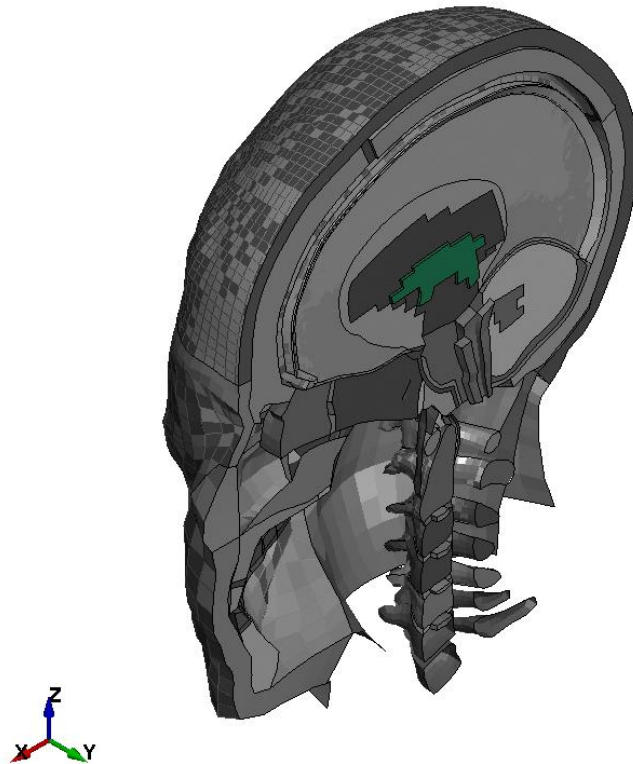
Figure 3.7: THUMS Head - Detail of the 3rd Ventricle

Required by the EuroNCAP protocol, two different sections of the neck are monitored: the upper neck and the lower neck and the same strategies for implementing the sensors are adopted in both areas.

Load sensors are modelled by using the keywords *DATABASE_CROSS_SECTION_SET in order to define load cells on the C1 vertebrae and the C7 vertebrae, and *DATABASE_CROSS_SECTION_PLANE for defining planes crossing the upper area of the neck and the lower area of the neck as it is visible in Figure 3.8. These sensors record both the loads transmitted through the neck and the moment to which it is subject.
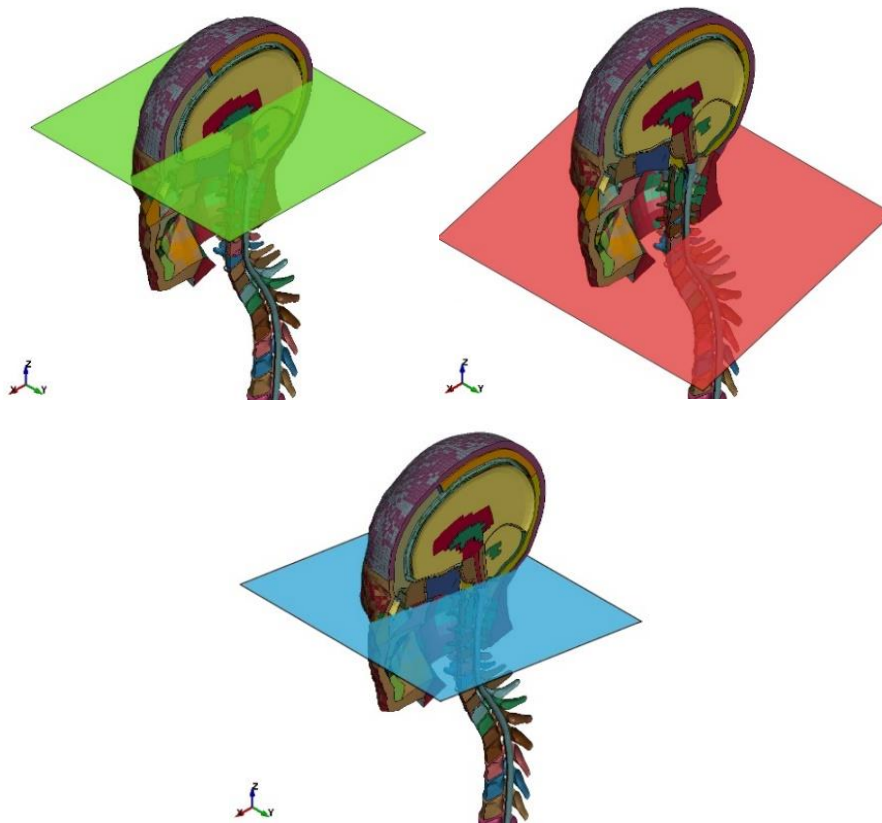
Figure 3.8: Head Cross Section Plane (GREEN), Lower Neck Cross Section Plane (RED), Upper Neck Cross Section Plane (BLU)

THORAX and PELVIS SENSORS

Multiple sensors are positioned in the thorax for describing the upper part of the body. Load cells are positioned on the most crucial vertebrae highlighted in Figure 3.10 such as the C1, C7, T12 and L5. Additionally, also the load transmitted through the Symphysis is being recorded.

1D discrete elements have been connected in the lateral direction between shoulder ribs, upper thorax ribs, middle thorax ribs, lower thorax ribs, upper and lower abdominal ribs in the lateral direction. These elements are able to measure the displacement, and the force transmitted between their extreme points. Figure 3.9 provides their disposition and anchorage points on the THUMS.
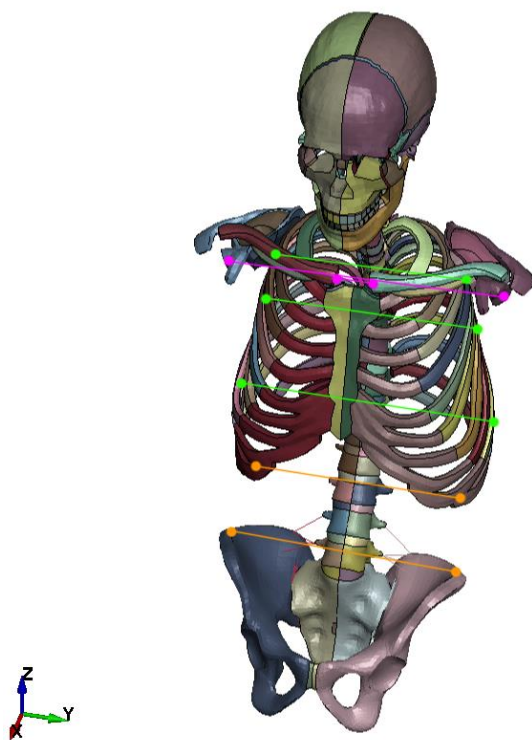
Figure 3.9:1D Discrete Elements on THUMS. Shoulders (MAGENTA); Thorax (GREEN); Abdomen (ORANGE)
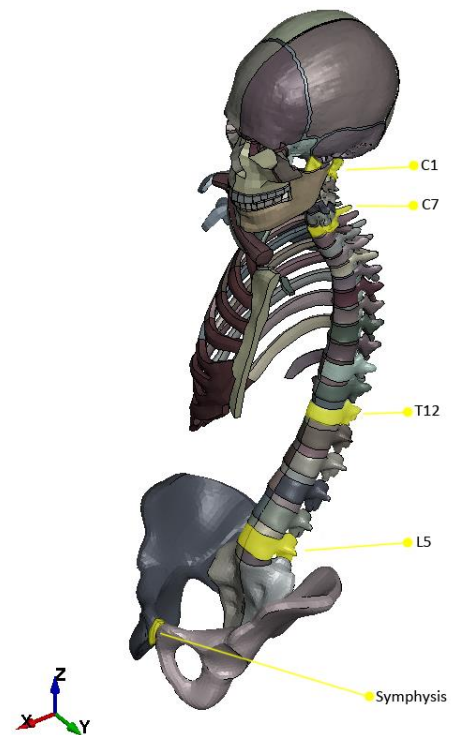
Figure 3.10: THUMS Load Sensors Position

Despite not being required by the EuroNCAP protocol, it is possible, in order to analyse in detail the deformation of the thorax and of the spine, to position markers or ribs and vertebrae so that it is possible to visualize instant by instant the deformation of the thorax circumference or the spine alignment. *DATABASE_HISTORY_NODES_ID cards are used to define these markers set and they monitor:

- *Cervical Vertebrae*
- *Thorax Vertebrae*
- *Lumbar Vertebrae*
- *Chest Ribs*
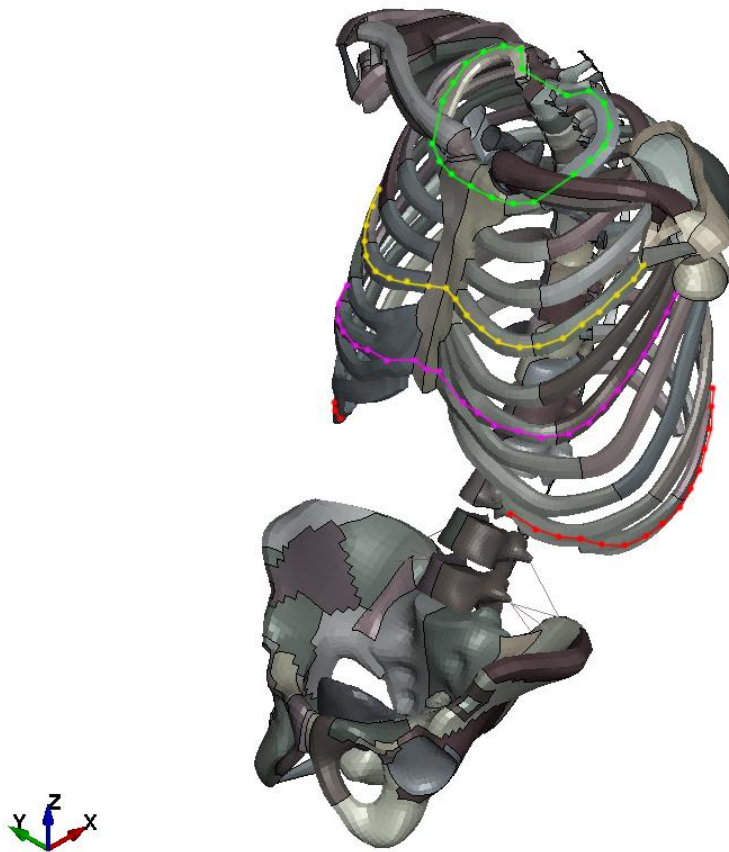
Figure 3.11: THUMS Model - highlight of Chestbands and Ribs Markers

INTERNAL ORGANS VOLUME SENSORS

The high detail provided by the THUMS model allows to further analyse the possible injuries occurring to the human body during an accident beyond what prescribed the EuroNCAP protocol since by nature, it has been designed to regulate the use of a real dummy, the WorldSID to be more specific. Specific sensors have been modelled for analysing the behaviour of the internal organ by using *AIRBAG_SIMPLE_PRESSURE_VOLUME keywords. These LS-DYNA cards are able to provide data on the change in volume of a closed surface and its normalized surface variation. In this work the organs groups taken into consideration for further analysis are:

- *Ribcage:* Enclosed surface of Pleura and Diaphragm
- *Right Lung:* Enclosed surface of Right Pleura Visceralis (Green)
- *Left Lung:* Enclosed surface of Left Pleura Visceralis (Orange)
- *Heart:* Enclosed surface of Pericardium
- *Pancreas:* Enclosed surface of Pancreas
- *Spleen*: Enclosed surface of Spleen
- *Liver*: Enclosed surface of Liver
- *Stomach*: Enclosed surface of Stomach (Red)
- *Small Intestine:* Enclosed surface of Small Intestine (Yellow)
- *Large Intestine:* Enclosed surface of Large Intestine (Purple)
- *Abdomen*: Enclosed surface of Peritoneum and Diaphragm
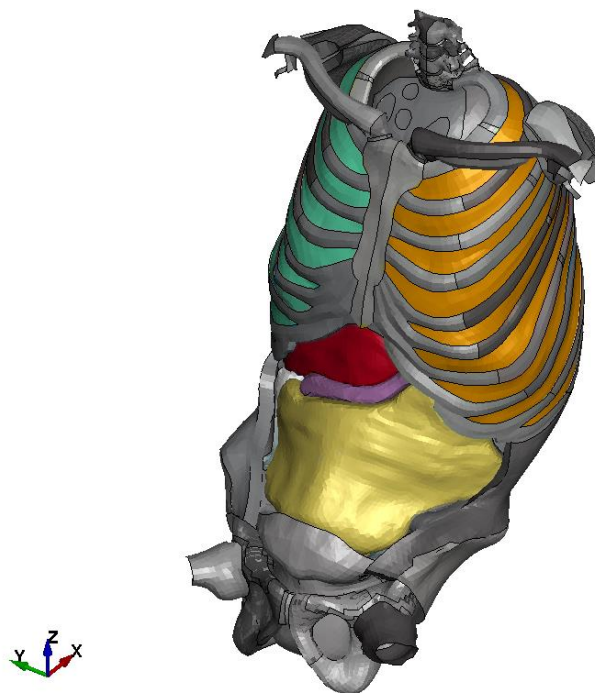
Figure 3.12: THUMS model - Internal organs highlight

3.2   Full-Scale Camry Model [5]

The Finite Element Model of the vehicle implemented in the simulation environment reproduce a mid-size passenger sedan and it is based on a 2012 Toyota Camry. Developed through a reverse engineering process by Center for Collision Safety and Analysis (CCSA) researchers under a contract with the Federal Highway Administration (FHWA), it was compared against several full-scale crash tests and a good correlation was obtained also in the case of the side NCAP Pole test [6]. The model conforms to the Manual for Assessing Safety Hardware requirements for a 1500A test vehicle. In its final version, it results in approximately 2.25 million elements and includes detailed modelling of the vehicle structure, suspension, steering, drivetrain, and interior components. This level of details, especially for what concerns the seat description, allows for integration of dummy models in the simulation.

Figure 3.13: Real and FE Model of 2012 Toyota Camry

The FE numerical simulations developed in this work were performed using LS-DYNA R11.1 non-linear explicit finite element code.

3.2.1   Model Description [5]

The model was developed on the basis of a production 2012 Toyota Camry through a reverse engineering process whose steps included systematically disassemble, catalogue, scan and measure each vehicle part. The data obtained in such a way, was then used for modelling these parts using the LS-DYNA software using shell, solid and beam elements.
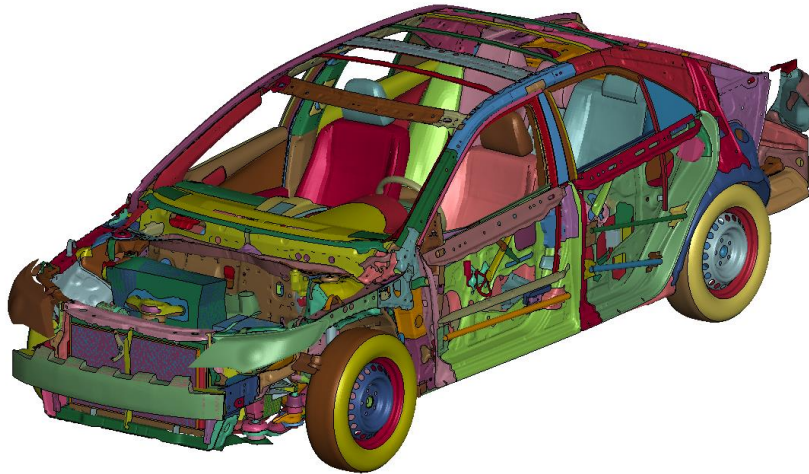
Figure 3.14: FE Model - Detail

Each component is connected either by spotwelds (*CONSTRAINED_SPOTWELD) in the case of structural components or Constrain Nodal Rigid Body (CNRB), entities able to simulate bolts, screws and clamps. This detailed process included functional capabilities of moving parts such as suspension and steering subsystems. Material data for the structural components of the model was obtained from manufacturer specification or, in the case they were not available, determined though sample testing. Non-structural components which are not relevant for the crashworthiness of the vehicle, such as the drivetrain and the engine, have been modelled with a coarser mesh and with less detailed models.

Figure 3.15: FE Model - Engine Bay Detail

Interior components of the front and rear door panels such as crash absorption foams and the window lifters mechanism have been included.
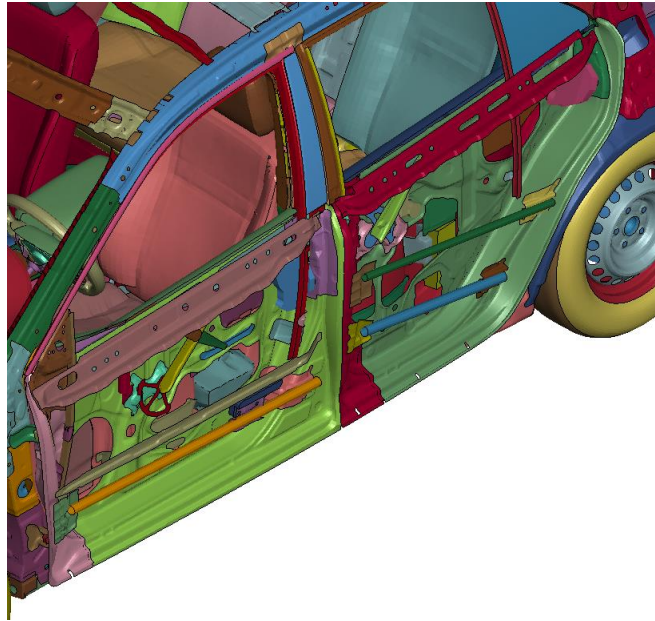
Figure 3.16: FE Model - Door Structure Detail

Suspension and steering subsystems are completely functional and modelled with detail in order to allow systems response in different simulation scenarios, such as irregular ground.

Figure 3.17: FE Model - Front (LEFT) and Rear (RIGHT) Suspension Detail

3.2.2 Accelerometers

For properly assess the vehicle dynamics during the impact, a total of 16 accelerometers have been defined on the model. The areas monitored by sensors are: Strut Towers, Lateral Sills and Seats attachment points. In addition to those, an accelerometer is positioned in proximity of the B-Pillar of the non-struck side as prescribed by the EuroNCAP Far-Side impact protocol and a similar one has been positioned on the driver side. The position of the sensors is highlighted in Figure 3.18.
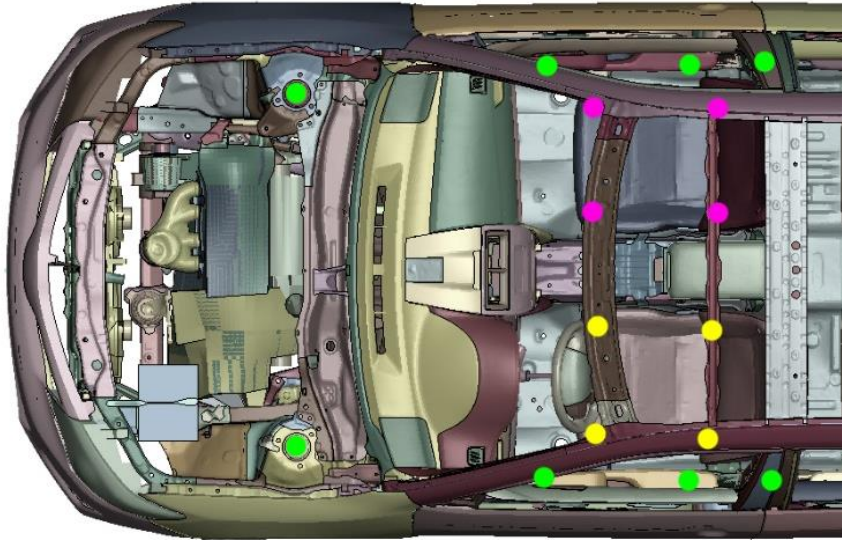
Figure 3.18: FE Model - Accelerometer Position Detail
Vehicle Structure (GREEN); Left Seat (YELLOW); Right Seat (MAGENTA)

The accelerometers are modelled by using the *ELEMENT_SEATBELT_ACCELEROMETER keyword in LS-DYNA. For a proper description of these sensors, they are defined on rigid elements, represented in this work by rigid cubes positioned as highlighted in Figure 3.18, which are attached to the structure by means of CNRB as it is possible to observe in Figure 3.19.
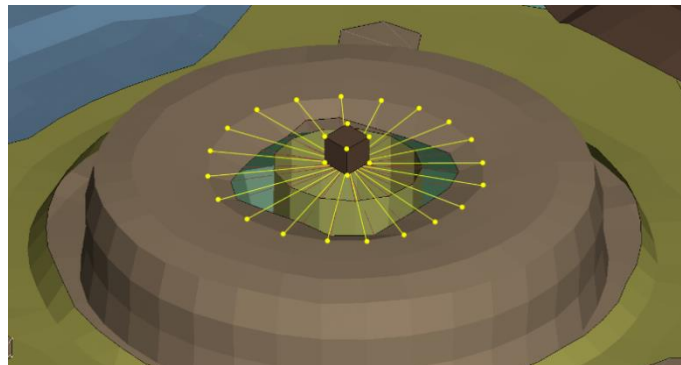
Figure 3.19: FE Model - Cube Accelerometer on Left Strut Tower Detail

The additional accelerometer positioned between the B-Pillar and the lower Sill, prescribed in its position by the EuroNCAP protocol as it is possible to see in Figure .20, has been defined differently to better represent the sensor adopted in the real crash test. In this case, some elements of the vehicle structure have been converted to rigid elements and a *ELEMENT_SEATBELT_ACCELEROMETER has been then defined on those elements..
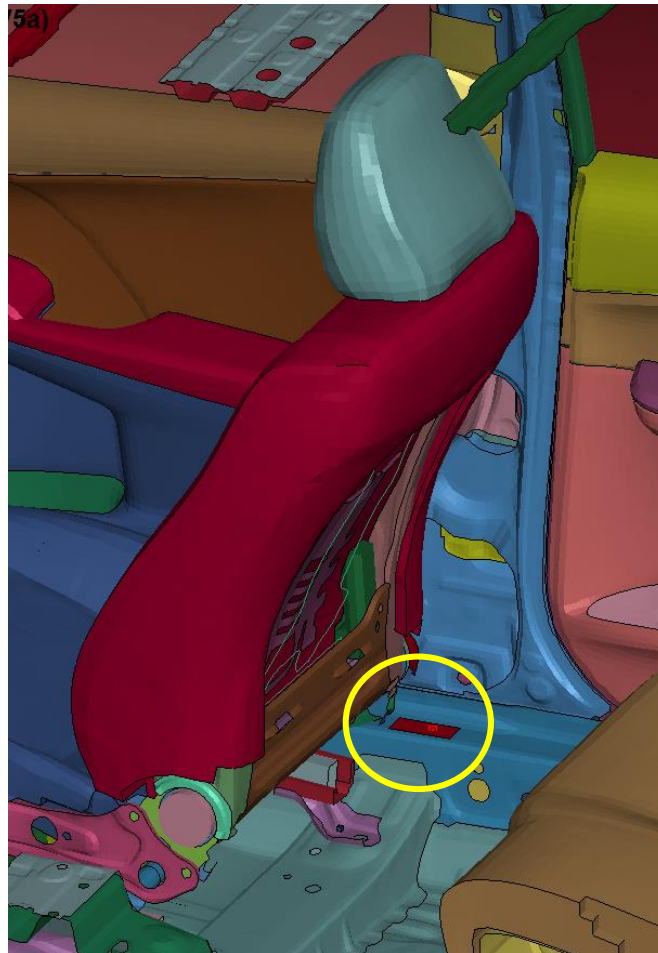
Figure 3.20: FE Model: EuroNCAP Sensor on Passenger Side - Detail

3.3 Sled Model

3.3.1 Purpose

Required by the EuroNCAP protocol to reduce the economic cost of crash tests, Far-Side safety rating is evaluated through the use of a sled model. In the actual practice, a production Body-In-White (BIW) of the vehicle is mounted on an accelerated sled as shown in Figure 3.21. This methodology brings within itself a number of advantages: the cost and time for multiple tests are greatly reduced, it is possible to verify multiple scenarios at different speed or vehicle angle and it can be useful in the early development stages of the vehicle. Furthermore, it is an easy platform where safety devices such as airbags, seatbelts and other active systems can be thoroughly tested. According to the test setup, the sled can be either accelerated or decelerated following what is called a sled pulse, representative of a previous crash test carried on in similar boundary conditions. In this thesis, a sled finite element model has been developed starting from the full vehicle model of a 2012 Toyota Camry. This model aims towards reproducing the BIW of the vehicle installed on a decelerating sled, according to the requirements prescribed by the EuroNCAP protocol.

Figure 3.21: EuroNCAP Sled Test [10]

3.3.2 Model Description

The sled model developed in this work has been obtained as a simplification of the complete vehicle model of a 2012 Toyota Camry described in detail in Section 4.2 the modelling process can be divided in the following steps:

1. *Sled structure modelling:* the components representative of the BIW structure have been extracted from the complete vehicle model with no modification, but some components have been trimmed in order to limit the environment to the structural parts relevant to our simulation.

2. *Sled structure polishing:* this process is aimed towards simplifying the description of the model an ensure its stability during movement. In this phase, the model has been subdivided in different subsystems which easier to be modified individually, the trimmed edges have been stiffened to increase stability and part of the vehicle subframe has been converted to rigid for implementing the kinematic onto the vehicle.

3. *Additional components modelling:* additional parts are required to be implemented for a complete model: Accelerometers are installed in relevant positions and foam spacers have been fitted to the passenger seat as prescribed by EuroNCAP.

4. *Sled model set-up:* Relevant effort has been dedicated to guarantee a proper run to completion of the simulation and the ease of use of this environment for further studies.

The final sled model, has been divided in different subsystems as follows :

- *BIW_with_rigid_sections.k:* File incorporating the structure of the sled
- *Left_seat_deformed.k:* Contains the driver seat pre-deformed following the THUMS contour
- *Right_seat.k:* Contains the passenger seat
- *Passenger_seat_spacers.k:* Contains the additional foams spacers
- *Smain.k:* Main file which recalls the different models. *CONTROL, *CONTACT, *DATABASE keywords are defined in this file.

3.3.3 Model Generation Process

Starting from the complete FE model of the 2012 Toyota Camry, the objective has been to obtain a sled model able to faithfully reproduce the interior environment of the vehicle. The complete modelling process is described in the following sections but, a brief overview is provided here.

As it is done in the actual practice, all the unnecessary components have been removed. This list comprehends: engine, suspensions, steering system, door panels and hood. Furthermore, the vehicle frame has been cut to remove all structural components rearward of the B-Pillar and to ensure stability, the trimmed edges have been converted to rigid. The kinematic of the sled has been applied to specific frame sections converted to rigid as well to reproduce what would happen in a realistic sled test. The model is equipped with 16 accelerometers positioned in the same locations of the complete vehicle FE model. Conform to the EuroNCAP protocol, foam spacers have been modelled and positioned in the gaps between the console, the passenger seat and the B-Pillar. The model has been organized in subsystems to increase the versatility of the model and to allow faster and easier problem-solving. The step-by-step process can be summarized as follows:

1. Removing unnecessary vehicle components
2. Cutting the vehicle frame to obtain a BIW model
3. Model division in subsystems: Structure, Left seat, Right seat
4. Stiffening of trimmed edges
5. Generation of rigid sections for defining the sled kinematics
6. Positioning of accelerometers sensors
7. Modelling and positioning of passenger seat spacers

In the following sections, the modelling process is reported in detail.
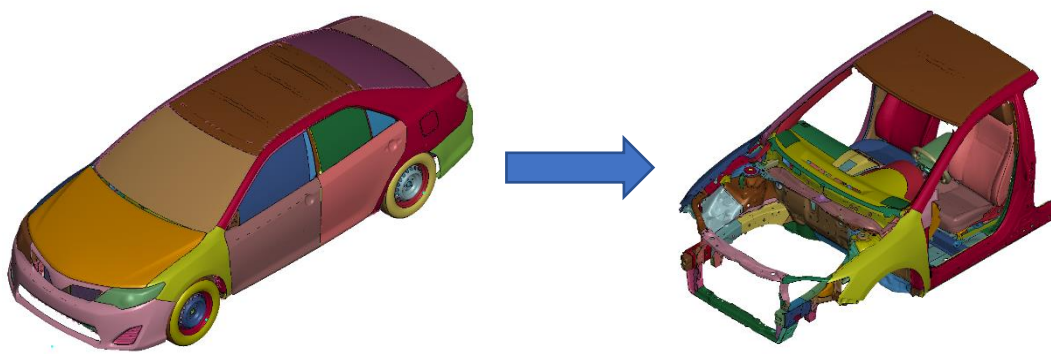
Figure 3.22: Complete and sled FE Model of a 2012 Toyota Camry

3.3.3.1 Removing unnecessary components

The first step of this process involves removing all the unnecessary components from the complete FE model. These components are not structural, are not relevant in our case scenario or are forced to be removed by the EuroNCAP protocol. Not structural parts which have been removed are the engine, the drivetrain, the suspension system, the steering system, the rear seats, the front doors, the rear doors, the hood and the trunk panels. Additionally, the rear subframe, sills and floor have been also removed. The windshield has also been removed as required by the EuroNCAP. The reason behind this choice is to increase the visibility of the camera equipment inside the vehicle during the real crash-test. During this process, a first manual clean-up of the model has been carried on for removing all CNRB that would not be connected to any part of the structure and would result in simulation errors if not removed. The model without these unnecessary components can be seen in Figure 4.23.
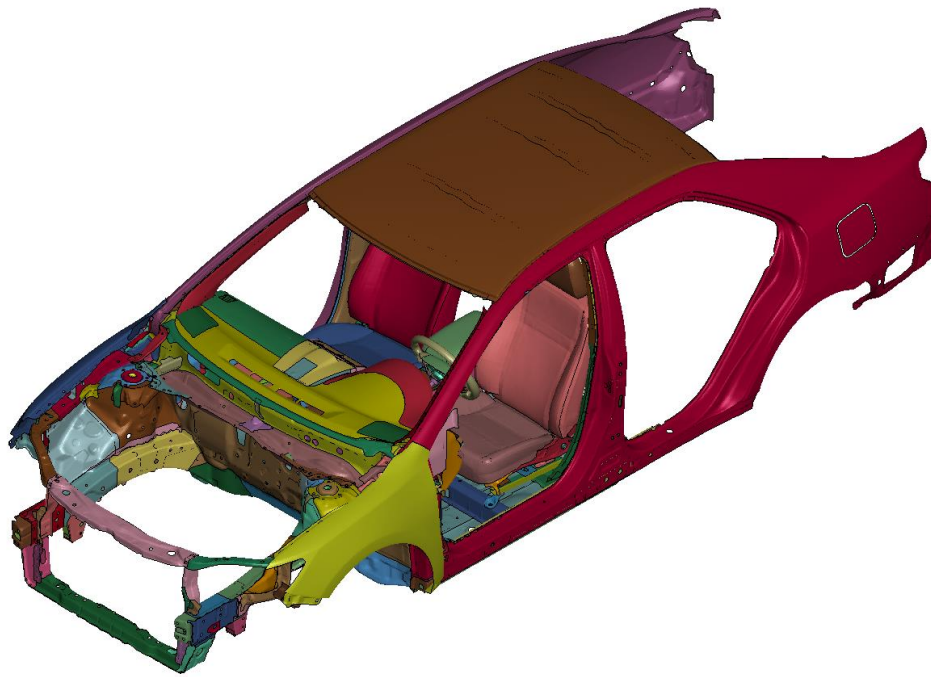
Figure 3.23: Vehicle model after unnecessary component removal

3.3.3.2 Cutting the vehicle frame

The necessary following step has been to cut the frame to remove the portion of the structure rearward of the B-Pillar as it is done in a real sled device. During this process, it is important to ensure stability of the sled model by avoiding excessive trimming of the vehicle structure and by paying attention to the shape of the cut edge. In order to not undermine the versatility of this model for multiple scenarios, it has been chosen to maintain the front end of the vehicle structure together with the roof frame. The trimming process has been carried on by selecting and

eliminating the unnecessary elements paying attention to resolve the possible errors that would emerge and by maintaining a smooth trimmed edge. A second clean-up has been carried out after this phase in order to remove all the CNRB left from the previous cleaning process and the errors that the cutting process would generate. The result of this phase can be seen in Figure 4.24.
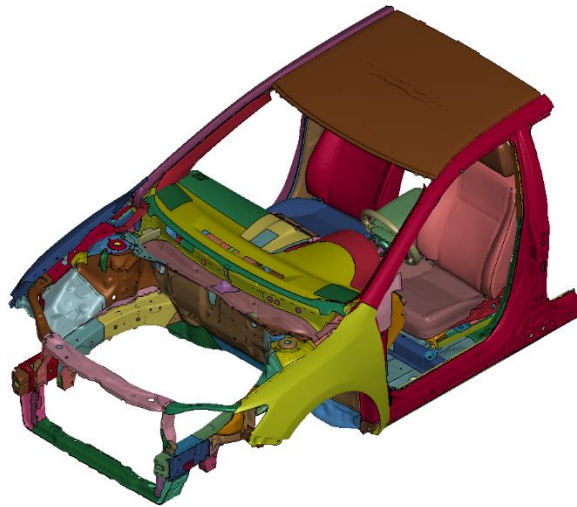
Figure 3.24: Vehicle model after cutting

3.3.3.3 Model division

Before proceeding with further modifications of the sled structure, in order to facilitate the next steps and work on different parts at the same time, with a consequent speed up of the modelling process, it has been decided to divide the model in multiple subsystems. From the modelling point of view, this also allows for a faster loading and saving time of the files when not all the elements are required to be modified.

The model has been divided in the following subsystems: structure, left seat and right seat. These subsystems have been obtained by isolating the left seat and right seat parts and saving them in separate files. The three subsystems are assembled in the same FE environment by being loaded thanks to the *INCLUDE keyword in the *Smain.k* file. The different files are the following:

- *BIW_with_rigid_sections.k*
- *Left_seat.k*
- *Right_seat.k*
- *Smain.k*

Significant attention has been dedicated towards ensuring that the connection between the different subsystems does not cause any errors. The seats are connected to the sled structure with the use of CNRB which are described in the respective files.

3.3.3.4 Stiffening of trimmed edges

As a result of the cutting process, the trimmed edges could experience an unrealistic behaviour during the simulation having potential consequences on the sled structure stability. This problem can be solved stiffening the areas that have been cut by transforming the elements of this region in rigid elements. A three-element wide belt has been modelled with the following properties:

- *SECTION_SHELL: with 1mm thickness (unchanged)
- *MAT_RIGID: with ρ=7.89e+3 kg/m^3, E=210 GPa, υ=0.3 (structural steel)

The thickness of the section has been decided on the basis of the elements in the proximity of the stiffened area. The material has been modelled as a structural steel with properties similar to other parts of the sled structure. A detail of the stiffening of the trimmed edges can be seen in Figure 4.25, an identical process has been carried on the cut ends of the upper roof assembly.
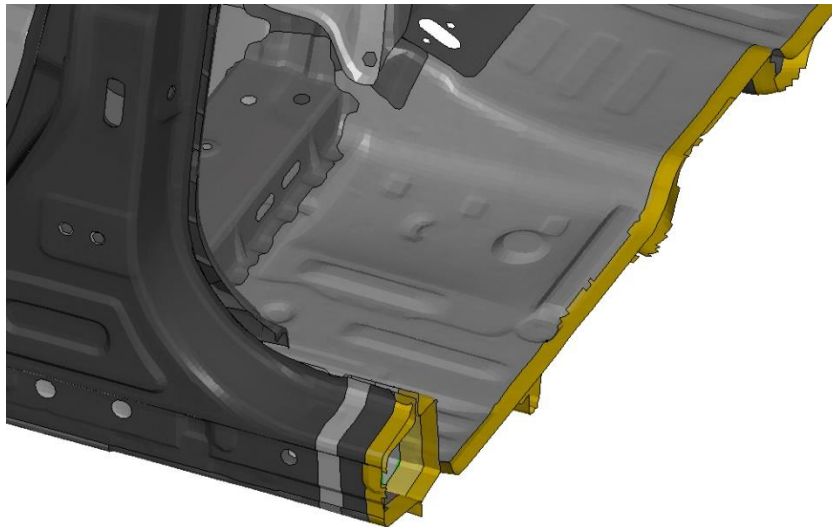
Figure 3.25: Detail of the floor stiffened edges

3.3.3.5 Rigid sections generation

A fundamental step is then to modify the sled such that it is possible to assign to it the desired kinematics. In this work, it has been chosen to characterize the motion of four regions of the sled structure. These regions are located, as shown in Figure 4.26, on the lateral lower sills in the rear of and front of the floor area. The reason for this choice has been dictated by the desire to reproduce the attachment between the BIW and the accelerated sled in the actual test practice. A

four elements wide belt for each region has been isolated and converted to rigid material with the following properties:

- *SECTION_SHELL: with 1mm thickness (unchanged)
- *MAT_RIGID: with ρ=7.89e+3 kg/m^3, E=210 GPa, υ=0.3 (structural steel)

The four rigid sections, due to the limited width with respect to the structure, are defined in the same part and a common movement is described for all of them. *CONSTRAINT_PRESCRIBED_MOTION have been used to assign velocity curves to the rigid sections. To be representative of the behaviour of the complete vehicle model, linear and rotational velocities have been prescribed along the X, Y and Z axis. A detail of front and rear rigid section is shown in Figure 4.27.
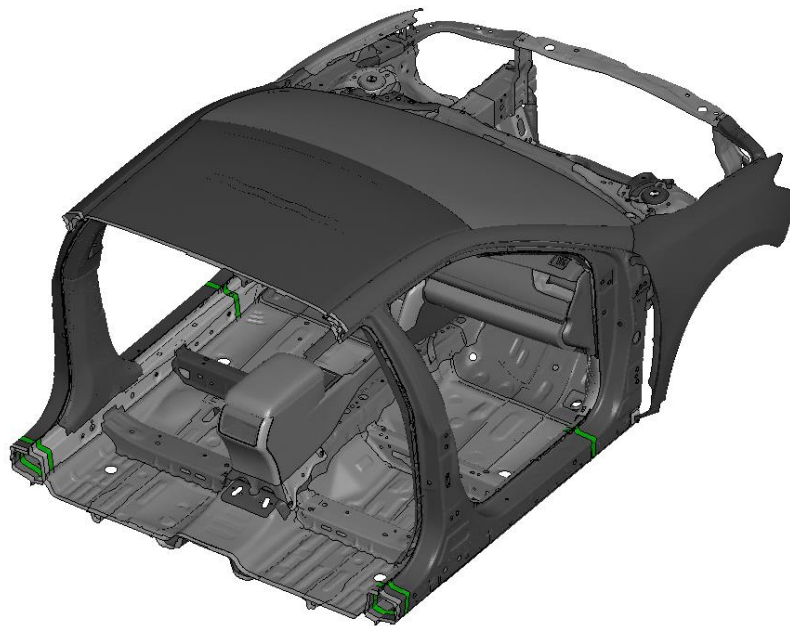
Figure 3.26: FE sled model with rigid sections (GREEN)
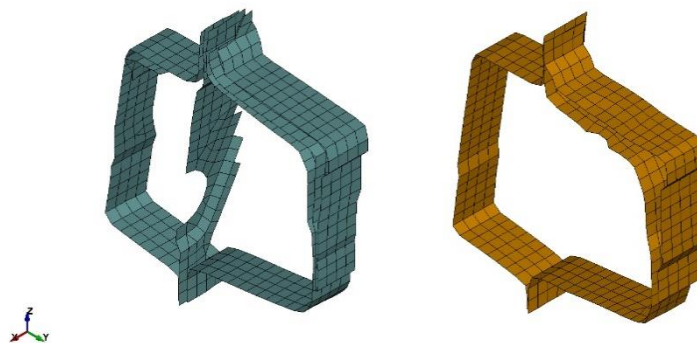
Figure 3.27: Front (LEFT) and Rear (RIGHT) Rigid Sections - Detail

3.3.3.6 Accelerometers

The sled model has been equipped with the same sensors system modelled for the complete Camry FE model. Therefore the 16 accelerometers are positioned in the same locations: Strut Towers, Lateral Sills, Seats attachment points and lower B-Pillar as it can be seen in Figure 4.28. For more details on the modelling of these sensors, refer to Section 4.2.2.
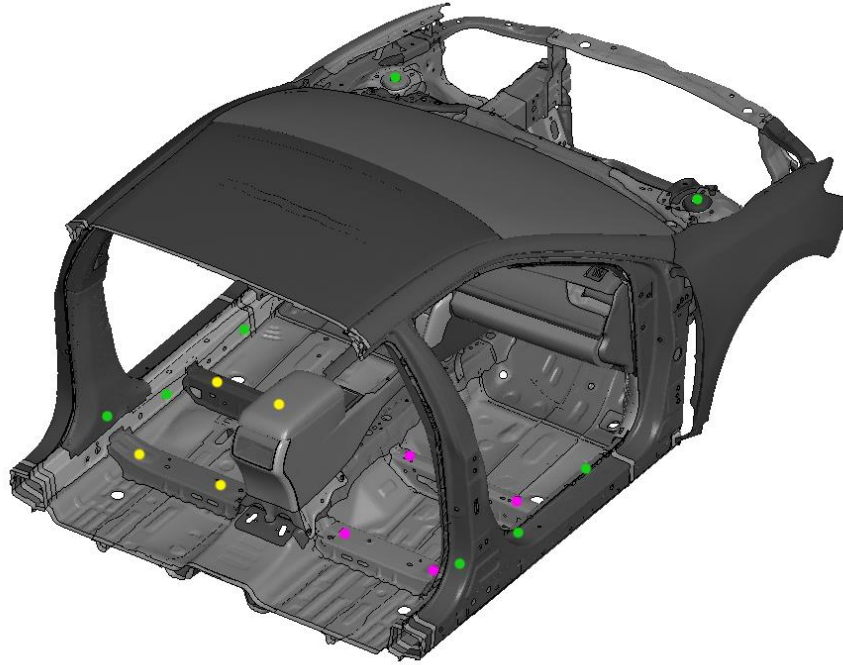
Figure 3.28: FE Sled Model - Accelerometer Position Detail
Vehicle Structure (GREEN); Left Seat (YELLOW); Right Seat (MAGENTA)

3.3.3.7 Passenger seat spacers

An additional component explicitly required by the EuroNCAP protocol is represented by foam spacers positioned in the lateral surrounding of the passenger seat as shown in Figure 4.29. These plastic material inserts assume the role of filling the gaps between the central console, passenger seat and B-Pillar with the aim of replicating the pole intrusion inside the vehicle during the sled test. The spacers should help transmit the forces between these three components but not enough data has been provided by the protocol to document the effectiveness of this measure towards reproducing the real crash test conditions in the sled environment. As a mean of evaluating the effect of the foam spacers, in this thesis the forces transmitted through these components will be evaluated.
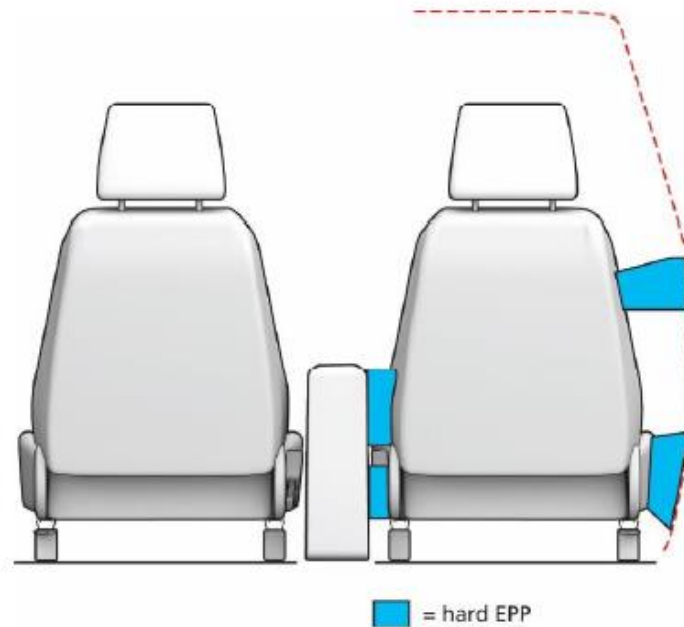
Figure 3.29: Passenger Seat Spacer position according to EuroNCAP protocol [10]

Three different components have been modelled: a spacer positioned between the central console and the left side of the passenger seat, a spacer positioned between the right side of the back seat cushion and the B-Pillar cover and a spacer positioned between the right side of the lower seat components and the B-Pillar cover. These components have been modelled following these steps:

1. Isolating the gap boundary components
2. Creating for each side of the gap a continuous surface
3. Creating by extrusion of one of the surfaces, a solid mesh that would fill the gap
4. Checking and modifying the mesh to avoid penetration with the gap boundary components
5. Re-meshing the spacer to have a smoother and more uniform mesh

Once these components have been modelled and included in the sled model as a separate file, it has been possible to define load sensors for the right and left side of the seat. These sensors are described through the use of *DATABASE_CROSS_SECTION_PLANE, as it can be seen in Figure 4.30, and they can measure the load transmitted between the parts involved.
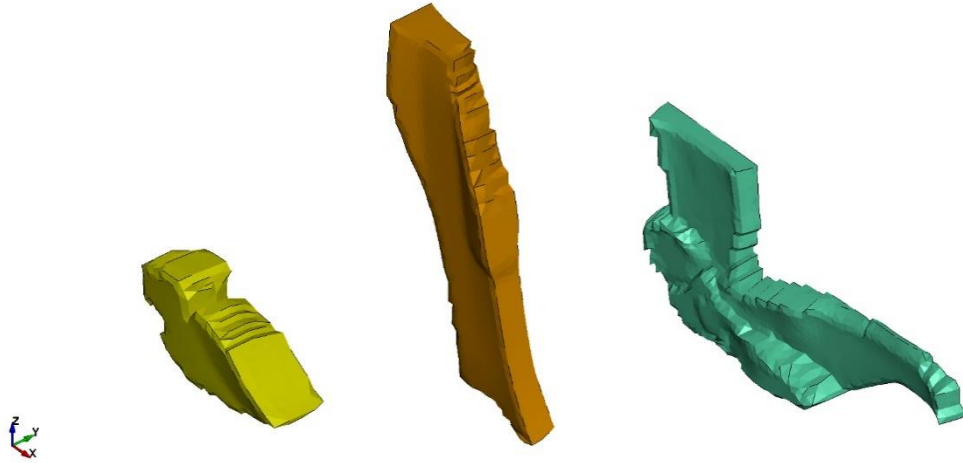
Figure 3.30: Passenger seat spacers - FE Model
Lower Right Seat (YELLOW); Upper Right Seat (ORANGE); Left Seat (GREEN)

Figure 3.31: Passenger seat spacers: Position detail (LEFT); Section Planes (RIGHT)

The EuroNCAP protocol also specifies the type of material required for the spacers. In the specifics, an Expanded Polypropylene (EPP) with a density of 60g/l and with a minimum compression stress of 340 kPa at 25% of compression strain. For including this material properties in the added components, different material cards available in the LS-DYNA code has been considered. Multiple sources [6, 21], indicated that for this type of foam, a versatile closed-cell polymer extensively used in the automotive industry for bumpers and pedestrian protection, the best compromise in terms of behaviour of the material and accuracy during the deformation is to

use a *MAT_FU_CHANG_FOAM description. This type of material model based on the constitutive equations for foam materials by Chang (1995) allows for defining nominal stress vs strain at different strain rates. The choice of this material card directly influenced the research of useful data for the material description since the two requirements of minimum compression strength and availability of stress vs strain data, at multiple strain rates, had to be met. A thorough research in the available databases and papers has been carried out and the material with the following characteristics has been chosen:

- ρ = 90g/l
- Compression stress @ 25% strain = 570 ÷ 698 kPa
- E = 12 MPa
- HU = 0.01
- SHAPE = 6

It is worth observing that the material selected is denser and considerably stiffer than the minimum required by EuroNCAP. This choice has been forced by the lack of publicly available material data that would fit the requirements, especially for the availability of compression data at multiple strain rates.

In the Fu Chang Foam model, the hysteric unloading factor HU and the shape unloading factor SHAPE characterize the behaviour of the material during the unloading phase and have been chosen by following LS-DYNA guidelines [8] and equal respectively to 0.01 and 6.
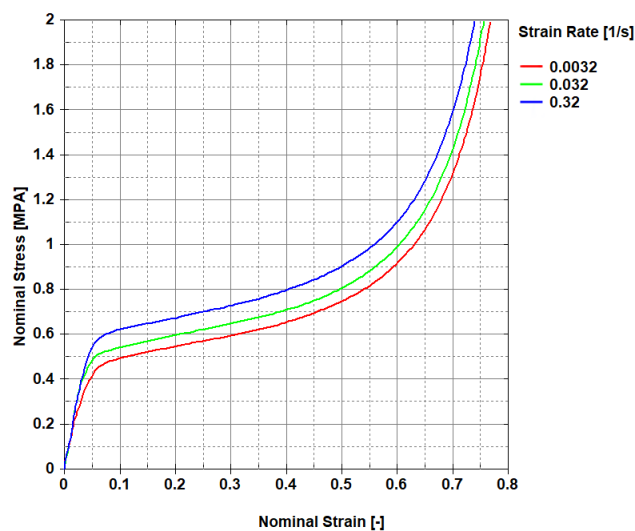
Figure 3.32: EPP90 Compression Stress vs Strain at different strain rates

While performing different validation tests involving the previously described spacers, a stability problem occurred when high strain rates were reached. To find a solution, the following changes

have been tested: increased material stiffness, increased material strain rate range, different element material formulation, different hourglass controls and different definitions of contact between the spacers and the sled environment. Unfortunately, none of these solutions proved to provide enough stability in the simulation. For this reason, a simpler and more stable material model has been adopted by replacing the *FU_CHANG_FOAM model with a *LOW_DENSITY_FOAM one. Referenced and used in other works (Civin, 2018 [7]), it does not take in account the material behaviour at different strain rates but, using the same material properties described in §4.3.3.7, material stability was achieved throughout the complete simulation. The stress-strain curve adopted in this model, describe the material when subject to a strain rate equal to 0.032 1/s, visible as the green curve in Figure 3.32. Other characteristics of the material such as density and elastic modulus have been kept unchanged.

Chapter 4: Full-Scale Test

The starting point of the Far-Side EuroNCAP assessment protocol is to be identified with a full-scale crash test involving the complete vehicle in a lateral impact. The resulting deceleration of the vehicle body will then be used to assign the proper kinematic to the sled model. Two different full-scale crash test can be performed: a lateral impact against an Advanced European Mobile Deformable Barrier (AE-MDB) at 60 km/h, and an oblique impact against a rigid pole at 32 km/h. Due to the severity of the impact and the higher intrusion inside the vehicle compartment, the latter has been chosen to be the representative test in this work. Described in Section 3.2.2, the same conditions have been reproduced in the virtual environment.

The complete base model used for the simulations required is composed by the following files:

- *Main.k*: File which includes the general keywords and the movement equations, it calls for the other files in the same virtual environment
- *Toyota_Camry.k*: File which includes the complete vehicle and the equipped sensor system
- *Pole.k:* File which includes the rigid pole and relative keywords
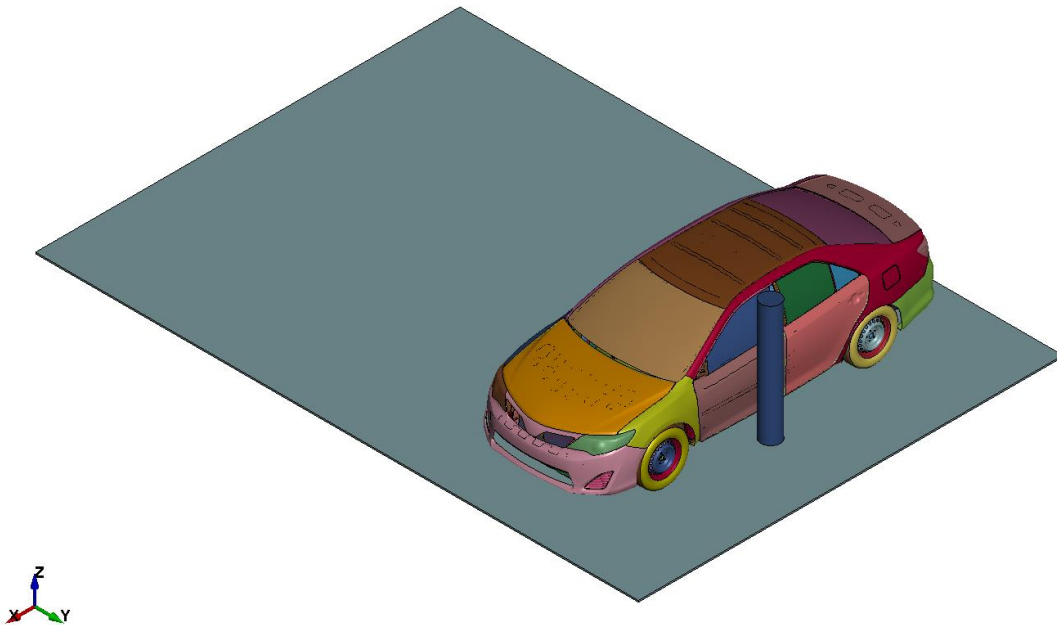- *Floor.k:* File which includes the rigid floor and relative keywords

Figure 4.1: Pole Test Model Setup

The pole has been modelled as a solid element cylinder with a height H equal to 1600mm and a diameter D of 254mm. It is positioned 1254mm rearward of the front axle and 1054mm to the left

of the vehicle longitudinal axis. It is described as a rigid material based on a structural steel. The floor uses the same material, it is modelled as a solid block 5600x8000mm and is 20mm thick. It covers a large area below the vehicle and, to replicate the real testing condition, it moves at the same initial speed of the vehicle. The pole is positioned 31mm above the surface of the floor to avoid potential interference between the two.

The movement has been described by assigning an initial velocity to the vehicle model and the floor, while the pole is rigidly fixed in space. Due to difficulties in rotating the vehicle to obtain the prescribed oblique angle of 15°, the model will initially move diagonally on the XY plane, at a speed of 32km/h.

*CONTACT_AUTOMATIC_SURFACE_TO_SURFACE keywords have been used to describe the direct contact between the outer vehicle surface and the rigid pole with the definition of segment contact sets. Similarly, the contact between the tires and the ground has been modelled in the same way, in this case the static and dynamic friction coefficients, have been set to values respectively of 0.2 and 0.1 to replicate the low friction condition recommended by the EuroNCAP protocol. Internal contacts between vehicle components such as doors, seats, and all other moving parts, has been modelled using *AUTOMATIC_SINGLE_SURFACE.
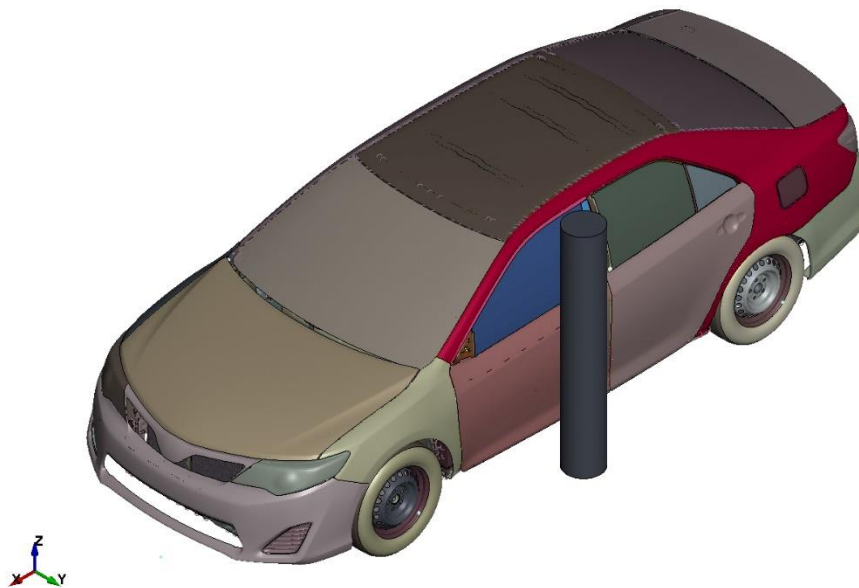
Figure 4.2: Pole Test Model - Vehicle Contact Surfaces

4.1 Validation of Rigid Sections

To validate the effect of the introduction of rigid sections in the vehicle model, described in Section 4.3, a comparison test has been carried on by evaluating the behaviour of the complete system under side impact conditions. The reference for this validation test is represented by the model without rigid sections and the comparison is carried on by evaluating the simulation energy, vehicle structure velocity and acceleration.

4.1.1 Energy

The first comparison that can be made between the two models concerns the energy balance during the simulation. This analysis can provide information on the general behaviour of the simulation and can highlight possible problems. In Figure 4.3, a direct comparison between the reference model (solid line) and the rigid section model (dashed line) is shown. It can be observed that the total energy can be considered constant for the whole length of the simulation and it is equal between the two models. The most significant difference between the two model concerns the internal energy and the sliding energy. The reason for this difference can be identified in the different deformation behaviour of the struck side sills where the rigid sections have been modelled. The increase of internal energy mirrors the creation of negative sliding energy and it can be considered a very localized problem with low impact on the overall validity of the solution. In both cases the hourglass energy is kept to a value below 10% of the total energy.
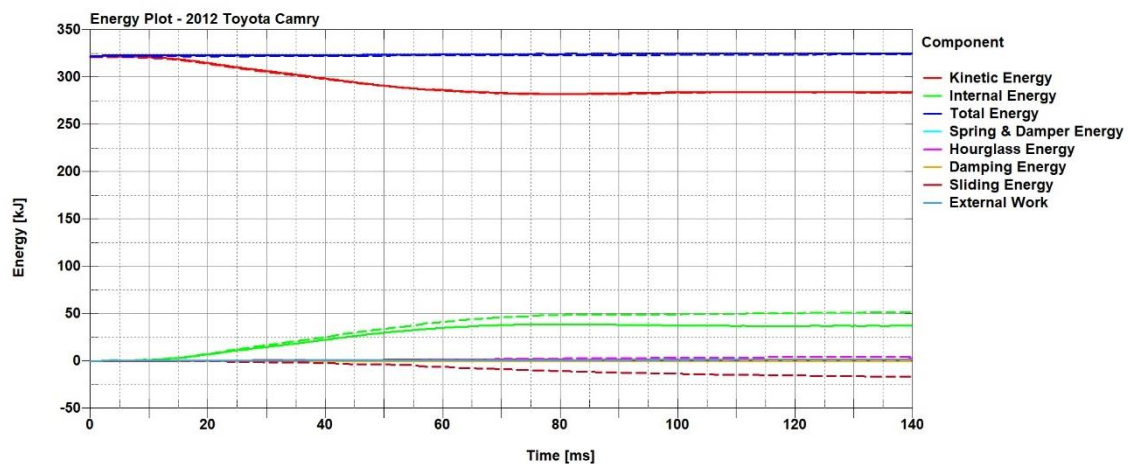

Figure 4.3: Energy Plot - 2012 Toyota Camry: Reference Model (solid line) vs Rigid Section Model (dashed line)

4.1.2 Accelerometer

Analysing the accelerations measured during the simulation by the sensor positioned on the lower part of the B-Pillar of the unstruck side, it can be observed that the general trend of the acceleration curves along X, Y and Z of the rigid section model provides a reasonable representation of the reference model during the crash scenario. The filter applied to the signal is a SAE CFC60, but a similar comparison has been carried on also using CFC108 and CFC180 filters and produced comparable results.
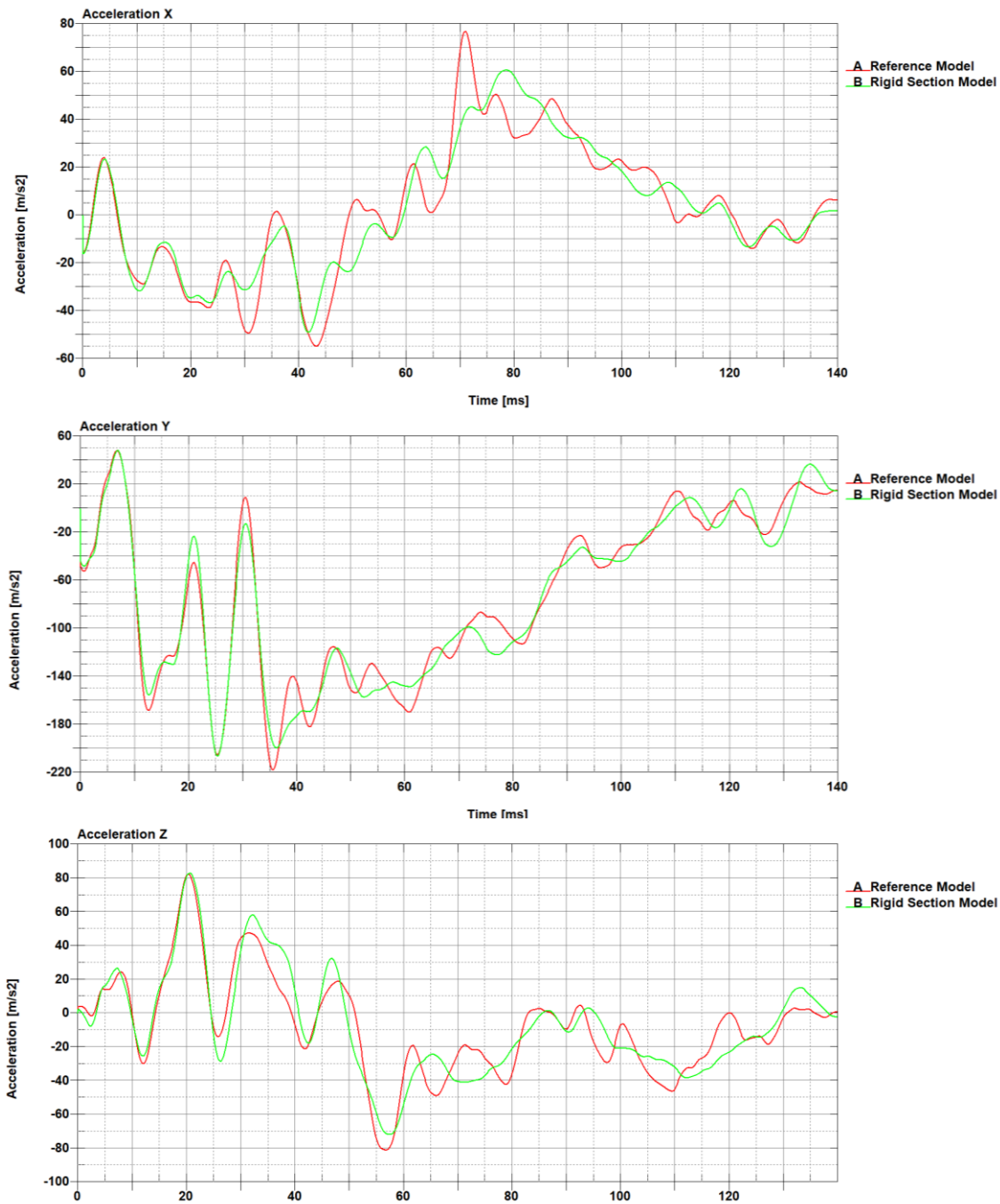

Figure 4.4: Acceleration Plot in X, Y and Z - 2012 Toyota Camry: Reference Model vs Rigid Section Model

Due to numerical noise occurring during the simulation in measuring the acceleration, it is relevant to evaluate the comparison between the velocity signal. As it is possible to observe in Figure 4.5, the two models behave similarly presenting no significant differences in the velocity output. For this comparison a SAE CFC180 filter has been used.
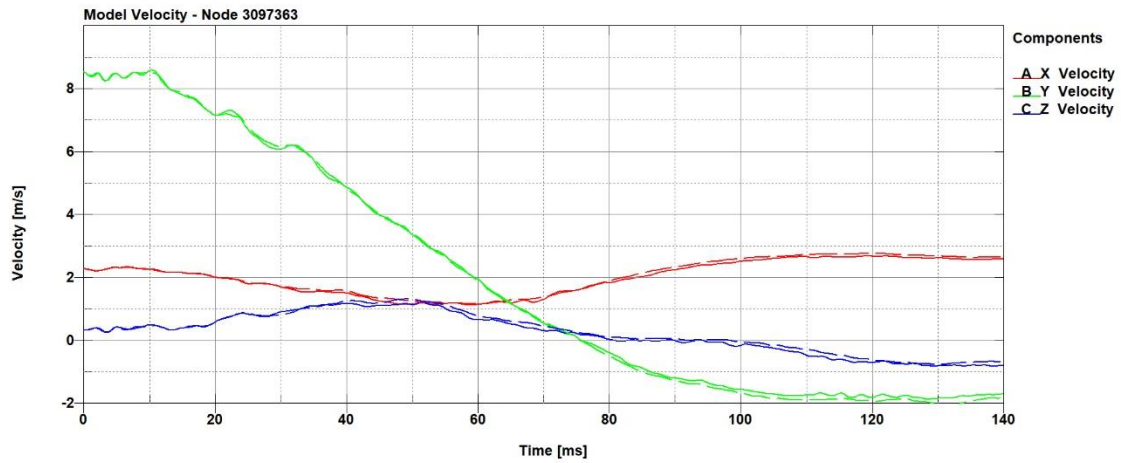

Figure 4.5: Velocity Plot - 2012 Toyota Camry: Reference Model (solid line) vs Rigid Section Model (dashed line)

4.2 Validation of Sled Model

To validate the sled model and to ensure that it behaves as desired, a comparison test has been carried on with reference to the simulation involving the complete vehicle model. The movement of the sled is directly obtained from the accelerometer positioned in the lower part of the B-Pillar of the side not directly subject to the impact as prescribed by the EuroNCAP protocol. *BOUNDARY_PRESCRIBED_MOTION_RIGID keywords are used to describe linear velocity and rotational velocity of the rigid sections in the 6 DOF.

4.2.1 Energy

To identify general simulation problems, it is useful to analyse the energy plot diagram. In this case since an external work is being applied to the sled in order to assign the movement to the model, a constant total energy throughout the simulation is not to be expected and this is observable in Figure 4.6. The hourglass energy represents about 10% of the total simulation energy, conform to the LS-DYNA guidelines. Another useful metric to highlight potential simulation problems is the energy ratio defined as the ratio between the total energy and the sum of internal and kinetic energy. In this case, it is constant and equal to 1 which is considered an optimal simulation result.
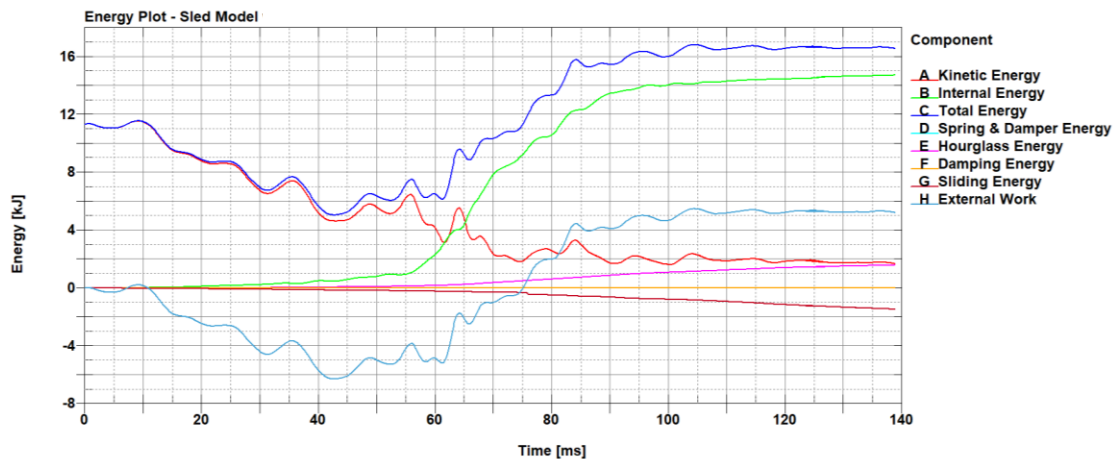

Figure 4.6: Energy Plot - Sled Model

4.2.2 Accelerometer

In order to compare the kinematic of the sled model the output of the accelerometer positioned on the structure have been evaluated. In the following Figure 4.7 – 4.12, the linear and rotational velocity of the two models are shown. The linear velocities plots are filtered using a SAE CFC60 filter while for the angular velocities a heavier filter was needed due to the high noise of the reading, they sue a SAE CFC20.
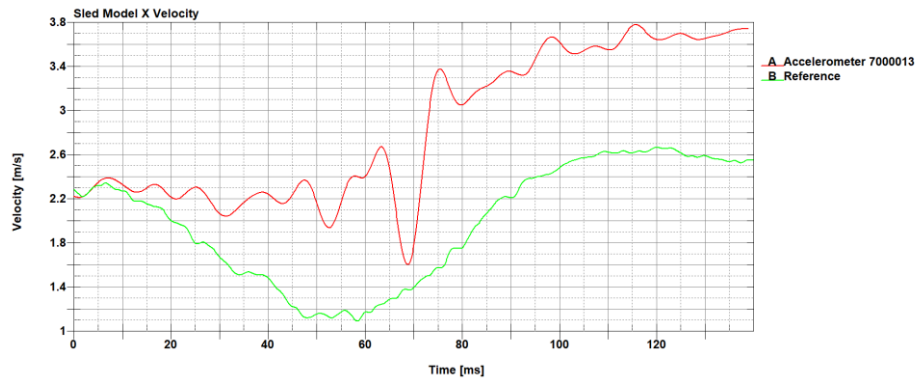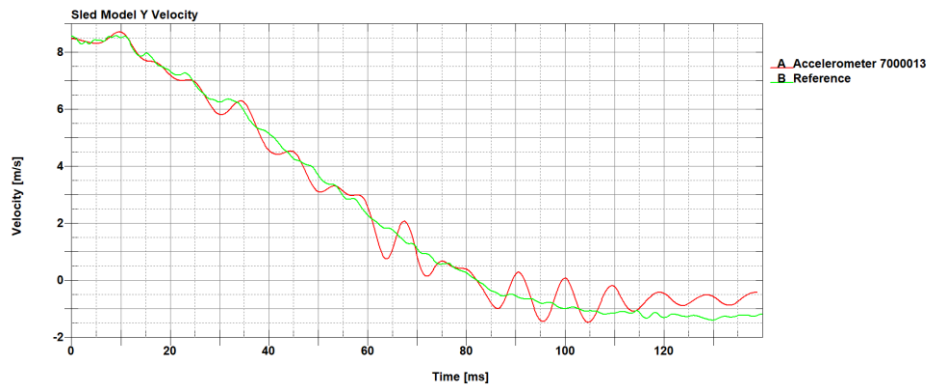

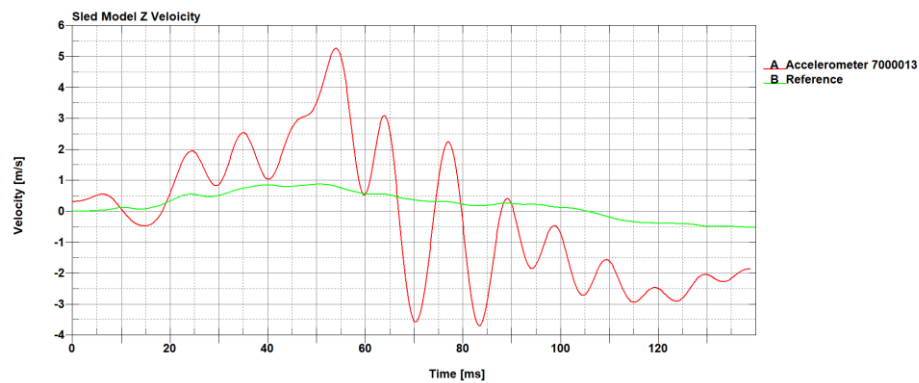*Figure 4.7: Sled Model X Velocity*

Figure 4.8: Sled Model Y Velocity

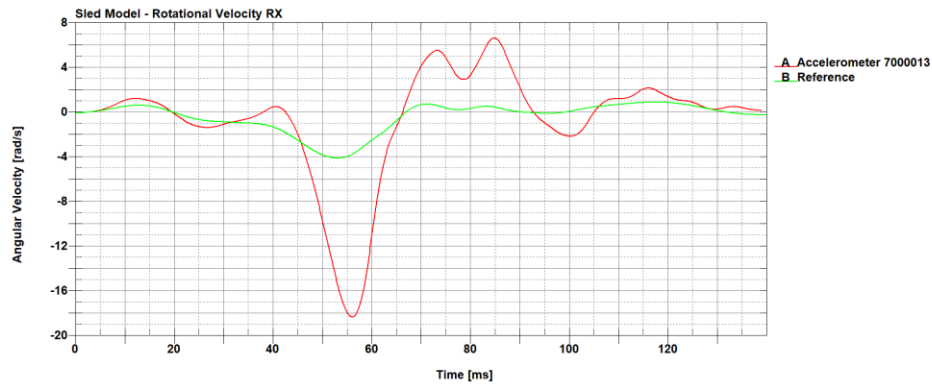

Figure 4.9: Sled Model Z Velocity

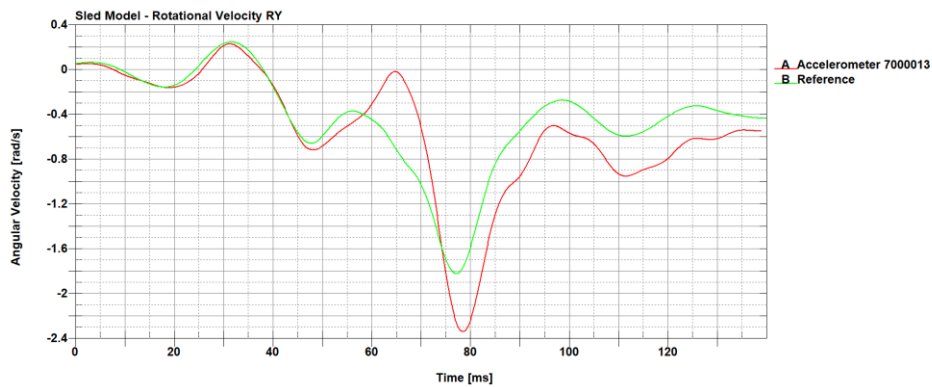*Figure 4.10: Sled Model RX Rotational Velocity*

Figure 4.11: Sled Model RY Rotational Velocity
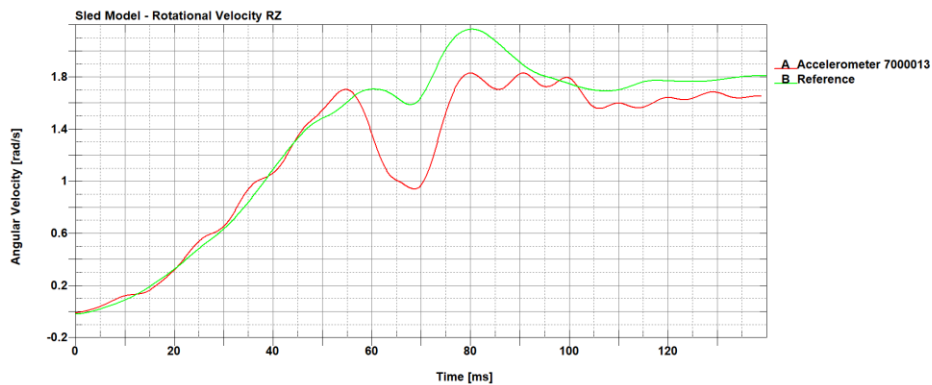
Figure 4.12: : Sled Model RZ Rotational Velocity

Analysing the results obtained, it is possible to observe the similar behaviour of the two models, but it is also noticeable the velocity oscillations captured by the accelerometer positioned on the sled model. The different response is most noticeable for what concerns the linear velocities in the X and Z directions. This behaviour can be attributed to two factors: the lower mass of the sled model and the behaviour of the lower structural components such as the sills and the floor, when subject to a constrained movement applied in localized sections. This results in high oscillation

of the sills, where the rigid sections and the accelerometers are located impacting the accelerometer reading.

The Pearson's correlation coefficient has been calculated to assign a measure of the relationship between the behaviour of the two models. The results reported in Table 2, show a strong correlation between the models with values above 0.7. [25]

	Velocity X	Velocity Y	Velocity Z	Rotational Velocity X	Rotational Velocity Y	Rotational Velocity Z
R	0.767	0.999	0.721	0.855	0.882	0.954

Table 2:Pearson's Correlation Coefficient

4.2.3 Visual Comparison

In Figure 4.13 – 4.19 a visual comparison between the sled model and the complete vehicle model is provided. As it is possible to observe, the general behaviour of the two models is comparable in terms of kinematic and rotation. The intrusion of the pole inside the vehicle compartment is not represented in the sled model and this leads to the different movement of the driver's seat.
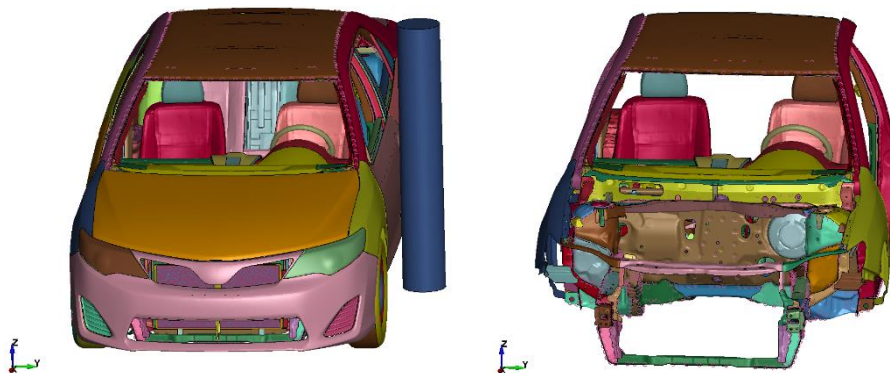
Figure 4.13: Full-scale and Sled models - t = 0ms
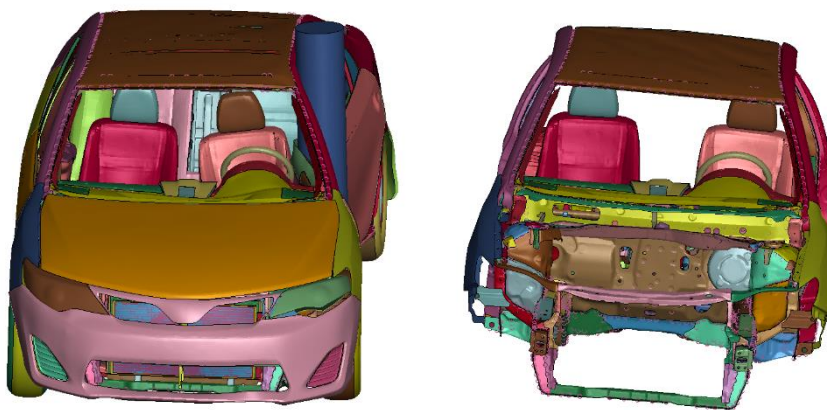

Figure 4.14: Full-scale and Sled models - t = 20ms

Figure 4.15: Full-scale and Sled models - t = 40ms

Figure 4.16: Full-scale and Sled models - t = 60ms
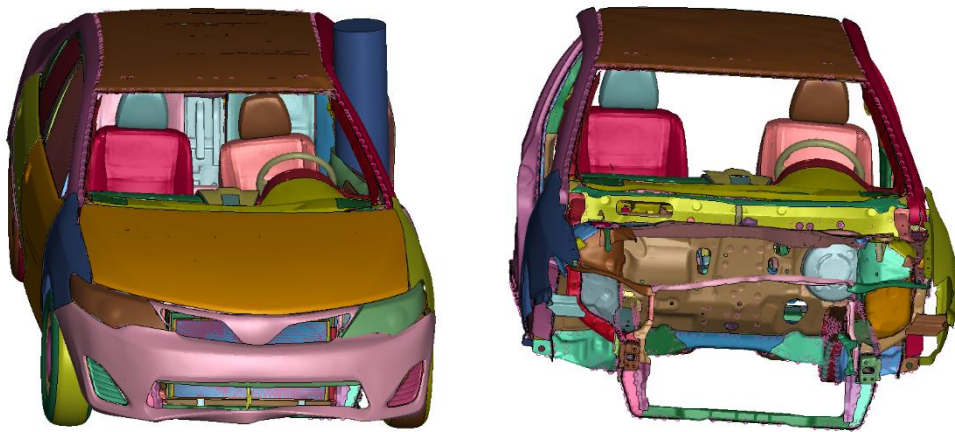

Figure 4.17: Full-scale and Sled models - t = 80ms

Figure 4.18: Full-scale and Sled models - t = 100ms

Figure 4.19: Full-scale and Sled models - t = 120ms

Figure 4.20: Full-scale and Sled models - t = 140ms

Chapter 5:   THUMS Implementation

5.1 Sitting Simulation

When an occupant sits inside a vehicle, the seat deforms itself to accommodate the weight of the person. In order to faithfully represent what happens in the reality, it is necessary to carry out a sitting simulation that would simulate this process. The resulting deformed seat is needed to avoid initial penetrations when the HBM is inserted in the vehicle between the body and the seat and provide an overall more realistic behaviour.

The process requires two models to be run:

- *THUMS:* For this type of simulation, the whole HBM is not required because of the high computational cost that would involve, therefore a simplification can be made. Assuming with good approximation that the deformation of the HBM while sitting is negligible, it is possible to convert the outer skin into a single part defined as a shell with rigid material.
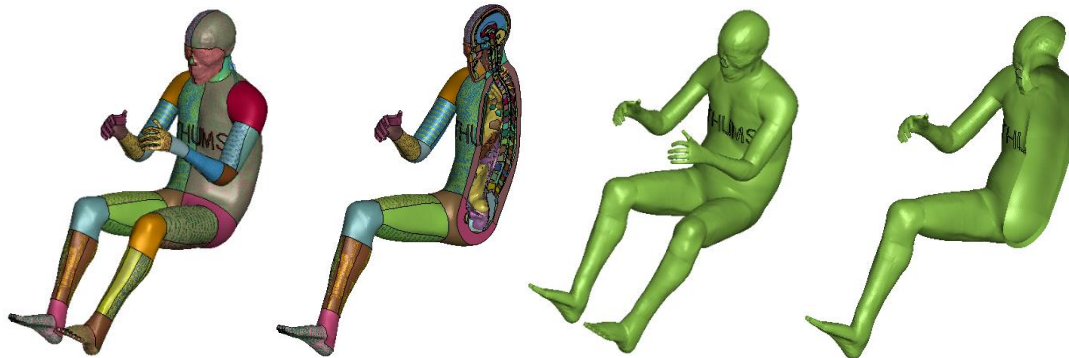

Figure 5.1: Comparison between full THUMS model and the rigid skin

- *Driver's Seat:* The FE model of the undeformed driver seat is isolated and exported from the complete system. This subsystem includes the seat structure, the seat cushions and their supports.

Figure 5.2: Driver Seat Subsystem

The seat is fixed in place so that rotational and translational degrees of freedom are locked. To this end, *BOUNDARY_SPC_SET are applied to the seat attachment points with the vehicle structure. To perform the sitting simulation, a fixed displacement of 50mm in X direction and -80mm in Z direction is assigned to the rigid skin by the keyword *BOUNDARY_PRESCRIBED_MOTION_RIGID. These quantities are consistent with the common practice adopted by automotive companies [17].
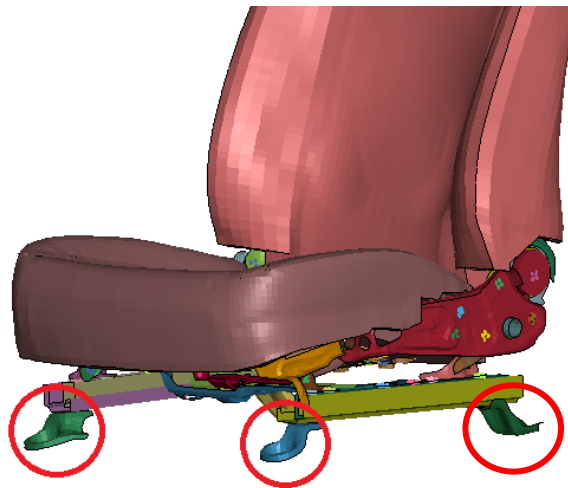
Figure 5.3: Detail of the constrained seat attachments

The contact between the seat cushions and the rigid skin is defined by the keyword *CONTACT_AUTOMATIC_SURFACE_TO_SURFACE.
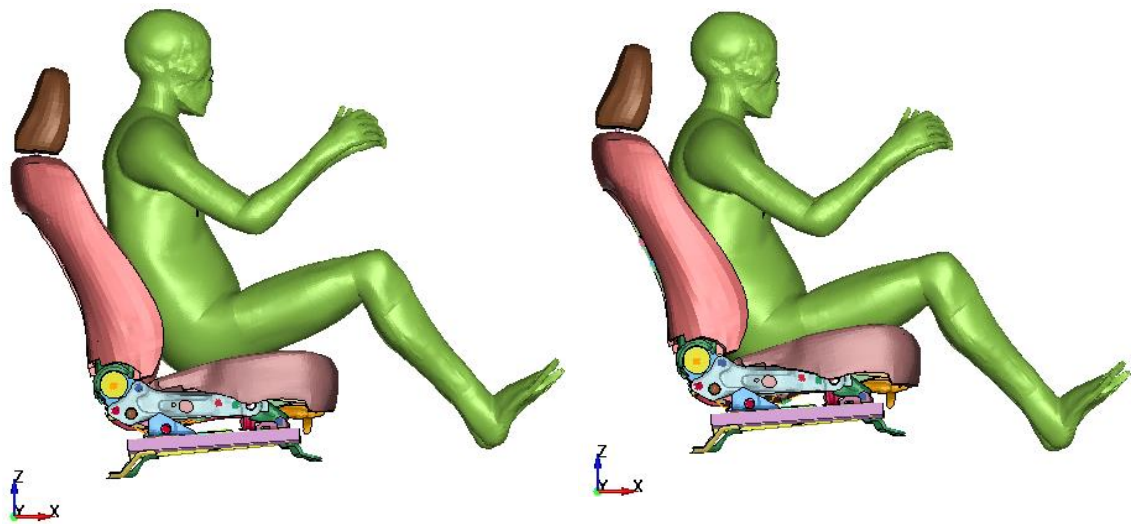
Figure 5.4: Seat and Skin model at first and last step of Sitting Simulation

The result of the sitting simulation, showing the deformed driver seat can be observed in Figure 5.5. The model is then included in the complete vehicle system for further simulation steps.
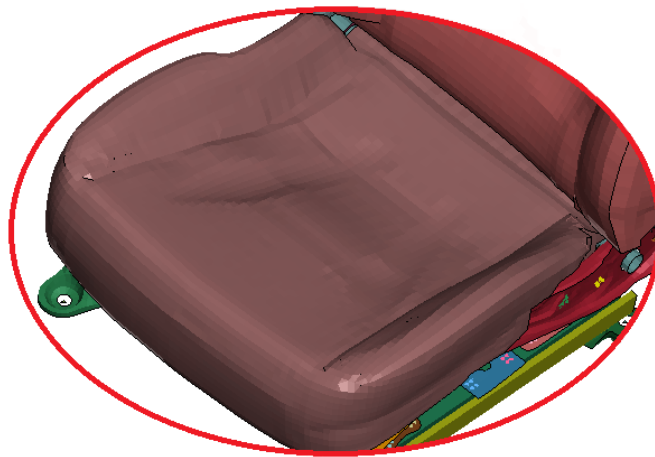
Figure 5.5: Deformed cushion seat - Detail

5.2   THUMS Positioning process

The THUMS provided is available in two standard positions: a standing one and a sitting one. Starting from the latter model, it is required to properly position the dummy model in order to fit the environment of our vehicle and satisfy the requirements laid by the EuroNCAP protocol. For the positioning process two software where used: PIPER and LS-DYNA. The PIPER software is an open source software developed in a European project. The software is aimed to scale and position Human Body Models. The steps required are the following:

1. Positioning of the THUMS through the PIPER software functionality
2. Creation of a script for the positioning simulation on LS-DYNA
3. Simulation with LS-DYNA

Inside the PIPER environment, it is possible to import a visual reference of the vehicle environment to facilitate the positioning process. Shown in Figure 5.6, a simplified model of the driver seat and the surrounding interior components is isolated for this purpose and loaded together with the THUMS model inside PIPER. Two features of the software have been used to
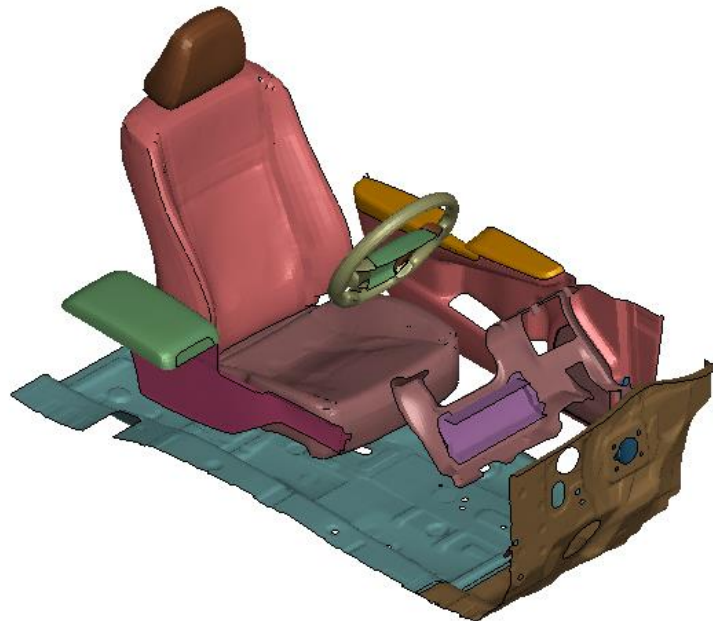
Figure 5.6: Environment subsystem for positioning

perform the positioning process: the landmark positioning and the joint positioning. Landmarks are useful to move the limbs in the desired position while by using the joint positioning, it is possible to fine tune their angle. Bones can be fixed in place to avoid unwanted movements during the positioning process. The distribution of landmarks and joints on the THUMS can be seen in Figure 5.7.
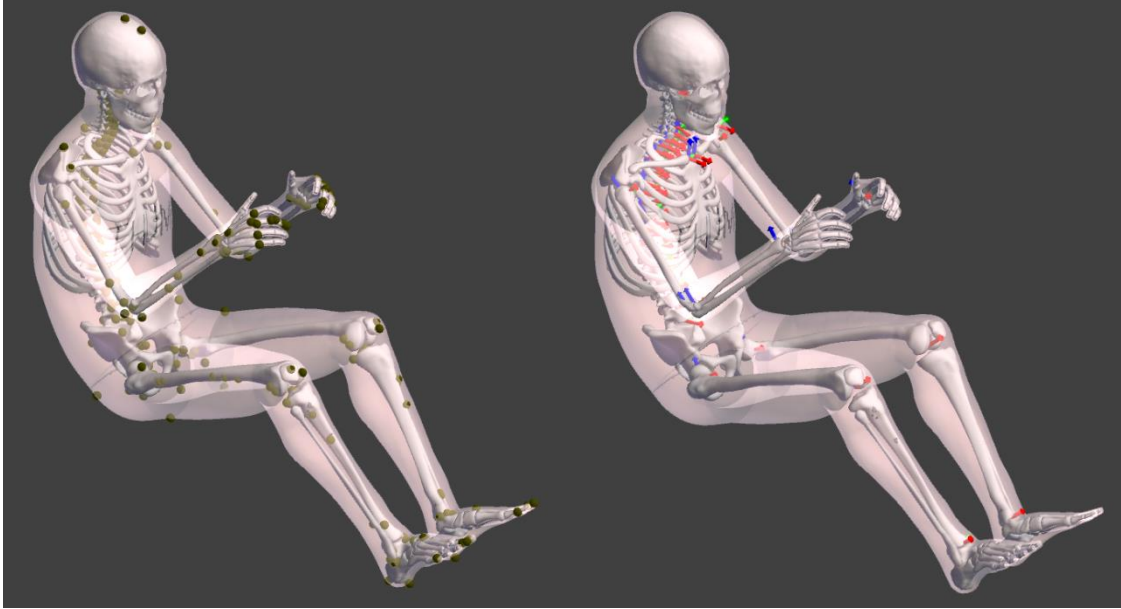
Figure 5.7: Landmarks (left) and Joints (right) Visualization in PIPER

In this work, the position of the limbs is the focus of the positioning process. The EuroNCAP protocol norms the position of the left and right feet to be compliant with a standard driving position, therefore the left foot is positioned on the accelerator pedal, the right foot flat on the floor due to the absence of a dedicated foot rest on the vehicle and the heels are resting on the floor. No specific positions are specified for what concerns the arms since in the actual practice a WorldSID dummy without complete upper limbs is used. For this reason, the hands have been positioned to be at "9 and 3" position representative of a realistic scenario.

Once the desired position has been obtained through iterative steps, in order for the position to be definitive and be able to be used in this work, a script file must be generated. This script is needed to set up a FE simulation that runs on LS-DYNA solver. PIPER is able to generate and run the script and the following files have been obtained:

- *CURVE.k*

- *ele_beam.k*

- *main.k*

- *motion.k*

- *nodeset_PIPER.k*

- *noeuds_extr_beam.k*

With the addition of the files required for loading the THUMS in the *main.k* file, the simulation can be run. The positioning results can be seen in Figure 5.8 and 5.9.
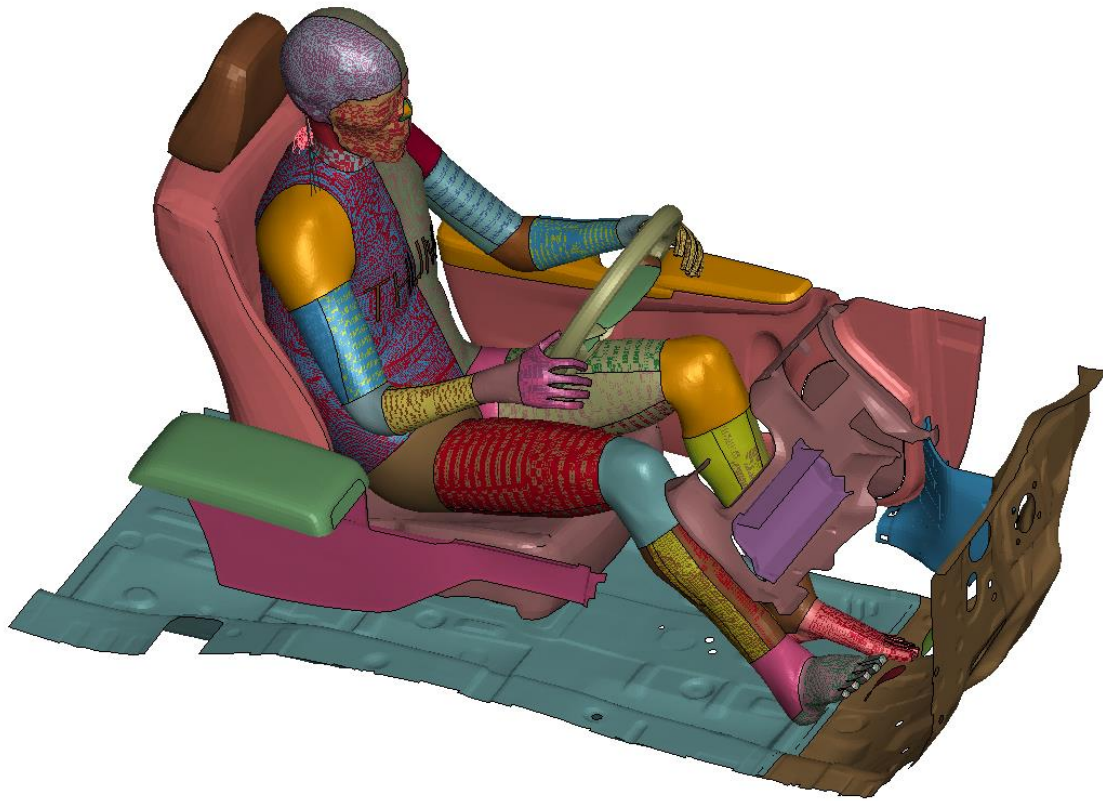
Figure 5.8: Final THUMS position in the vehicle environment
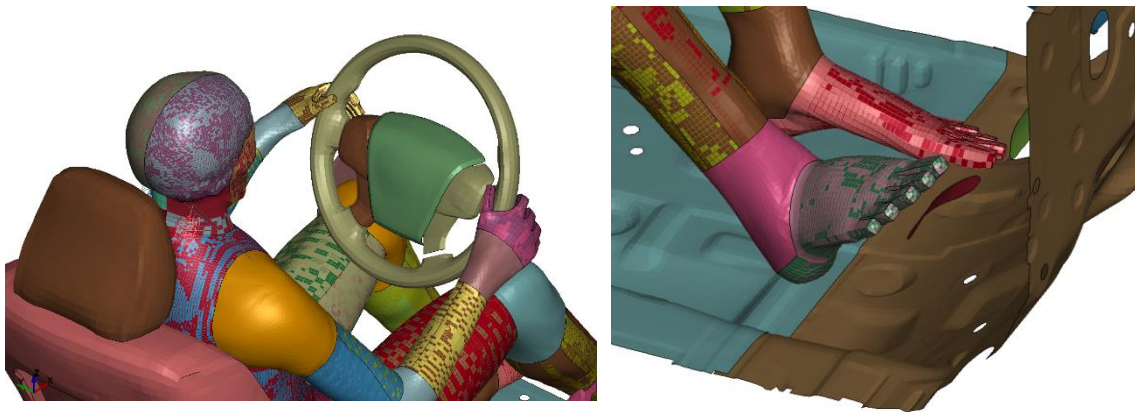
Figure 5.9: Positioning Details - Steering Wheel and Feet Position

Chapter 6:   Seatbelt

6.1 Introduction

A fundamental component of the active safety system of the vehicle is represented by the seatbelts. The role of the seatbelt system is to constrain the occupant to the seat avoiding dangerous movements and possible collisions with the interior environment of the vehicle.
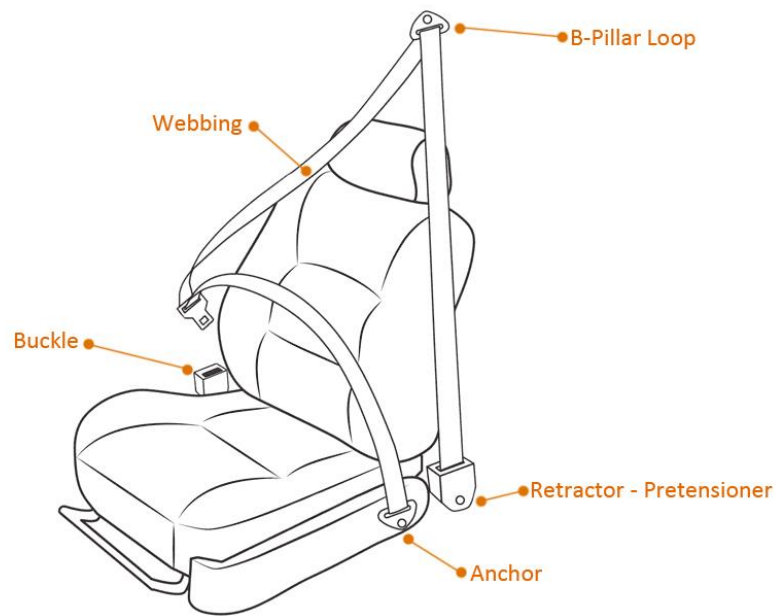

Figure 6.1: Seatbelt system components

The traditional components of the system, highlighted in Figure 6.1, are the following:

- *Webbing:* Constructed in a resistant synthetic fabric material, it provides the resistance to the inertia of the human body and distributes the load on a large area to reduce localized loads. The webbing has a length between 2500mm and 3400mm, a width of 47mm and a thickness of 1.2mm.
- *Buckle:* Positioned close to the hip of the occupant, represent the latch mechanism to which the sliding tongue is engaged.
- *Anchor:* Positioned in the lower part of the B-pillar, represents the end of the seatbelt.
- *Pillar loop:* Fixed to the B-pillar, is the upper anchor point of the seatbelt system.
- *Height adjuster:* This device can be installed in proximity of the pillar loop with the objective to regulate the height of the upper D-ring to better accommodate the driver's height.

- *Retractor:* Positioned in the lower part of the B-pillar, has the aim to ensure that the seatbelt does not cause discomfort to the occupants and needs to interrupt the spooling of the webbing when activated. Integral part of the retractor is the load limiter which helps to avoid injuries from the seatbelt.

- *Pretensioner:* Integral component to the retractor assembly, reduces the slack of the seatbelt before the impact with the secondary objective to reduce the effect of Out-Of-Position (OOP) sitting posture. It can be activated by a pyrotechnic charge.

The seatbelt assembly is explicitly required in the EuroNCAP far-side assessment protocol due to the significant effect that the engagement between the belt and the human body has in reducing the severity of the injuries on the occupants [11, 28].

6.2 System Description

The belt chosen for the simulation is a three-point seatbelt that can be divided in three belt sections:

- B-Pillar belt
- Shoulder and Torso belt
- Lab belt

Each of these sections is created independently so that it is possible to isolate the areas where a more detailed modelling is needed. Two different strategies have been followed during the modelling: the regions where no direct contact with the THUMS occurs have been modelled with 1D elements while 2D shell elements have been used to describe the seatbelt in the shoulder and lap sections.

The procedure to implement the seatbelt into the complete model is integrated inside LS-PrePost software and requires the following steps:

1. *Isolate the necessary FE models:*
   The required models as reference to model the seatbelts are the deformed driver's seat, the positioned THUMS model and the vehicle structure.

2. *Identify the anchors on the vehicle structure:*
   The three-point seatbelt model is defined in this way because it requires three attachment point on the structure. The retractor, positioned in the lower part of the B-Pillar represent, includes the beginning and end of the seatbelt loop, the D-Ring, positioned above and rearward of the occupant shoulder represent the second anchor,

and the buckle positioned to the left of the driver's hip represent the third and last point. In the vehicle model provided, these attachment points have been identified as nodes on the vehicle structure where the element belonging to the seatbelt would anchor. Their position is highlighted in Figure 6.2.

The components needed to properly describe the restraint seatbelt, such as the retractor and the buckle for example, are not included in the original model of the vehicle. For this reason, it has been chosen to attach the seatbelt system to specific points of the sled structure.
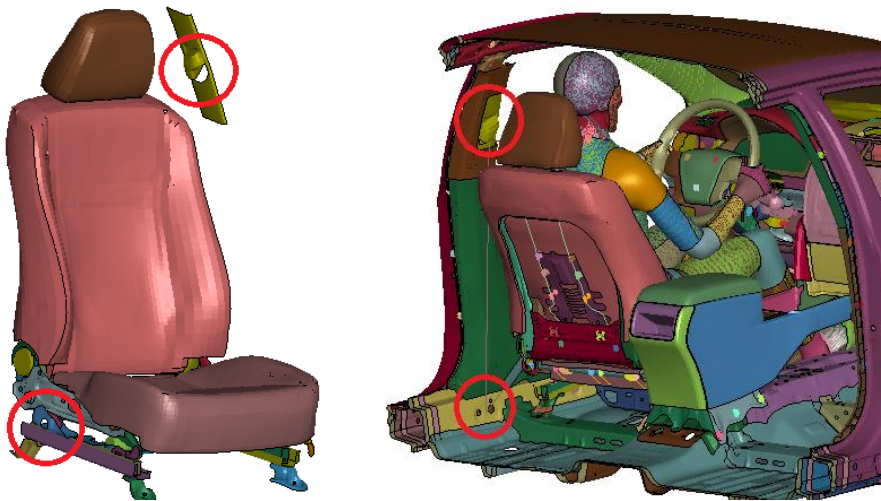

Figure 6.2: Anchors Location - Detail

3. *Create Thorax and Lap element sets:*

   For the software function to properly fit the seatbelt around the HBM, it is needed to define two different segment sets that would represent the surface elements of the thorax and lap respectively. This is done through the keyword *SET_SEGMENT.

4. *Perform the seatbelt fitting:*

   Using the *Seatbelt fitting* command provided by LS-PP, it is possible to specify the anchors point of the seatbelt defining each of the three seatbelt sections. During this
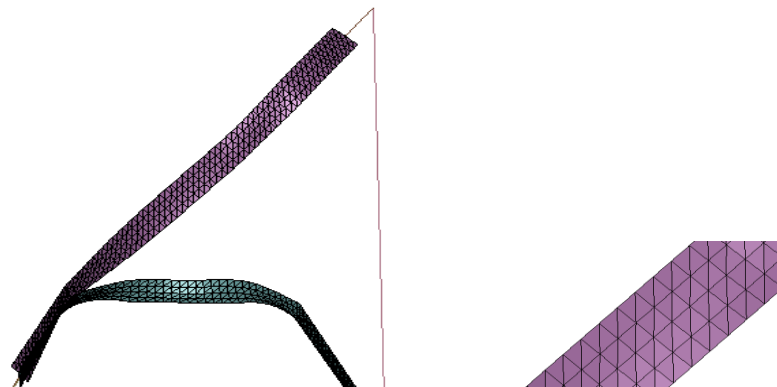

Figure 6.3: Seatbelt Model with Mesh detail

phase it is possible to select how to model the seatbelt by selecting the size and the type of elements to be used in the mesh. With reference to the segment sets created in the former passage, and by using the *Stretch* command, the seatbelt model will be generated, and it will fit the contour of the THUMS.

Figure 6.4: THUMS with Seatbelt

6.3   Seatbelt Parameters

To be completely functional and behave as the real counterpart would, a series of parameters need to be defined for refine the seatbelt model. In the following sections the passages required to define the seatbelt anchors and material are reported as well as the description of additional components such as the retractor and the pretensioner.

6.3.1   D-Rings and Buckle

The seatbelt models generated in the previous phases, define the three sections independently but, to reproduce the seatbelt loop, it is required that these segments behave as a single component. To this end, we need to define *ELEMENT_SEATBELT_SLIPRING in correspondence of the buckle and the upper D-ring. This keyword represents the seatbelt loop in these locations and in the LS-DYNA code, it allows for the elements in proximity of the anchor to pass through the loop and continue their movement. To be modelled the following input parameters are required:

- *SBID1:* This defines the first of the two seatbelt elements adjacent to the slipring. One of the two nodes that make up the beam element needs to also be one of the nodes of SBID2
- *SBID2:* This defines the second of the two seatbelt elements adjacent to the slipring. One of the two nodes that make up the beam element needs to also be one of the nodes of SBID1
- *SBRNID:* Defines a node belonging to the structure whose coordinates correspond exactly to the common node of SBID1 and SBID2
- *FC:* Is the coefficient that models the Coulomb friction of the slipring. Considering the relatively low friction between the seatbelt material and the D-ring, a coefficient of 0.15 has been chosen following the LSTC guidelines [19]

In this work, two location have been identified for positioning the slipring element: the buckle and the pillar loop and the chosen SBRNID nodes belongs to the original vehicle structure.

6.3.2   Webbing

The webbing of the seatbelt is modelled to replicate its real counterpart. It is made of a polyester fabric material with high resistance to cuts, scratches, and tensile stress. To reduce the computational cost of the simulation, the webbing model is composed by 1D and 2D elements according to the region of the seatbelt.

1D Beam elements have been used to describe the seatbelt regions in proximity of the sliprings and the B-Pillar belt. This part is characterized by *SECTION_SEATBELT and *MAT_SEATBELT keywords to describe its section and material properties. While the definition of the section in this case is trivial and does not require any additional parameter, the definition of the material requires more attention and the following inputs need to be provided:

- _MPUL – Mass per unit length:_ It defines the density of the material. In this work it has been set to 8e-5 kg/m
- _LLCID and ULCID:_ Define the loading and unloading curves measured in strain over force. They have been defined equal to each other with their trend is showed in Figure 6.5
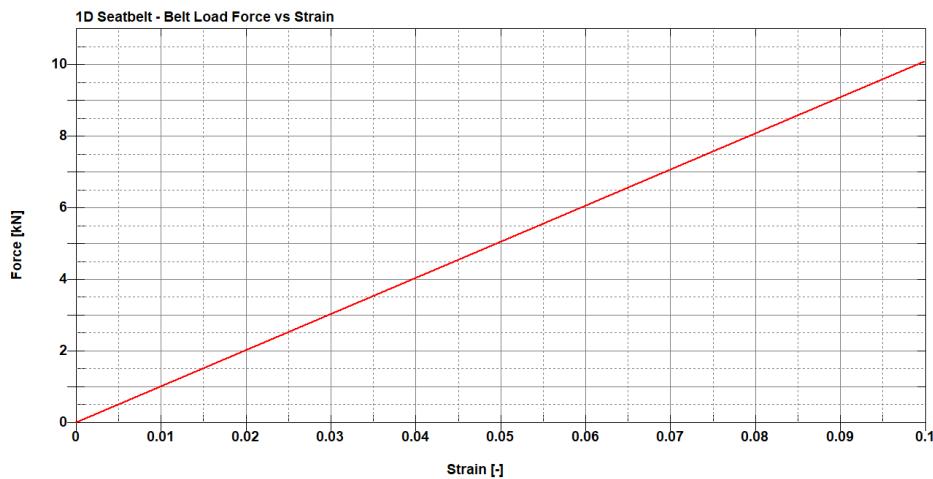
Figure 6.5: 1D Seatbelt - Belt Load Force vs Strain

- _LMIN:_ This parameter establishes the minimum length that each element in contact with a slipring or a retractor can assume. According to the guidelines provided by LSTC [19] it has been set to 3mm

The sections of the fabric belt have been modelled with 2D triangular shell elements and they are characterized by *SECTION_SHELL and *MAT_FABRIC keywords. In this case, due to the typical behaviour of the material used and the different response when subject to lateral and longitudinal loads, a more accurate description is needed. To this end, in the *SECTION_SHELL keyword, the possibility to include "fabric angles" is included allowing to align the main axis of each element. The definition of the fabric material, requires the following input parameters:

- _RO:_ Defines the mass density and it is equal to 1e-6 kg/mm^2
- _E:_ Defines the material Young modulus. It can be assigned separately for the longitudinal and lateral directions but in this case, it has been defined equal to 2 GPa for both

- *PR:* Defines the material Poisson Ratio. It can be assigned separately for the longitudinal and lateral directions but in this case, it has been defined equal to 0.3 for both
- *GAB:* Defines the shear modulus direction of the principal axis and it is equal to 0.769 [19]
- *LCA:* Defines the stress vs strain curve along the longitudinal fibre axis. Its trend is shown in Figure 6.6
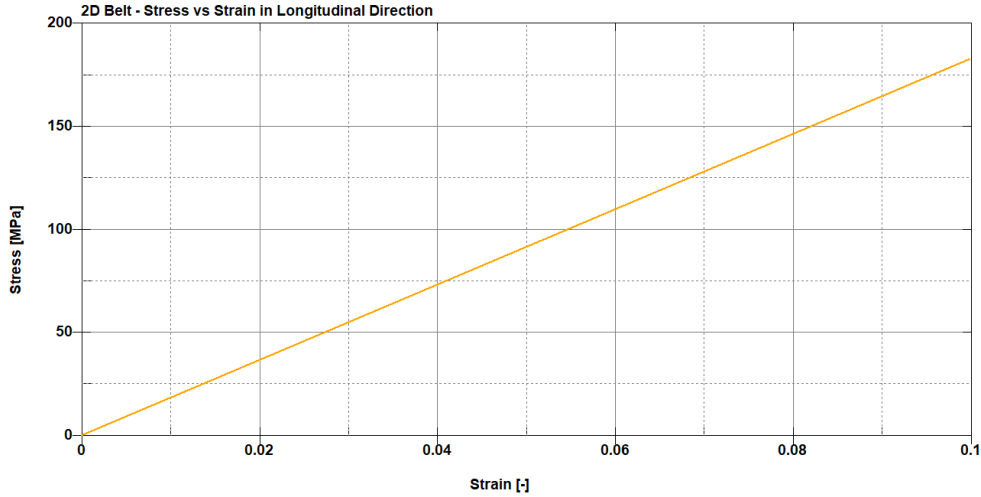

Figure 6.6: 2D Belt - Stress vs Strain in Longitudinal Direction

- *LCB:* Defines the stress vs strain curve along the transversal fibre axis. Its trend is shown in Figure 6.7
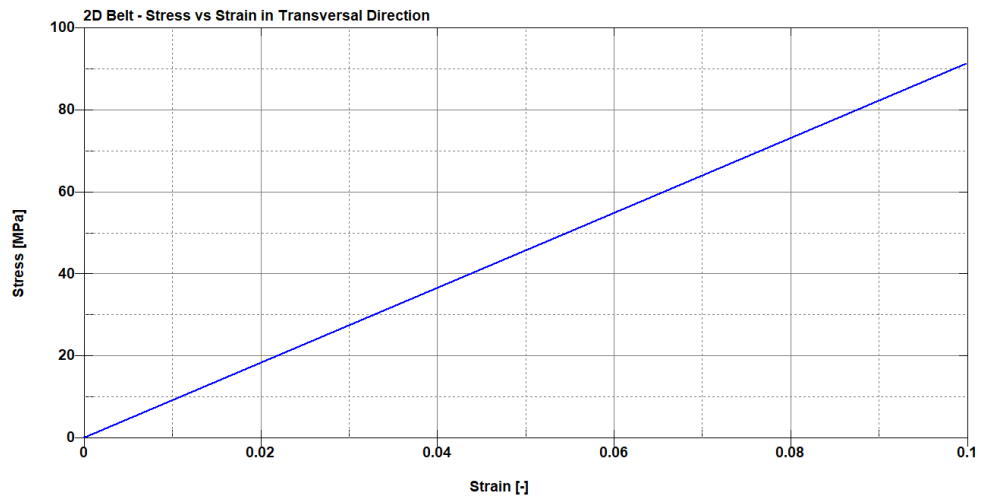
Figure 6.7: 2D Belt - Stress vs Strain in Transversal Direction

6.3.3 Retractor

During normal operation the retractor mechanism, to which the webbing is attached on one end, applies a counteracting torque with the help of a spring to the spooling of the seatbelt. This ensures that the belt is always in tension avoiding any possible slack. When the vehicle is involved in an

accident, a locking mechanism is triggered either by the deceleration of the car or the seatbelt movement. When the retractor is "locked-up", some amount of belt can still be spooled out according to a force-deflection curve. In LS-DYNA it is possible to properly reproduce this behaviour in the keyword *ELEMENT_SEATBELT_RETRACTOR and it requires the following inputs:

- *SBRNID:* Corresponds to the node ID of the retractor positioned on the vehicle structure. Its coordinates are required to be equal in coordinates to one of the two nodes of the seatbelt element SBID

- *SBID:* Identifies the seatbelt element ID positioned in correspondence of the retractor. One of its two node is required to be equal in coordinates to SBRNID

- *SID1:* Sensor ID which regulates the triggering mechanism

- *TDEL:* Defines the time delay between the sensor trigger and the retractor lockup. It has been set to 0ms

- *PULL:* Is the amount of belt that the retractor is able to spool out before locking. In this case it has been set to 10mm.

- *LLCID* and *ULCID:* These curves define the retractor pay out vs the force applied to it. It is equal for loading and unloading, its general trend can be seen in Figure 6.8
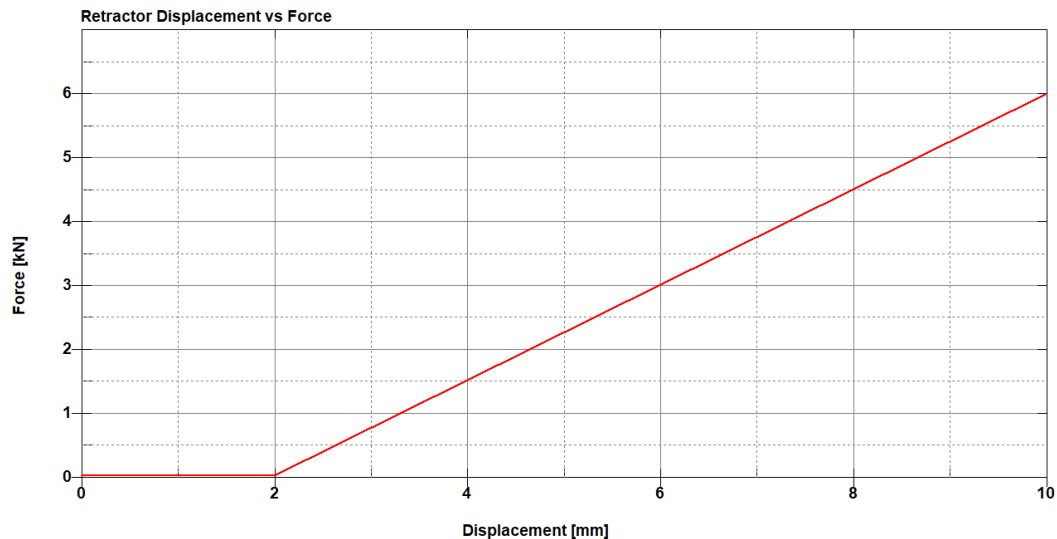
Figure 6.8: Retractor Displacement vs Force

- *LFED:* is a parameter used to determine when to pull-out an absorbed element. It is usually set to the average belt element, 10mm in this case [19]

The retractor lock-up is triggered by a user-defined sensor modelled with the keyword *ELEMENT_SEATBELT_SENSOR. Different strategies can be used as triggers, in this case it has been chosen a time delay of 1ms for the sensor to send the signal to the retractor to lock-up.

6.3.4 Pretensioner

The pretensioner, which is usually an integral component of the retractor housing has the role of tighten the belt in the event of a crash to move the occupant in a more optimal crash position. This device takes advantage of a pyrotechnic charge which is ignited as soon as a collision is detected winding up the belt around the retractor spool.

This behaviour is modelled in LS-DYNA with the keyword *ELEMENT_SEATBELT_PRETENSIONER as follows:

- *SBPRTY:* This parameter defines the type of pretensioner that is being modelled. In this work a pyrotechnic retractor is considered
- *SBSID:* Sensor ID which regulates the pretensioner trigger
- *SBRID:* Identifies the interested retractor ID
- *TIME:* Defines the time delay between the sensor trigger and the pretensioner activation. It has been set to 0ms
- *PTLCID:* Describes the belt pull in vs time curve. The extremely rapid response provided by the pyrotechnic charge is shown in Figure 6.9
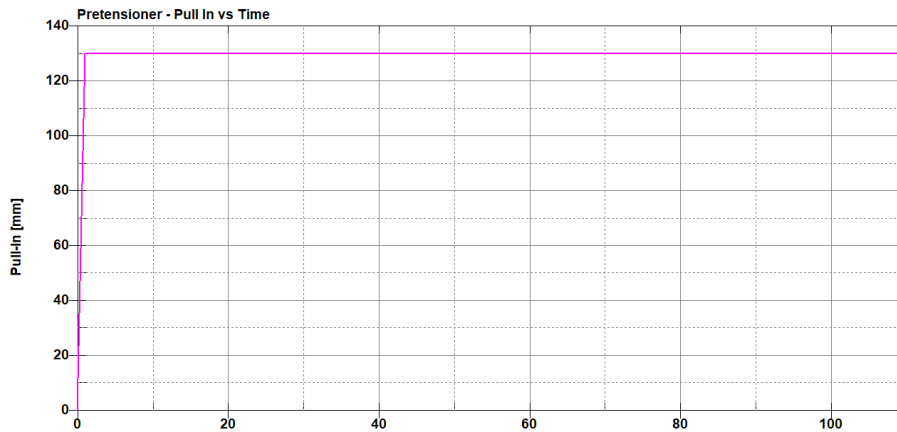
Figure 6.9: Pretensioner Pull In displacement vs Time

- *LMTFRC:* Defines the limiting force of the pretensioner. When the set limit is reached the control strategy will be determined by the retractor. In this work it has been set to 2.5kN

The pretensioner ignition is triggered by a user-defined sensor modelled with the keyword *ELEMENT_SEATBELT_SENSOR. This parameter represents the delay between the impact and the command to activate the pretensioner. It usually ranges between 10ms and 30 ms but specific values are not usually available to the public, for this reason it has been chosen a value of 13ms in accordance with the LSTC guidelines [19].

Chapter 7: Sled Simulation with THUMS

With all the necessary components modelled and the THUMS correctly positioned within the vehicle structure, the final simulation involving the sled model has been performed. The kinematic of the sled has been extracted from the oblique side impact test performed as reference for the validation tests and it has been assigned as a velocity pulse to the rigid sections of the simplified model previously described. The simulation time is equal to a period of 180ms.

The complete model used for this simulation is the combination of the following files:

- *BIW_with_rigid_sections.k:* File incorporating the structure of the sled
- *Left_seat_deformed.k:* Contains the driver seat pre-deformed following the THUMS contour
- *Right_seat.k:* Contains the passenger seat
- *Passenger_seat_spacers.k:* Contains the additional foams spacers
- *Smain.k:* File that allows to include all the components in a single simulation, general control and database keywords are defined here
- *Seatbelt.k:* Contains the seatbelt system consisting of the seatbelt, pretensioner, retractor and sliprings
- *THUMS.k:* Contains the complete THUMS model positioned on the deformed driver's seat
- *THUMS_sensors.k:* Includes in the model all the sensors required installed on the THUMS model
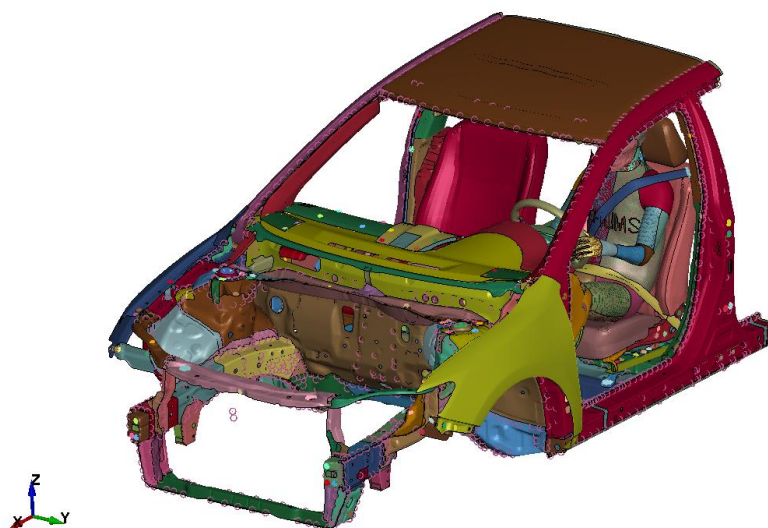
Figure 7.1: Sled Model with THUMS

7.1 Results

7.1.1 Visual Analysis

Analysing the visual output of the simulation it is possible to assess the general behaviour of the THUMS and compare it to other results available in the literature. In figure 7.2-7.11 snapshots of the simulations are taken every 20ms to provide a photographic reference to the following analysis.

The accident can be divided in different phases:

- *0 – 40 ms:* This represent the initial phase of the simulation. During this period the THUMS moves towards the passenger side unopposed in its movement due to its inertia and the distance between its body and the central console. In this phase the pretensioner is activated.
- *41 – 80 ms:* During this second phase, the THUMS comes in contact with the central console and the seatbelt system applies significant force on the occupant shoulder to limit its rotation.
- *81 – 120 ms:* In this period the whole right-side ribcage of the THUMS is in contact with the central console and the upper torso shows a strong lateral rotation. In this phase the seatbelt is strongly engaged with the left shoulder and biceps but, due to the occupant's movement the seatbelt is slipping towards the lower part of the arm reducing its restraint effectiveness.
- *121 – 180 ms:* In this phase the seatbelt is engaged with the left elbow pit before slipping away. The rotation of the upper body is not restrained and pivots around the central console structure. During this period the head and neck are dragged along with the torso rotation and the maximum lateral extension is reached.

Figure 7.2: Sled Model with THUMS - t = 0 ms

Figure 7.3: Sled Model with THUMS - t = 20 ms

Figure 7.4: Sled Model with THUMS - t = 40 ms

Figure 7.5: Sled Model with THUMS - t = 60 ms
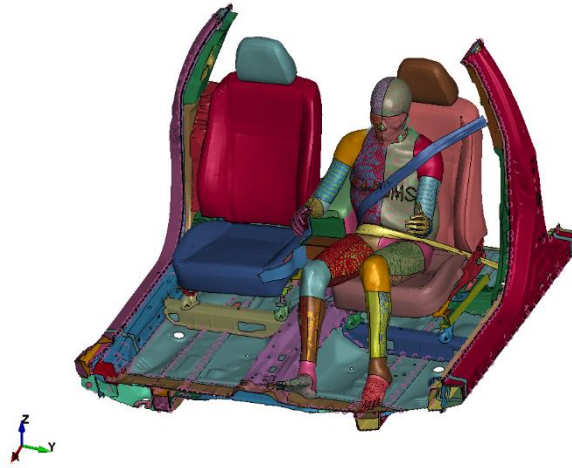
Figure 7.6: Sled Model with THUMS - t = 80 ms

Figure 7.7: Sled Model with THUMS - t =100 ms

Figure 7.8: Sled Model with THUMS - t = 120 ms

Figure 7.9: Sled Model with THUMS - t = 140 ms

Figure 7.10: Sled Model with THUMS - t = 160 ms

Figure 7.11: Sled Model with THUMS - t = 180 ms

7.1.2 Energy Balance

To evaluate the simulation validity, it is important to analyse the energy evolution in its principal components. As it was for the sled model without the THUMS model, the total energy nonlinear behaviour is the consequence of the external work required to assign the pulse to the structure. More significant is the development of hourglass and negative sliding energies. For what concerns the hourglass energies they are a result of the behaviour of the sled structure shown as a linear trend comparable to what shown in the validation test. Negative sliding energies on the other end can be the result of sliding nodes between contact surfaces. In our case this behaviour can be isolated to the contact between the seatbelt and the THUMS. The effect of the sliding energy is reflected in the behaviour of the energy ratio which, with optimal results, should be very close to the unity.
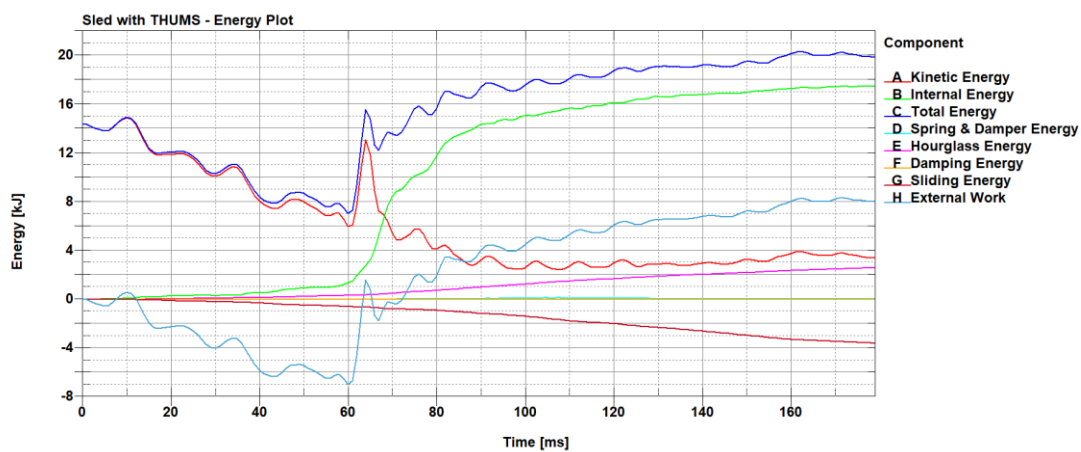
Figure 7.12: Sled with THUMS - Energy Plot
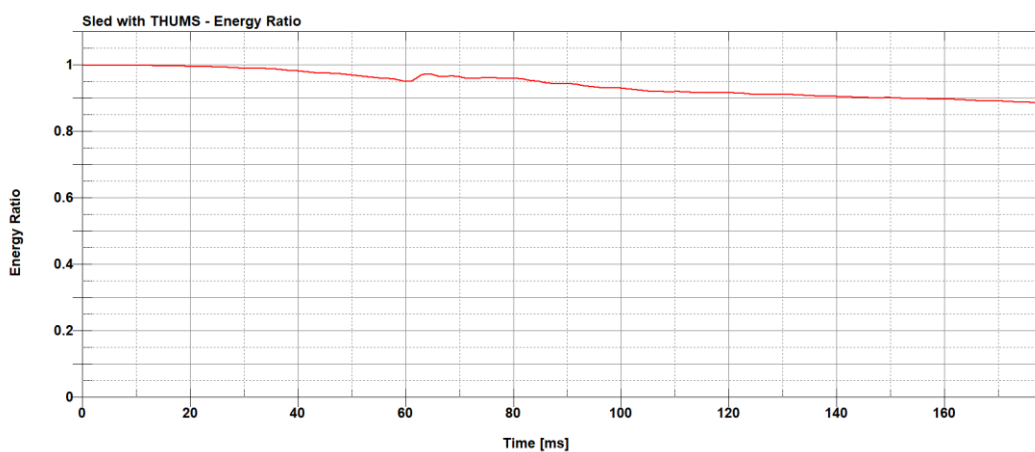
Figure 7.13: Sled with THUMS - Energy Ratio

7.1.3 THUMS Signals – Head

The accelerations and velocities to which it is subject the occupant's head, are significant to understand the overall severity of the crash. High decelerations would highlight a direct contact with the interior environment of the vehicle.

In Figure 7.14 it is possible to observe the acceleration of the head centre of gravity during the simulation. The three components of this motion provide a different point of view of the crash event: the most significant contributor to the combined resultant acceleration is the vertical motion of the head caused by the rotation of the THUMS body around the central console. The deceleration along X can be considered of secondary importance when compared to the other components of motion.
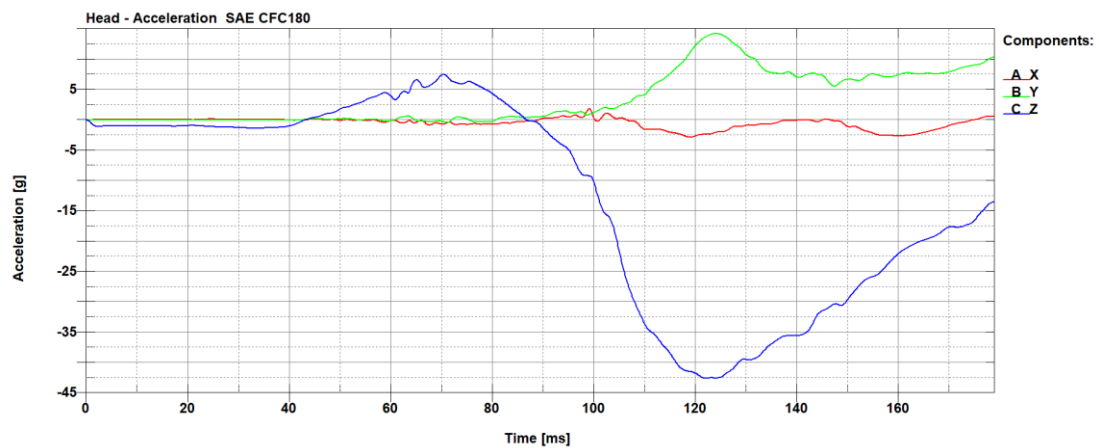
Figure 7.14: Head CG - Acceleration Plot
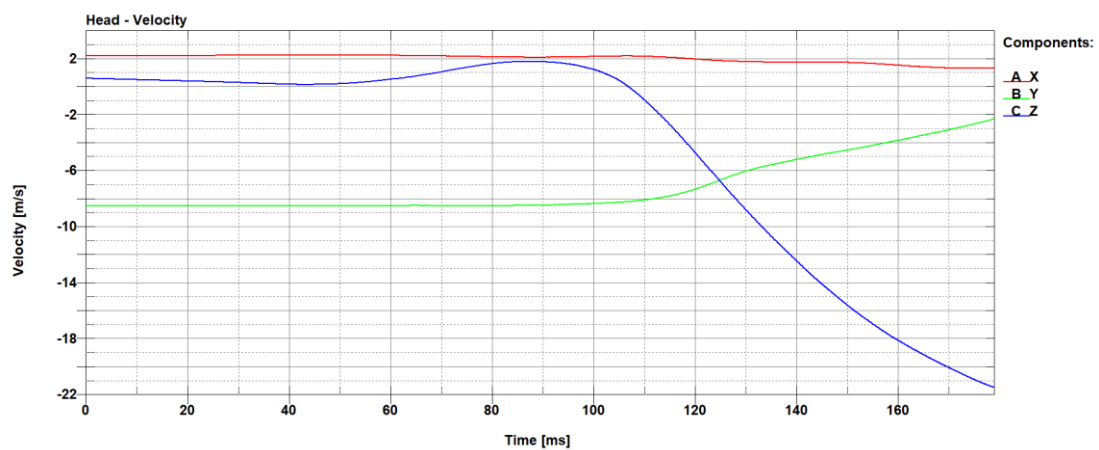
Figure 7.15: Head CG - Velocity Plot
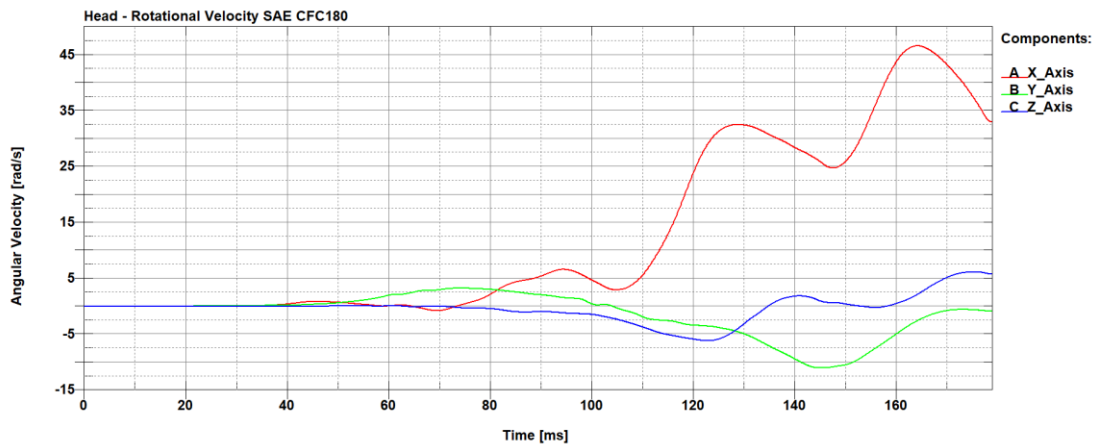
Figure 7.16: Head CG - Rotational Velocity Plot
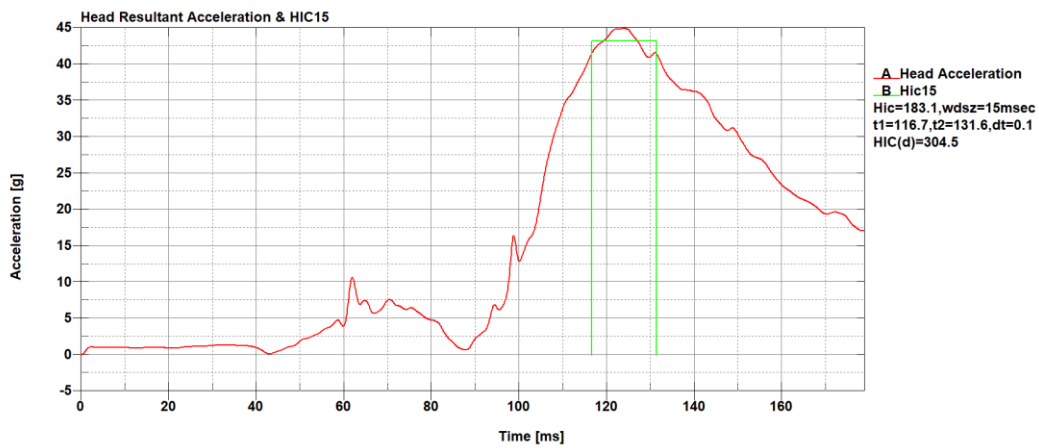
Figure 7.17: Head HIC15 – HIC=183.1 at t = 118÷131ms

The Head Injury Criterion (HIC) can be calculated from the resultant head acceleration to provide a measure of the injury level sustained by the occupant. This value is obtained by taking in consideration the cumulative effect of the resultant acceleration over an extended period of time. As suggested by the EuroNCAP protocol, the moving window used is equal to 15ms and the correspondent HIC15 parameter is therefore calculated. The results reported in Figure 8.18 show an HIC15 value of 183.1 between 116 and 131 ms. This value represents a reasonable result for this kind of event when the head does not come in contact with hard interior surfaces and it is within the performance limit of 500 set by the far-side assessment protocol.

7.1.4   THUMS Signals – Neck

The neck loading represent another crucial parameter during a far-side impact due to the large lateral rotation on the body. The upper and lower portions of the neck are being considered as suggested by the EuroNCAP far side protocol. In Figure 7.18-7.23 it is possible to observe the neck vertical tension, lateral bending moment and forward bending moment for these sections.
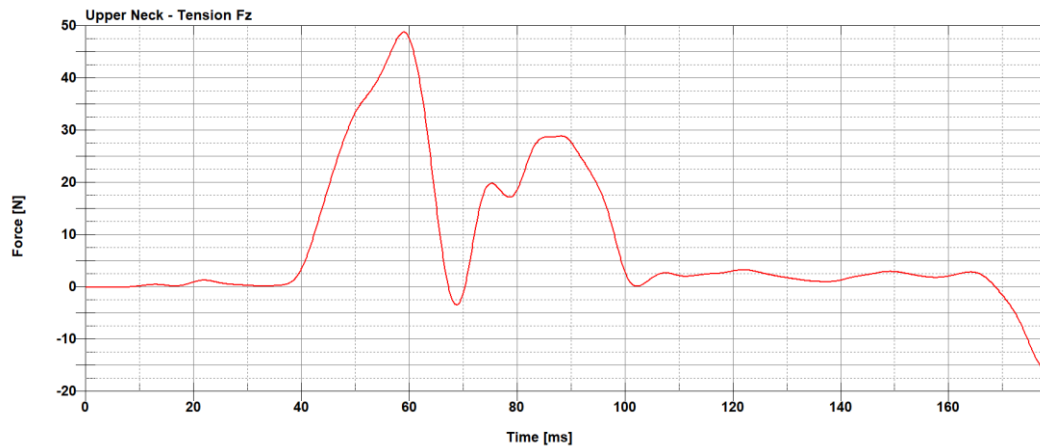
Figure 7.18: Upper Neck - Tension Fz
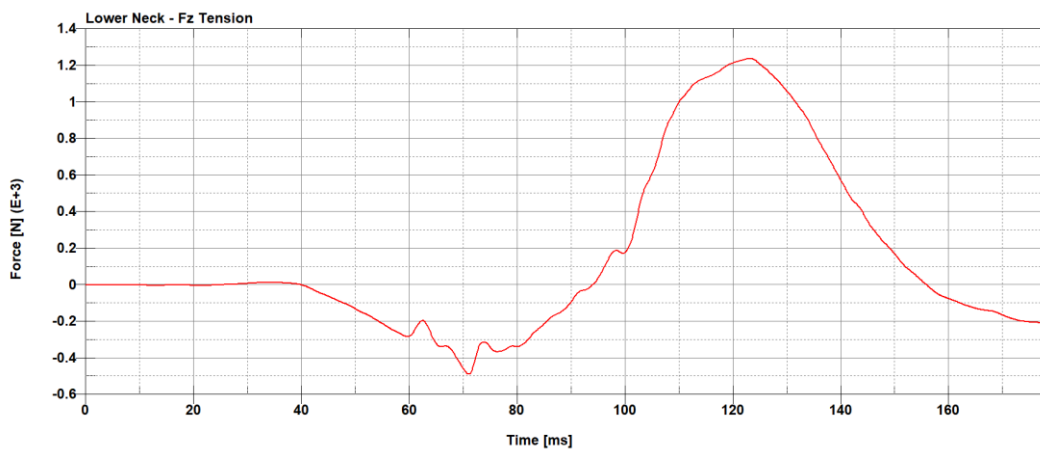
Figure 7.19: Lower Neck - Tension Fz
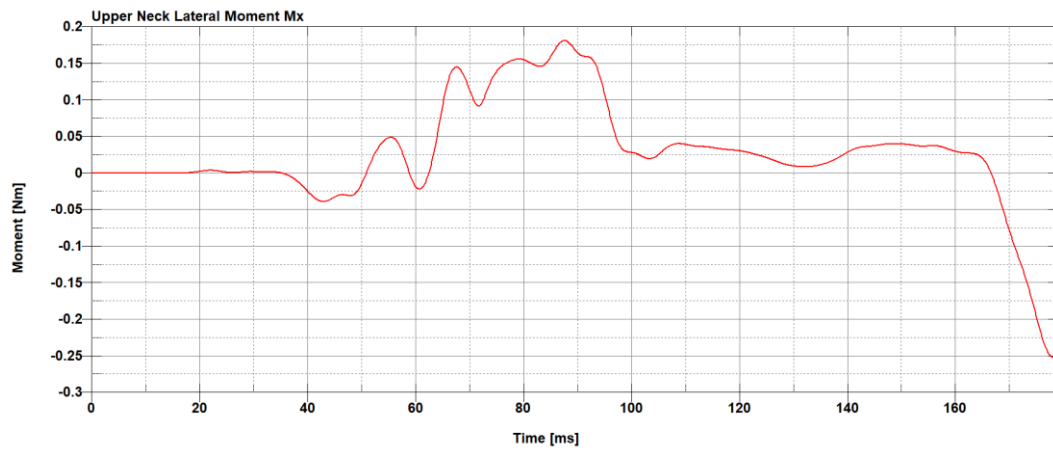
Figure 7.20: Upper Neck - Lateral Moment Mx
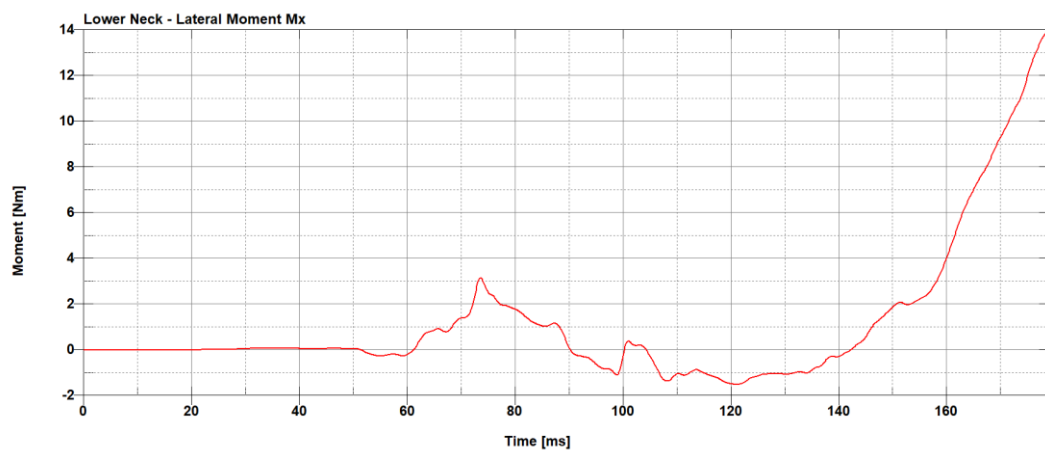
Figure 7.21: Lower Neck - Lateral Moment Mx
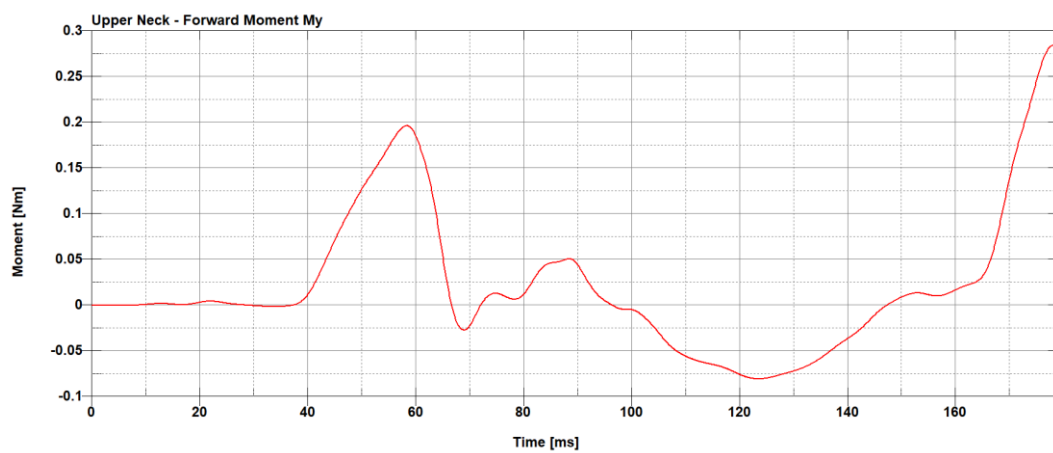
Figure 7.22: Upper Neck - Forward Moment My
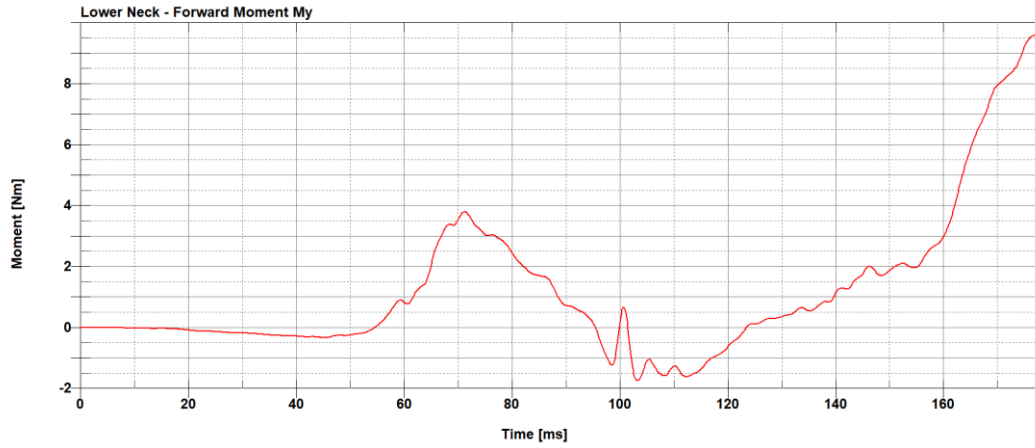
Figure 7.23: Lower Neck - Forward Moment My

Observing these plots, it is immediately clear that the lower portion of the neck is subject to much more severe loading than the upper section. The maximum vertical tension reaches 1.24 kN, the lateral bending moment 13.9 Nm and the forward bending moment 9.67 Nm. These values are significant but within the limits imposed by the EuroNCAP protocol respectively of 3.4 kN, 248 Nm and 50 Nm. The limited loading on the upper neck is corroborated by the visual behaviour of the THUMS but further investigation shall be conducted to better understand the differences between the HBM used and the WorldSID dummy used in the real practice.

From these results it is possible to also evaluate the Neck Injury Criterion (NIC) obtained as follows:

$$NIC = \frac{Fz}{Fzc} + \frac{My}{Myc};$$

Where Fz and My represent the maximum tension and moment experienced by the neck while Fzc and Myc represent reference value considered to be critical for neck injuries. In this evaluation values for a mid-size male are used and are respectively equal to 4500N and 310Nm.

$$NIC = \frac{1240N}{4500N} + \frac{9.67Nm}{310Nm} = 0.307 < 1$$

Substituting the results obtained in the simulation, a value of 0.307 for the NIC is obtained, considerably below the unit threshold.

7.1.5 THUMS Signals – Chest and Abdomen

Discrete elements positioned across the ribcage of the THUMS model are used to evaluate the lateral deformation of the occupant during a far side accident. The EuroNCAP protocol provides performance limits for the chest and abdomen portion of the upper body. Optimal results are deformations equal or below 28mm for the thorax and 47mm for the abdomen while the maximum values acceptable are respectively 50mm and 65mm. The attachment points of the discrete elements are provided in Section §4.1.3. In Figure 7.24-7.27 the time evolution of the lateral displacement of the upper body are reported.
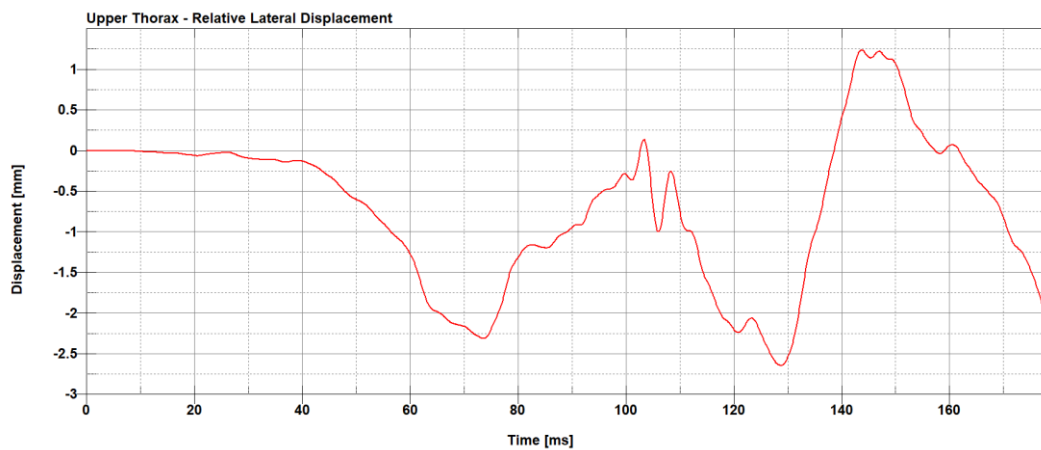
Figure 7.24: Upper Thorax - Relative Lateral Displacement
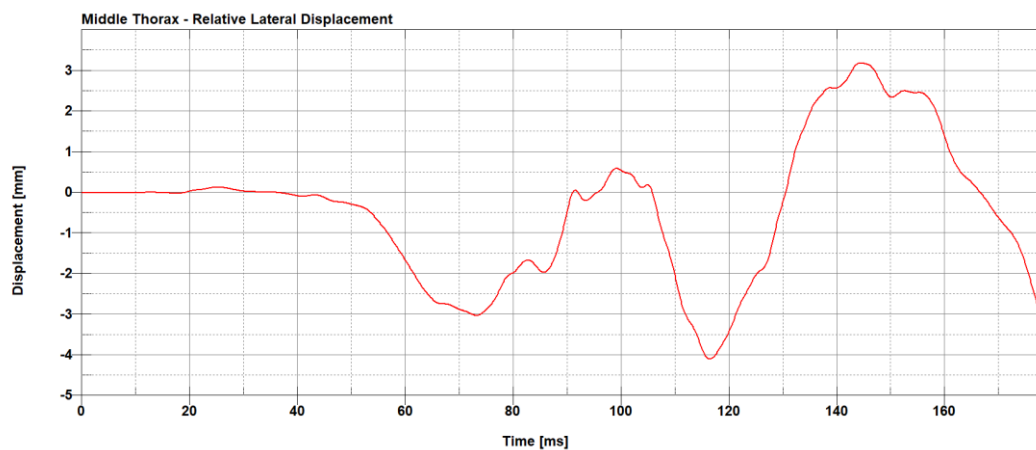
Figure 7.25: Middle Thorax - Relative Lateral Displacement
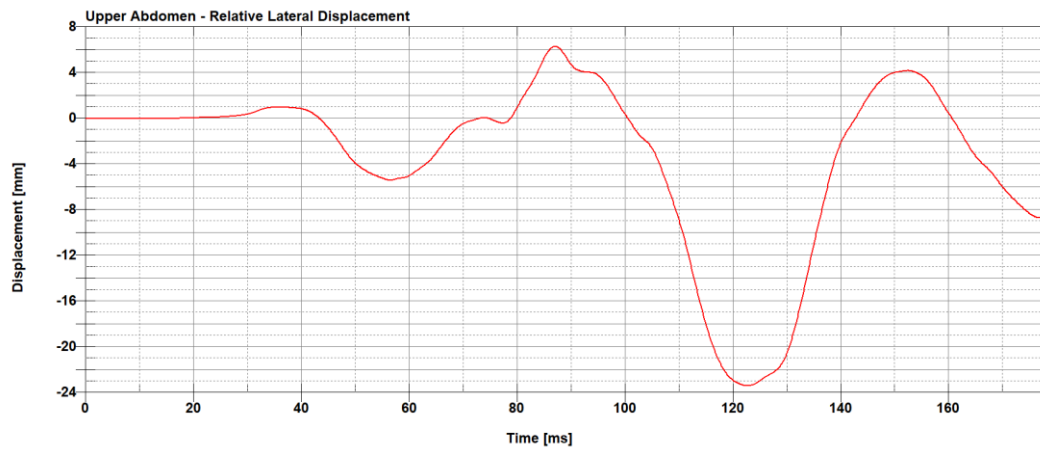
Figure 7.26: Upper Abdomen - Relative Lateral Displacement
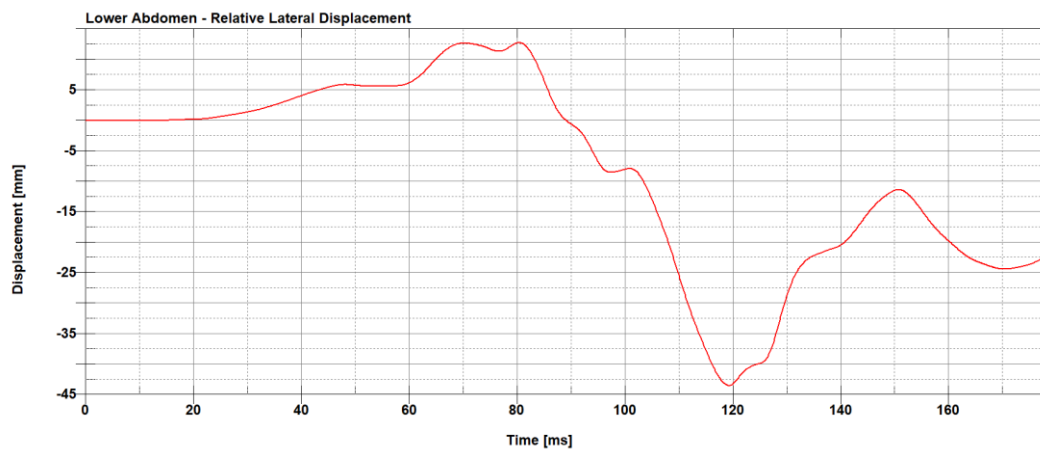
Figure 7.27:Lower Abdomen - Relative Lateral Displacement

From the results above, it is possible to observe the different behaviour experienced by the chest and abdomen regions with the former, showing limited deformations when compared to the lower part of the torso. This is motivated by the higher stiffness of the upper area due to the ribcage but also by the significant action of the seatbelt on the right side of the abdomen. Additional discrete elements have been placed between the clavicles and the rotator cuffs, their results are not directly a measure of the chest lateral deformation but rather a measure of the relative position of the shoulders. Their result is reported in Appendix B.

The maximum compression of the chest is equal to 4.08mm while the maximum compression of the abdomen is equal to 43.40mm. Both results are within the EuroNCAP higher performance limits.

7.1.6   THUMS Signals – Internal Organs Volume & Surface Area

The THUMS capabilities allow for thorough investigations of the behaviour of the internal organs of the human body and what happens to them during an accident. The organs considered are the lungs, the heart, the pancreas, the spleen, the liver, the stomach, the intestine and two larger regions such as the ribcage and the whole abdomen. Despite the volume time evolution of these organs is not subject to direct analysis in this work, the results obtained are reported in Appendix A for possible future studies on the matter.

RIBCAGE
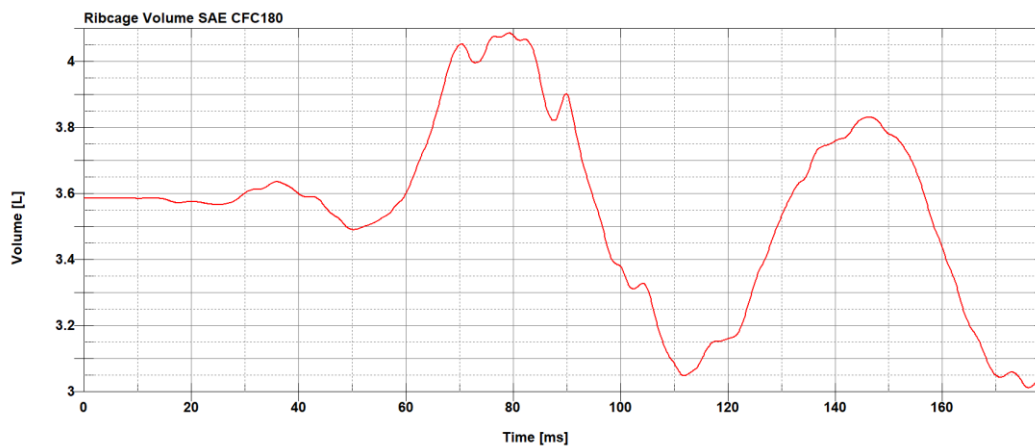
Figure 7.28: Ribcage - Volume
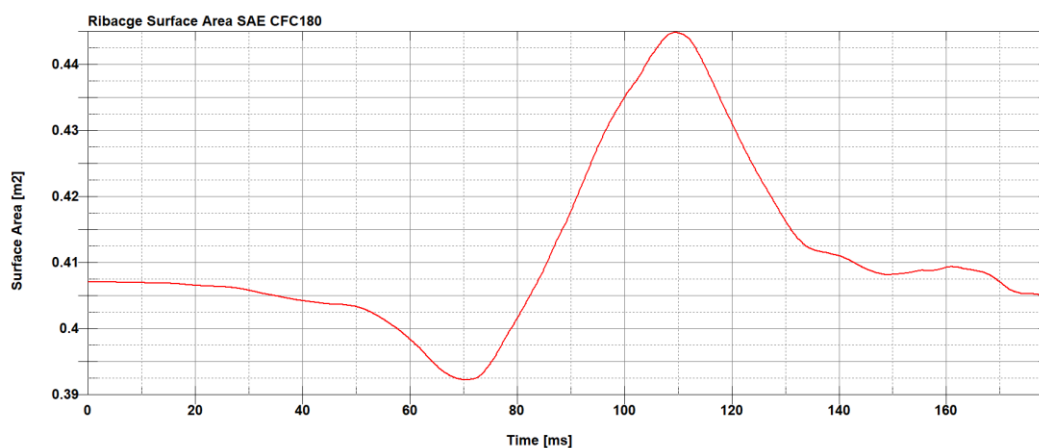
Figure 7.29: Ribcage - Surface Area

7.1.7 THUMS Signals – Spine Deformation

The placement of *DATABASE_NODOUT keywords on THUMS spine at each vertebra, allows to visualize the movement and deformation of the spine during the simulation. In the Figure 7.30 and 7.31 the vertebrae positions projected on the YZ plane and XZ plane are reported at 5 different instants of the accident: 0 ms, 45 ms, 90 ms, 135 ms, 180ms.

The results obtained show the potential of this methodology in highlighting possible criticalities and more in-depth analysis of the spine deformation during crash events.
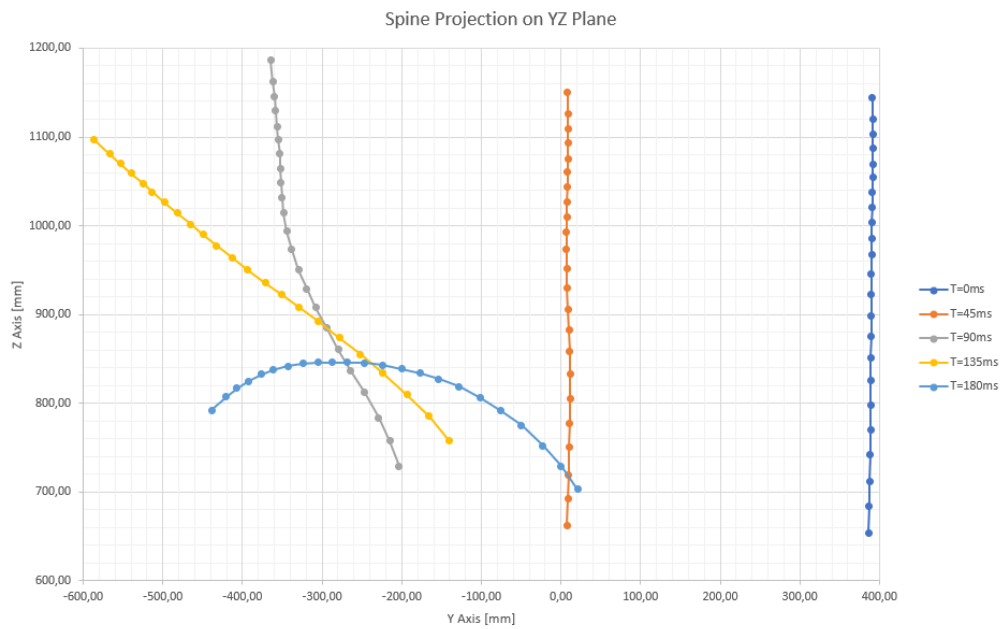
Figure 7.30: Spine Projection on YZ Plane
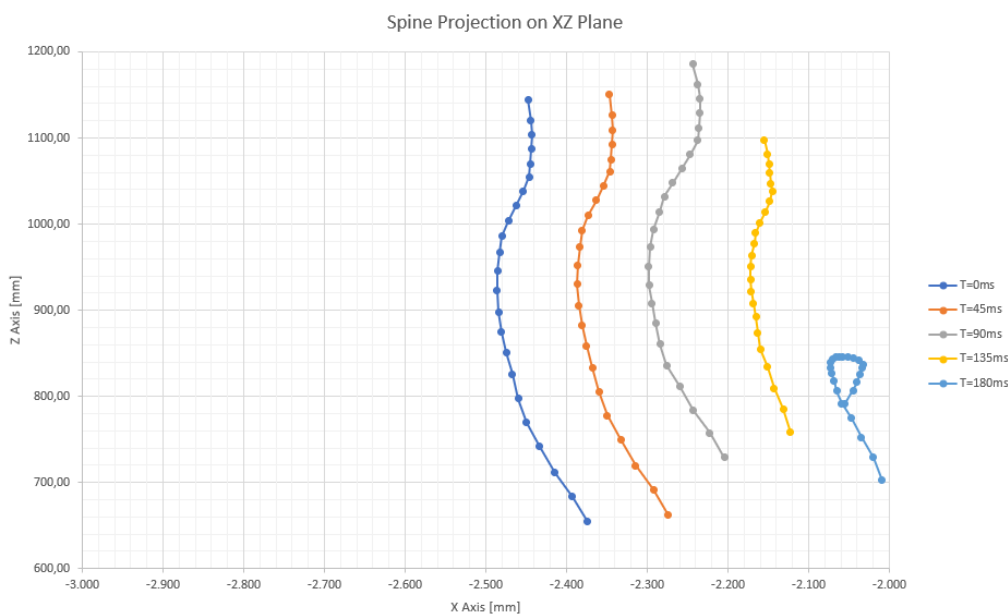
Figure 7.31: Spine Projection on XZ Plane

7.1.8 THUMS Signals - Load Limits

The EuroNCAP far-side assessment protocol includes some score modifiers that take in account the loading of the pelvis area. This has been evaluated in this model by measuring the load transmitted between the left and right ilium at the symphysis and the lumbar spine load experienced by the vertebrae L5. The results obtained are reported below in Figures 7.32 – 7.35.
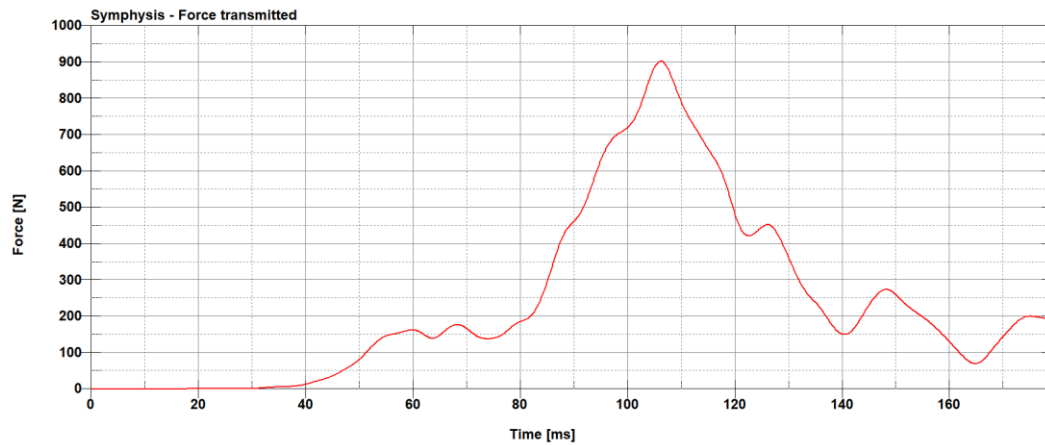
Figure 7.32: Symphysis - Force Transmitted
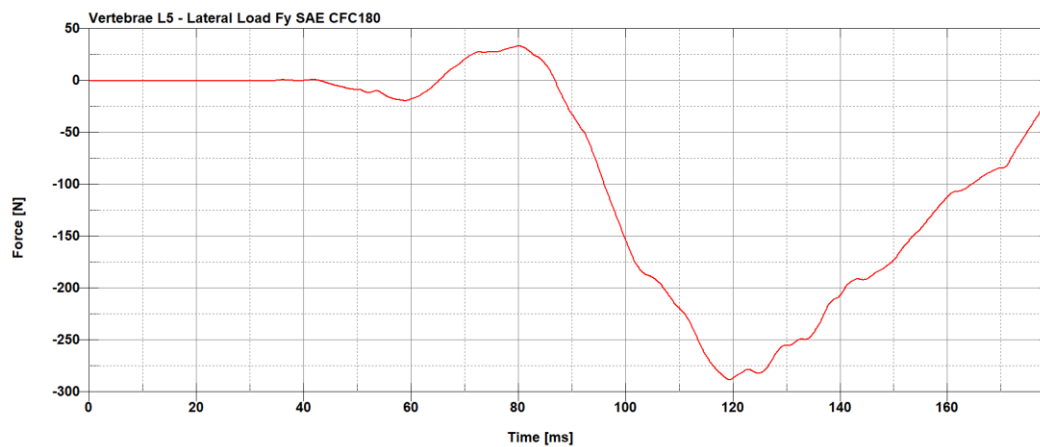
Figure 7.33: Lumbar L5 - Lateral Load
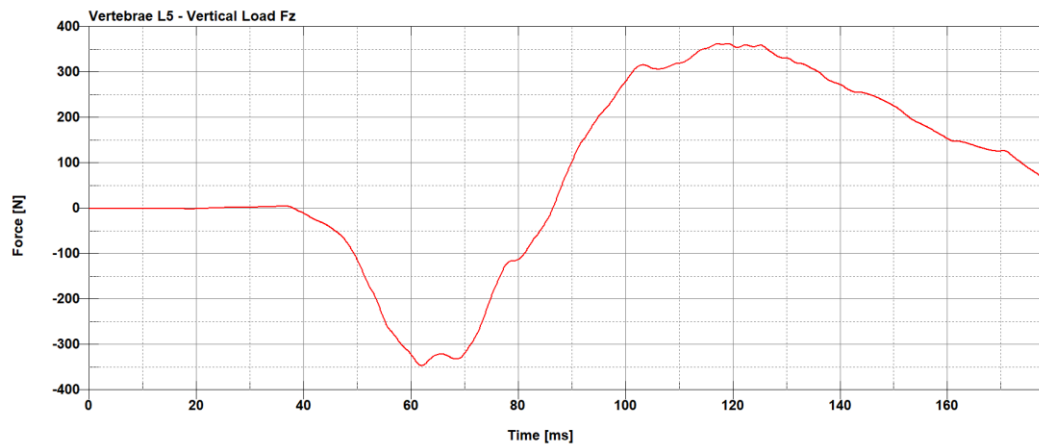
Figure 7.34: Lumbar L5 - Vertical Load
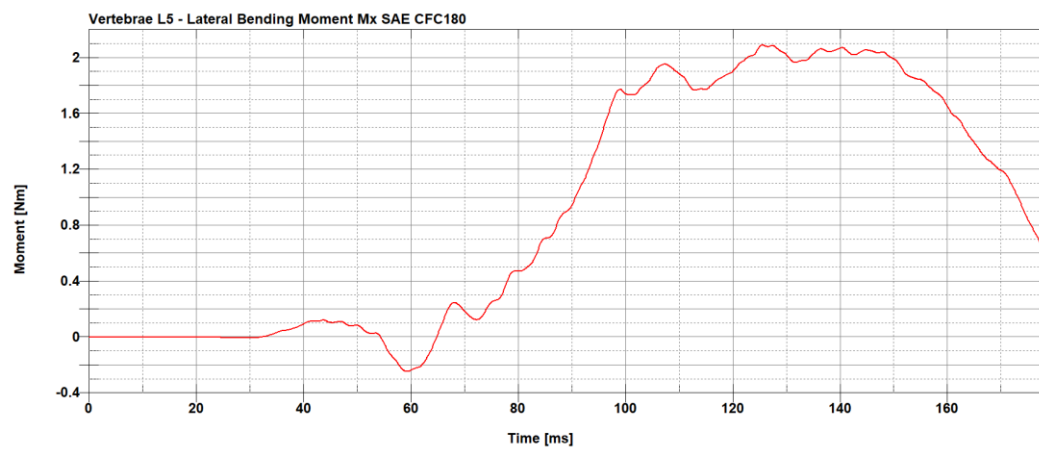
Figure 7.35: Lumbar L5 - Lateral Bending Moment

From the results above, the maximum force transmitted by the symphysis is equal to approximately 900 N which is within the threshold of 2.8kN.

The loading on the lumbar vertebrae L5 shows a lateral force with a maximum of 288N and a vertical tension with a maximum of 363 N and a vertical compression with a maximum of 346N. These values are significantly below their respective thresholds of 2.0 kN and 3.5 kN.

7.2 EuroNCAP Evaluation

The first step towards obtaining a complete EuroNCAP far-side assessment score is to evaluate the maximum head excursion during the accident. To this end the visual output of the simulation is reviewed and a score is assigned to each body portion: head, neck, and chest according to the zone reached during the THUMS movement. A maximum score of 12 points can be achieved with all body parts being within the green zone (Reference to Figure 3.3).

Observing Figure 7.36, the head reaches the red zone, the neck the yellow zone and the chest the green zone therefore, the obtained score is equal respectively to 0, 2 and 4 for a total of 6 points.
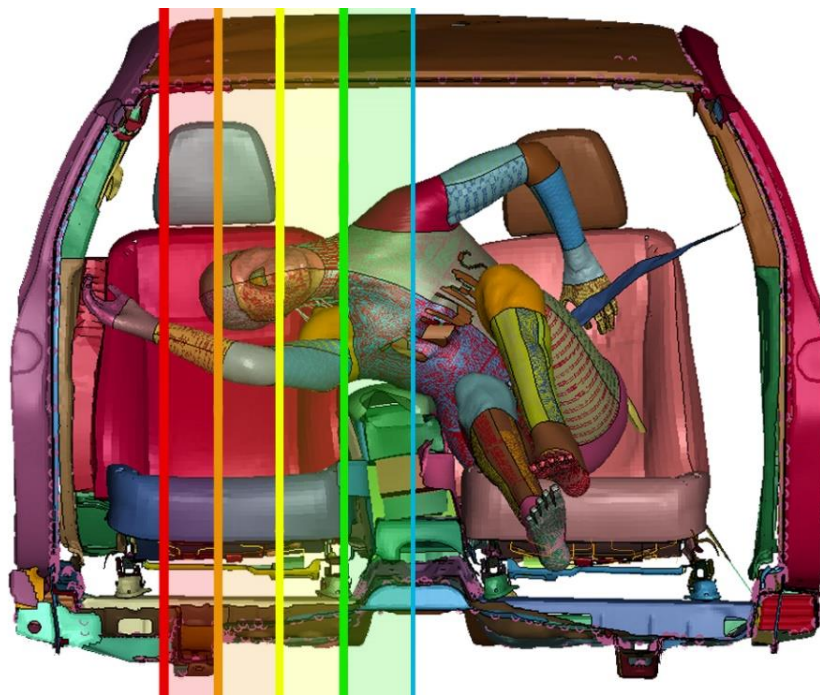
Figure 7.36: THUMS Head Excursion Assessment

The next step is, for each part, scale the obtained score according to the criteria obtained from the sensors positioned on the THUMS. In case of multiple parameters for the same body parts, the worst-case scenario is being considered.

Analysing the results analysed in the previous chapter it is possible to compare them to the performance limits imposed by the protocol. In this case, the maximum values obtained for each of the three body segments is well within the maximum score threshold therefore the full 6 points are not scaled down. The breakdown of the points can be seen in Table 3.

Dummy Criteria		Performance Limits		THUMS Score	Points
	Criteria	High	Low		
Head	HIC15	500	700	183.1	0/0
	3ms Acceleration	72g	80g	45g	
Upper Neck	Tension Fz		3.74 kN	48 N	2/2
	Lateral Moment Mx	162 Nm	248 Nm	0.15 Nm	
	Forward Moment My		50 Nm	0.25 Nm	
Lower Neck	Tension Fz		3.74 kN	1240 N	
	Lateral Moment Mx	162 Nm	248 Nm	14 Nm	
	Forward Moment My		100 Nm	9.5 Nm	
Chest & Abdomen	Chest lateral compression	28 mm	50 mm	4.08 mm	4/4
	Abdomen lateral compression	47mm	65 mm	43.4 mm	
Total					6/6

Table 3: Dummy Criteria applied to THUMS

Finally, some modifiers are required to take in consideration the loading on the lumbar region. Some thresholds are therefore imposed on the load transmitted by the symphysis and the loading of the lumbar, here represented by the load cell positioned on the vertebrae L5. Exceeding any of these limits, would reduce the final score by 4 points but, as it is possible to see from Table 4, none of these parameters is beyond the imposed threshold. The final score from the far-side assessment score applied to this simulation involving a THUMS model is equal to 6 points.

Pelvis & Lumbar Criteria			THUMS Score
Criteria	Performance Limits	Modifier	
Pubic Symphysis	2.8 kN		900 N
Lumbar Fy	2.0 kN	-4 points	288 N
Lumbar Fz	3.5 kN		363 N
Lumbar Mx	120 Nm		2 Nm

Table 4: Pelvis & Lumbar Criteria applied to THUMS

7.3 Passenger Seat Spacer

To monitor the force transmitted by the passenger seat foam spacers, load sensors have been positioned on the added components.

In Figure 7.37, the load evolution through the two spacers is shown. The component positioned between the B-pillar and the passenger seat experience the highest load reaching 4kN while the central console spacers is subject to a maximum of 1.5kN. These results combined with the visual output, show the effectiveness of the spacers in closing the air gaps between the three components but it is difficult to evaluate the actual loading that would properly reproduce the vehicle structure deformation during the full-scale crash test.
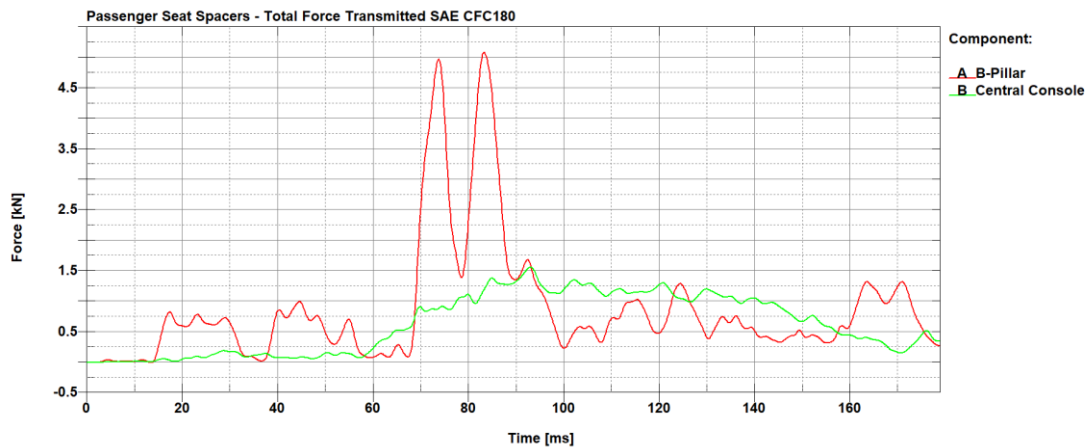
Figure 7.37: Passenger Seat Spacers - Force Transmitted

Chapter 8:   Conclusions

In this thesis, a Human Body Model has been used to evaluate the far-side protection provided to a mid-size vehicle occupant according to the EuroNCAP assessment protocol. The work begun by analysing the 2012 Toyota Camry FE model provided by CCSA and by extracting from it a simplified sled consisting of the vehicle's Body-In-White, front seats, central console and dashboard. After dividing the model in its main subsystems, some parts were required for stiffening the structure's cut edges while others were necessary to assign a prescribed movement to the sled. Following the EuroNCAP protocol procedures, the input pulse has been obtained by performing a representative oblique side impact against a rigid pole at 32km/h.

To evaluate that the modifications to the original model would not significantly alter the behaviour of the sled, two different validation tests have been performed:

- The first one has been performed considering the original model with and without the addition of rigid sections
- The second one has been performed between the original and sled model

The first comparison produced the expected results and showed that the insertion of rigid sections in specific regions, did not significantly alter the behaviour of the vehicle during the impact. Some discrepancies were detected in the acceleration readings but were not significant enough to influence the sled motion.

The second comparison, on the other hand, highlighted some discrepancies between the behaviour of the two models. The sled model showed some elastic phenomena and vibration of the structure and it was reflected in the sensors reading. The velocity output resulted in a high number of oscillations with low amplitude. The reasons for this different behaviour can be identified in two factors: the reduced mass of the sled and the behaviour of the vehicle structure when subjected to localized lateral loads. Despite these discrepancies, by evaluating the correlation factor between the two signals, a moderate to strong correlation has been identified.

Once the sled model has been validated, the THUMS model required some attention to be properly inserted inside the vehicle. Through the use of the PIPER software, the human body has been positioned in a standard driving position on the driver's seat, a seatbelt restraining system has been modelled and fitted to secure the HBM to the seat during the crash event and a sensor array has been defined on the body to monitor its behaviour. Accelerometers and load sensors have been positioned in critical areas such as the head, neck, thorax and pelvis while additional

sensors have been used to monitor the volume of internal organs and the deformation of the spine in order to take full advantage of the expanded possibilities made available by the high level of detail provided by the THUMS,.

The model obtained reproduce with good accuracy the internal environment of the vehicle and its interaction with the occupant during a far-side impact. The THUMS movement show a realistic behaviour consistent with the actual practice but experiencing a large lateral displacement. Using the EuroNCAP assessment protocol as reference the results are within the upper performance limits. It is also important to notice that some improvements could be implemented. The first step could be to evaluate different methods to assign the kinematics to the model to avoid instabilities and structure oscillations. The second step would be to tune the seatbelt parameters in order to increase the retention provided thus limiting the rotation and displacement of the occupant.

The results obtained are useful to identify the different stages of the crash and the critical factors affecting the HBM as well as providing an early safety assessment of the vehicle. Furthermore, the reduced computational load and the significantly faster running time required by the simplified model are useful aspects that can facilitate the assessment of the model in different scenarios. This can be crucial in the automotive industry towards steering the car development and taking pre-emptive action for increasing the safety level provided to the occupants.

Chapter 9:   BIBLIOGRAPHY

[1] L. Adena, F. Caimmi, L. Leonardi, M. Nacucchi, et al., (2019), *"Compression of polystyrene and polypropylene foams for energy absorption applications: A combined mechanical and microstructural study"*, Journal of Cellular Plastics, Vol. 55, No. 1, pp 49-72

[2] M.W.J. Arun, S. Umale, J. R. Humm, N. Yoganandan, et al., (2016), *"Evaluation of kinematics and injuries to restrained occupants in far-side crashes using full scale vehicle and human body models"*, Traffic Injury Prevention Vol. 17, No. 61, pp 116-123

[3] N. Baker, S. Henry, T. Laituri, (2018) *"A Side Impact Taxonomy for USA Field Data"*, SAE Technical Paper 2018-01-1331

[4] R. Bouix, P. Viot, J. L. Lataillade, (2009), *"Polypropylene foam behaviour under dynamic loadings: Strain rate, density and microstructure effects"*, International Journal of Impact Engineering, Vol. 36, pp 329-342

[5] CCSA, (2016), *"Development & Validation of a Finite Element Model for the 2012 Toyota Camry Passenger Sedan"*, doi:10.13021/G8N88

[6] CCSA, *"2012 Toyota Camry Detailed Model V5 – Validation"*, doi:10.13021/G8TS3

[7] S. Civin, *"Material Characterization and Finite Element simulation of Ice Hockey Helmets under rotational impact conditions"*, Master's Degree thesis in Product Innovation Engineering, Università degli Studi di Padova, a.a. 2017/2018

[8] B. Croop, H. Lobo, (2009), *"Selecting Material Models for the Simulation of Foams in LS-DYNA"*, 7th European Ls-DYNA Conference

[9] J. Ellway, K. Hallbauer, T. Kerz, (2019), *"The development of a EuroNCAP far side occupant test and assessment procedure"*, Paper Number 19-0278

[10] EuroNCAP (2020), *"Far Side Occupant Test & Assessment Protocol"*, Version 2.0.1

[11] EuroNCAP (2015), *"Oblique Pole Side Impact Testing Protocol"*, Version 7.0.2

[12] A. Filatov, J.M. Scanlon, A. Bruno, S.S.K. Danthurthi, et al., (2019), *"Effects of Innovation in Automated Vehicles on Occupant Compartment Designs, Evaluation, and Safety: A Review of Public Marketing, Literature, and Standards,"* SAE Technical Paper 2019-01-1223

[13] J.L. Forman, F. Lopez-Valdes, D.J. Lessley, P. Riley, et al., (2013), *"Occupant Kinematics and Shoulder Belt Retention in Far-Side Lateral and Oblique Collisions: A Parametric Study"*, Stapp Car Crash Journal, Vol. 57, pp 343-385

[14] C. Furbish, J. Welcher, J. Brink, et al., (2019), *"Occupant Kinematics and Loading in Low Speed Lateral Impacts"*, SAE Int. J. Advances & Curr. Prac. In Mobility 1(4):1470-1490

[15] H.C. Gabler, K. Digges, B.N. Flldes, L. Sparke, (2005), *"Side Impact Injury Risk for Belted Far Side Passenger Vehicle Occupants"*, SAE Techincal Paper 2005-01-0287

[16] J. George, M. Davis, S. Sharpe, J. Olberding, et al., (2020) *"Evaluation of Occupant Kinematics during Low- to Moderate-Speed Side Impacts"*, SAE Technical Paper 2020-01-1222

[17] F. Germanetti, *"Finite Element Simulation of Impact of Autonomous Vehicle with Human Body Model in Out-of-Position Configuration"*, Master's Degree thesis in Automotive Engineering, Politecnico di Torino, a.a. 2019/2020

[18] A. J. Golman, K. A. Danelson, L. E. Miller, J.D. Stitzel, (2014), *"Injury prediction in a side impact crash using human body model simulation"*, Accident Analysis and Prevention Journal, Vol. 64, pp 1-8

[19] S. Guha, (2011), *"Occupant Modelling Workshops & Other Learning Aids"*, LSTC, www.lstc.com/training_workshops

[20] M. Hitosugi, S. Tokudome, (2011), *"Injury severity of occupants in lateral collisions in standard and small vehicles: Analysis of ITARDA's in-depth investigation data"*, International Journal of Crashworthiness, Vol.16, No. 6, pp 657-663

[21] Y. Kitagawa, S. Hayashi, K. Yamada, M. Gotoh, (2017), *"Occupant Kinematics in Simulated Autonomous Driving Vehicle Collisions: Influence of Seating Position, Direction and Angle"*, Stapp Crash Jurnal, Vol. 61, pp 101-155

[22] B. Pipkorn, K. J. Larsson, D. P. Rapela, C. Markusic, et al., (2018*), "Occupant Protection in Far-Side Impacts"*, IRCOBI Conference1 IRC-18-16

[23] K. Ramaswamy, V. Virupaksha, J. Polan, B. Tripathy, (2017), *"Validation of Expanded Polypropylene (EPP) Foam Material Models for Low Speed Bumper and Pedestrian Protection Applications"*, SAE Technical Paper 2017-01-0363

[24] K. Ramaswamy, B. Patham, B. Savic, B. Tripathy, (2017*), "Stable and Accurate LS-DYNA Simulations with Foam Material Models: Optimization of Finite Element Model Parameters"*, SAE Int. J. Mater. Manuf. Vol.10, No. 2

[25] P. Schober, C. Boer, L.A. Schwarte, (2018), *"Correlation Coefficients: Appropriate Use and Interpretation"*, Anesthesia & Analgesia, Vol. 126, No. 5

[26] D. Soliman, *"Finite element modelling of vehicles in human body models for passive safety"*, Master's Degree thesis in Automotive Engineering, Politecnico di Torino, a.a. 2019/2020

[27] S. R. Sopher, G. C. Granthen, (2011), *"Material and Design Innovation Techniques for Expanded Polypropylene (EPP) Products Used in Automotive Interior Applications"*, SAE Int. J. Mater. Manuf., Vol. 4, No. 1

[28] B. Suderman, I. Scher, R. Ching, (2014), *"Likelihood of Lumbar Spine Injuries for Far-Side Occupants in Low to Moderate Speed Lateral Impacts"*, SAE TEchincal Paper 2014-01-0494

[29] M. Toney-Bolger, S. Sherman, J. Isaacs, C. Garman, et al., (2020), *"An Evaluation of Near- and Far-Side Occupant Responses to Low- to Moderate-Speed Side Impacts"*, SAE Technical Paper 2020-01-1218

[30] Toyota Central R&D Labs. Inc., (2020), *"THUMS AM50 Occupant Model Version 4.1"*, Toyota Motor Corporation

[31] S. Umale, N. Yoganandan, F. A. Pintar, M.W.J. Arun, (2018), *"Factors influencing effectiveness of occupant retention under far-side impacts: A parametric study"*, Journal of the Mechanical Behavior of Biomedical Materials, Vol. 84, pp 235-248

[32] J. Vychytill, J. Hlucha, L. Kovar, M. Kostikova, et al., (2020), *"Innovative Active Head Restraint System in a Car: Safety Assessment with Virtual Human Body Model"*, SAE Int. J. Advances & Curr. Prac. In Mobility 2(4):2107-2124

[33] World Health Organization (2015), *"Global status report on road safety 2015"*

[34] I. Yeh, (2007), *"LSDYNA Seat Belt Modelling Guideline"*, ftp.lstc.com
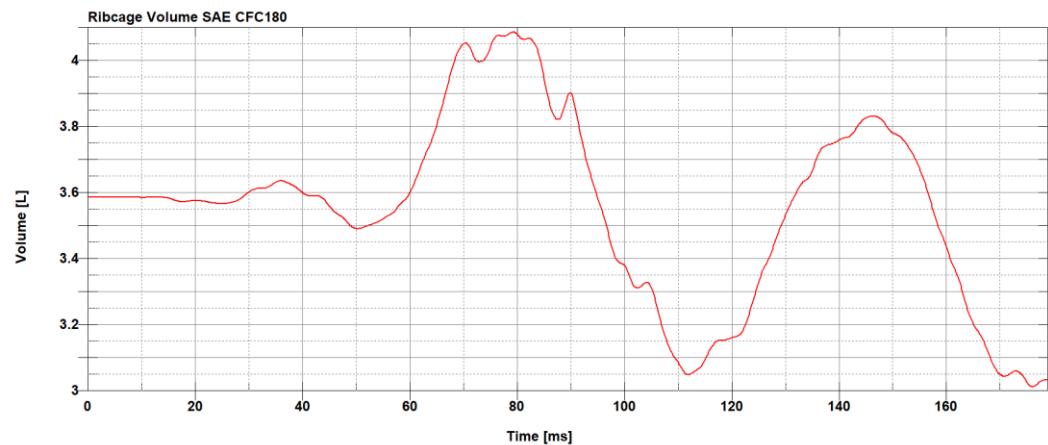
Appendix A

RIBCAGE

Appendix A 1: Ribcage - Volume
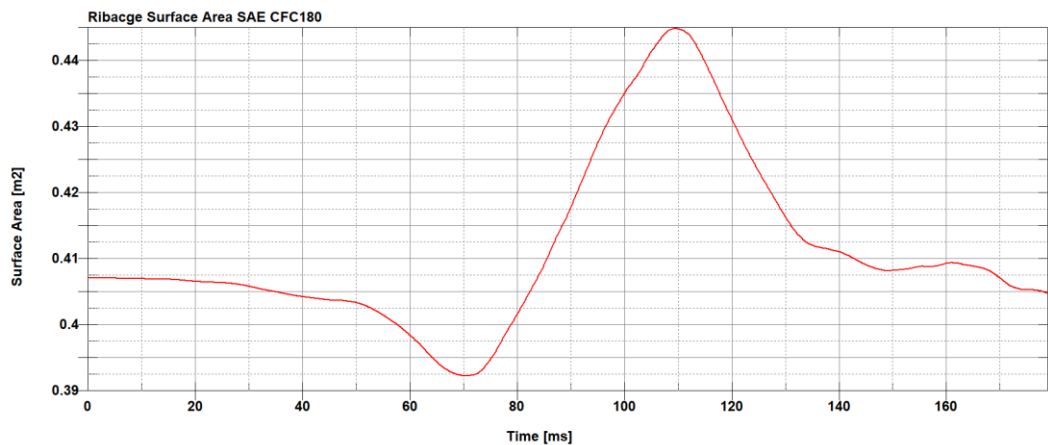
Appendix A 2: Ribcage - Surface Area
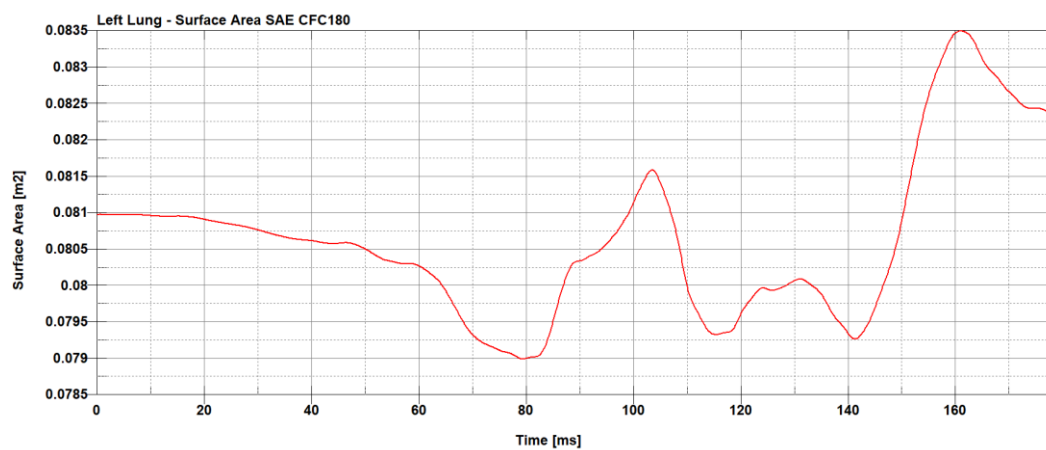
RIGHT LUNG
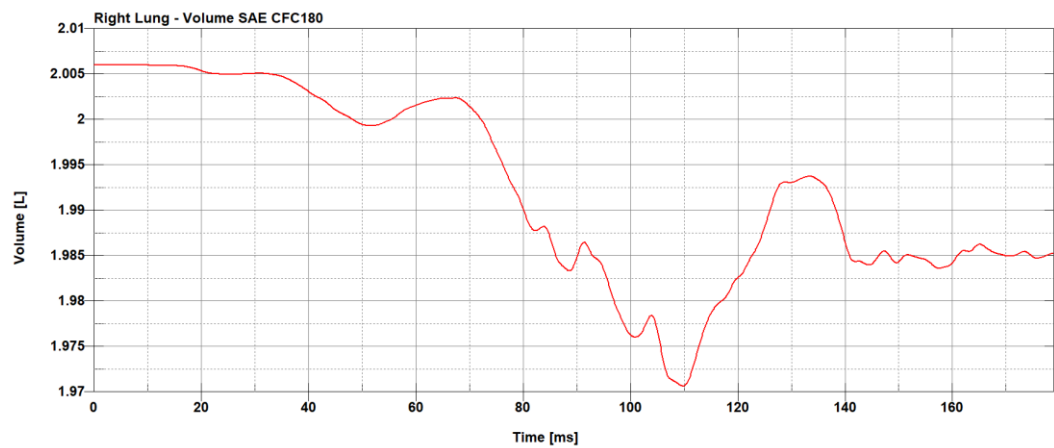
Appendix A 3: Right Lung - Volume
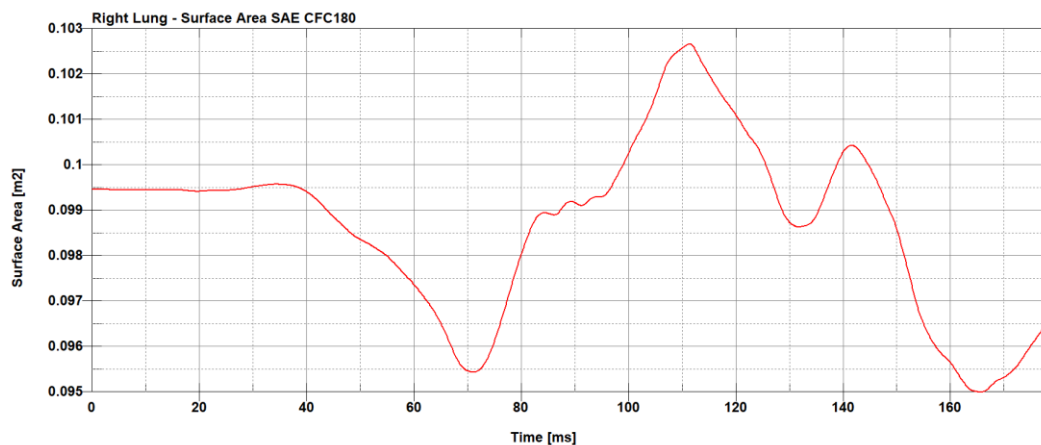
Appendix A 4: Right Lung - Surface Area
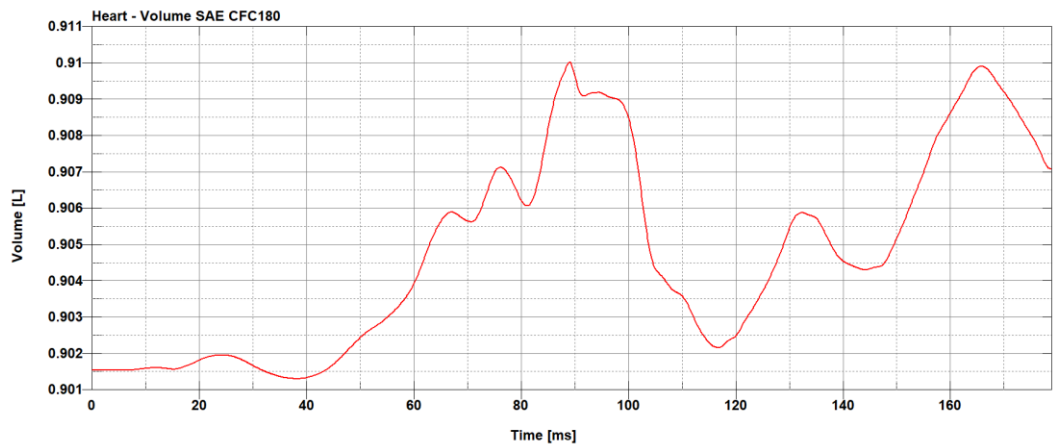
LEFT LUNG
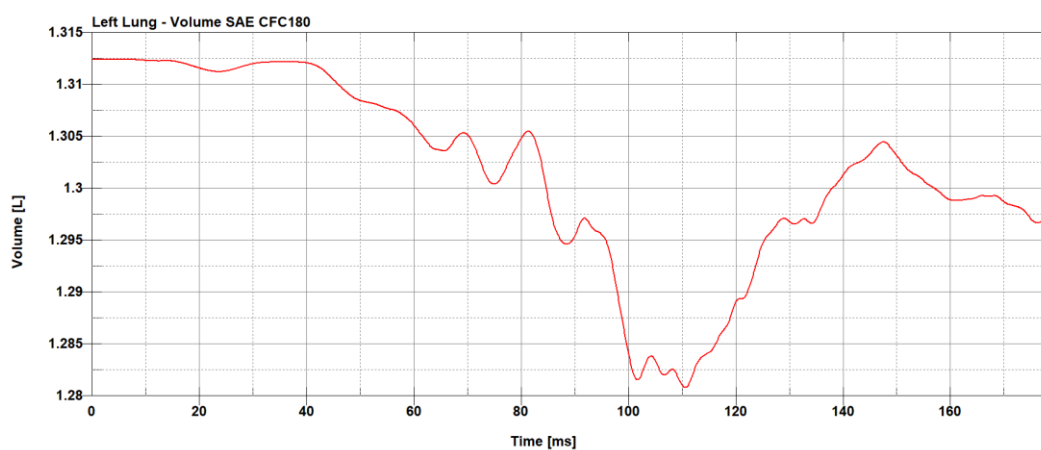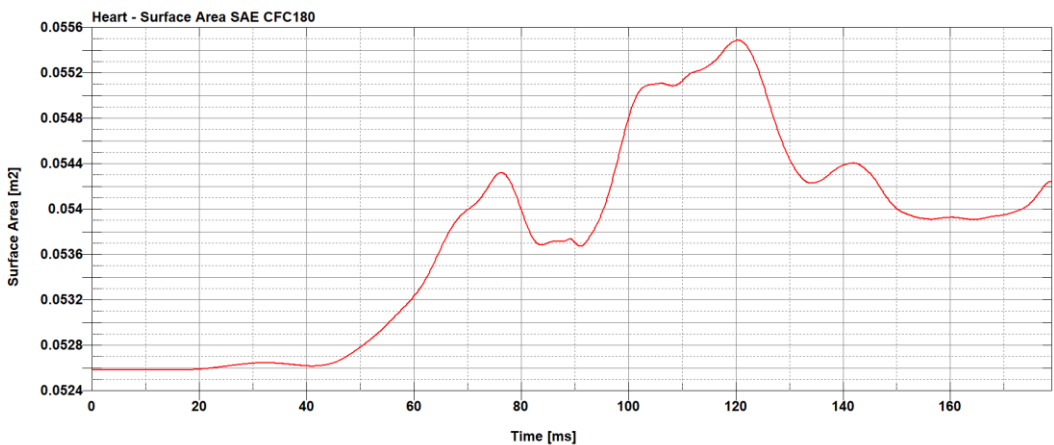

Appendix A 5: Left Lung - Volume

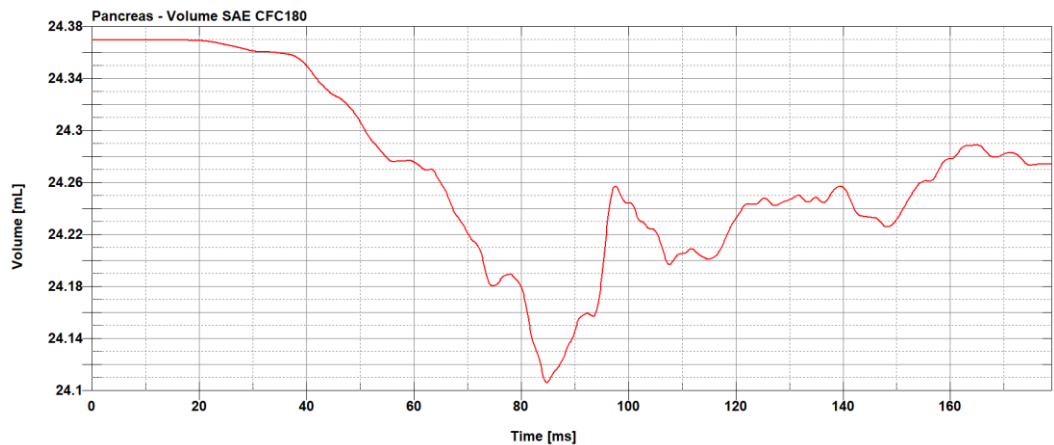*Appendix A 6: Left Lung - Surface Area*
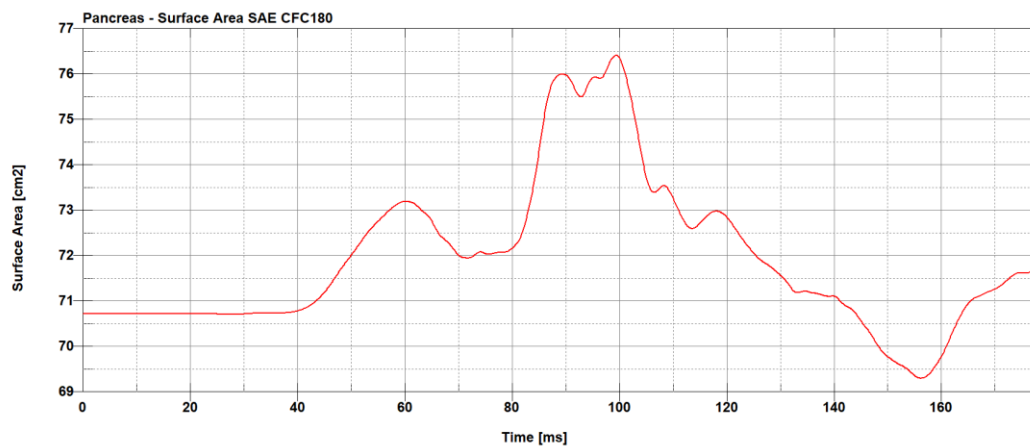
102

HEART

Appendix A 7: Heart - Volume
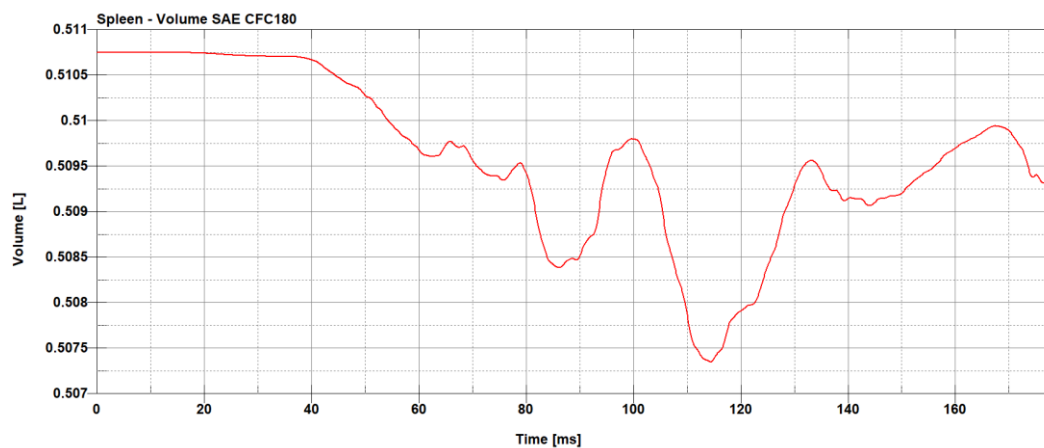

Appendix A 8: Heart - Surface Area

PANCREAS

Appendix A 9: Pancreas - Volume
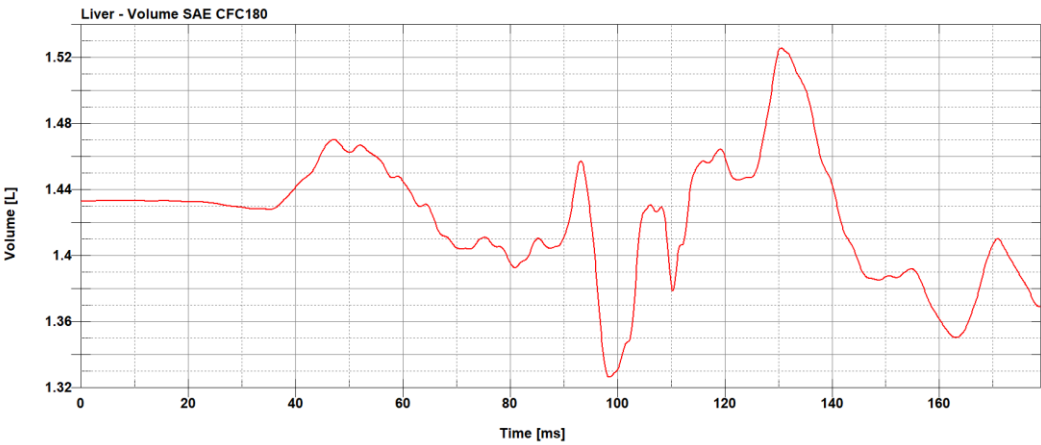
Appendix A 10: Pancreas - Surface Area

SPLEEN

Appendix A 11: Spleen - Volume
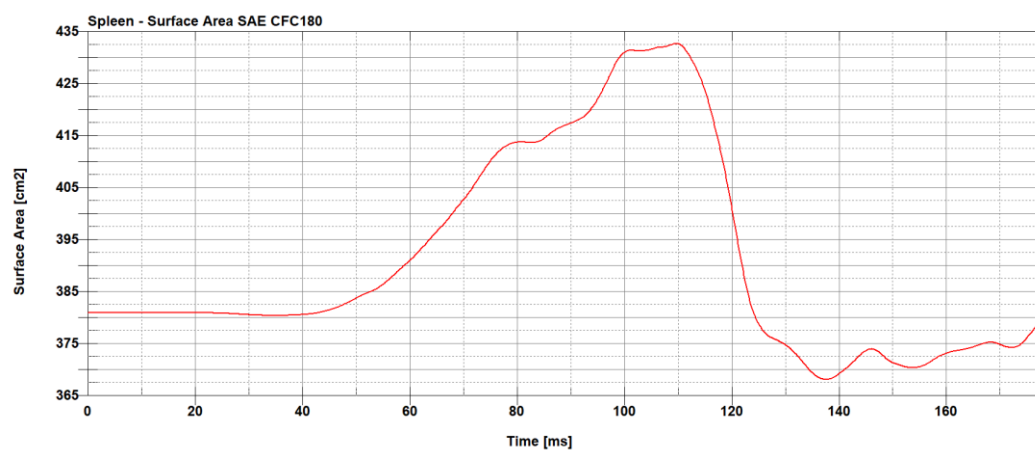
Appendix A 12: Spleen - Surface Area

104

LIVER

Appendix A 13: Liver - Volume
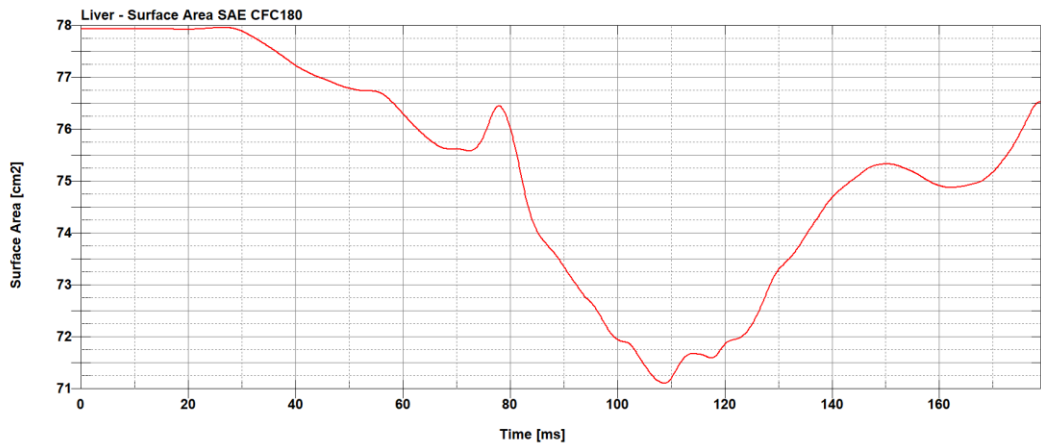
Appendix A 14: Liver - Surface Area

STOMACH
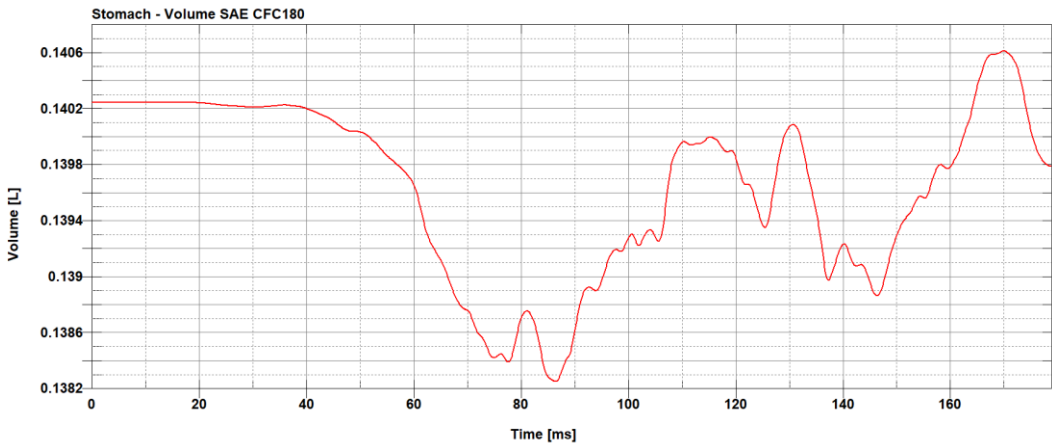
Appendix A 15: Stomach - Volume
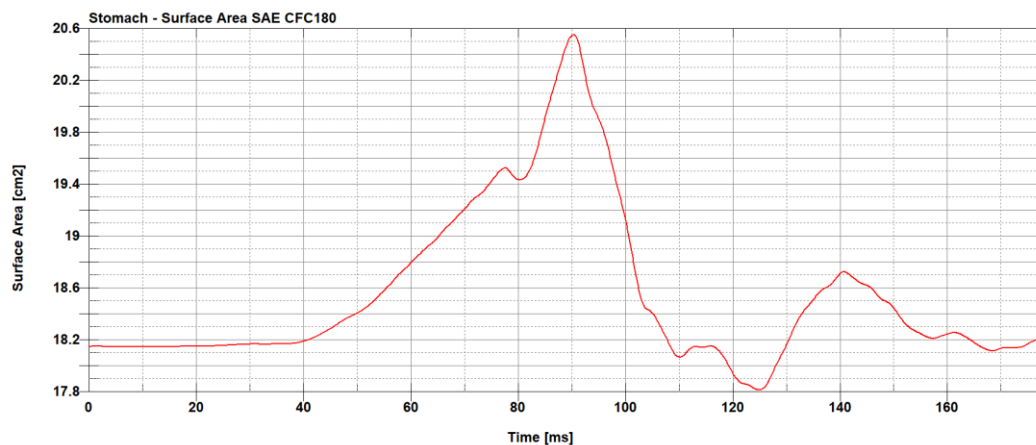
Appendix A 16: Stomach - Surface Area

LARGE INTESTINE
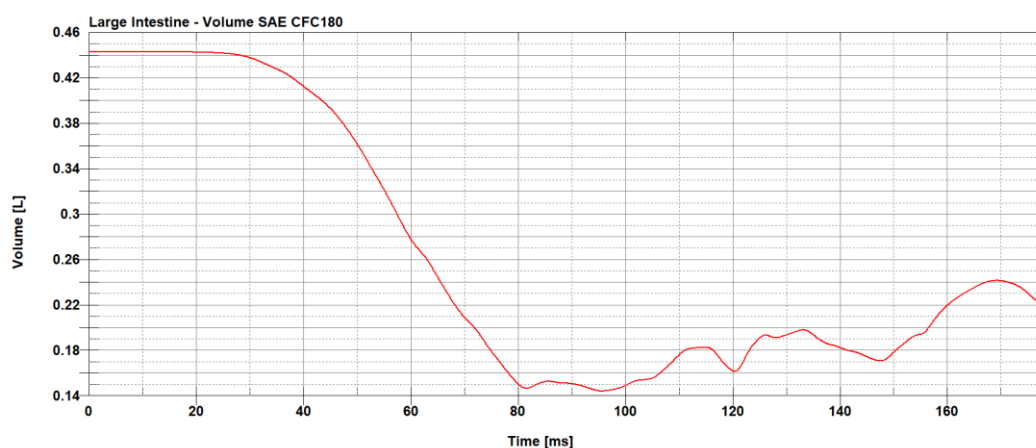
Appendix A 17: Large Intestine - Volume
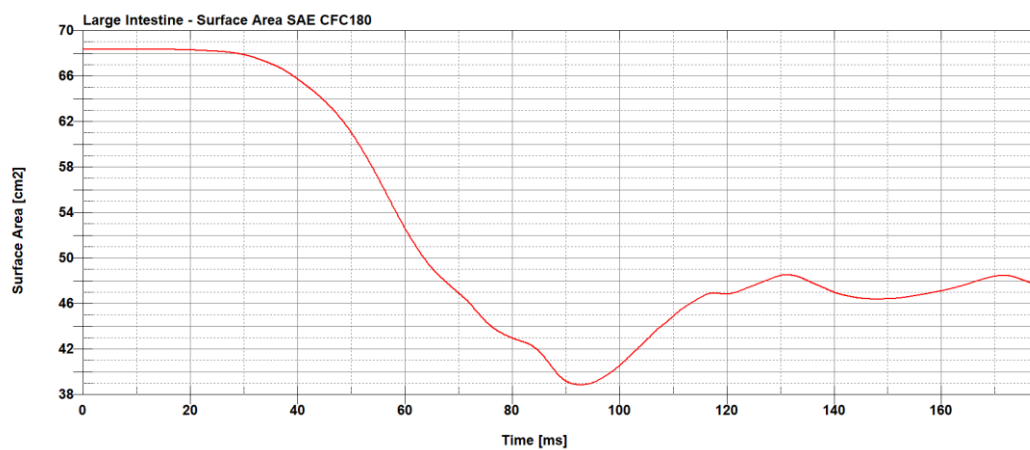
Appendix A 18: Large Intestine - Surface Area

SMALL INTESTINE
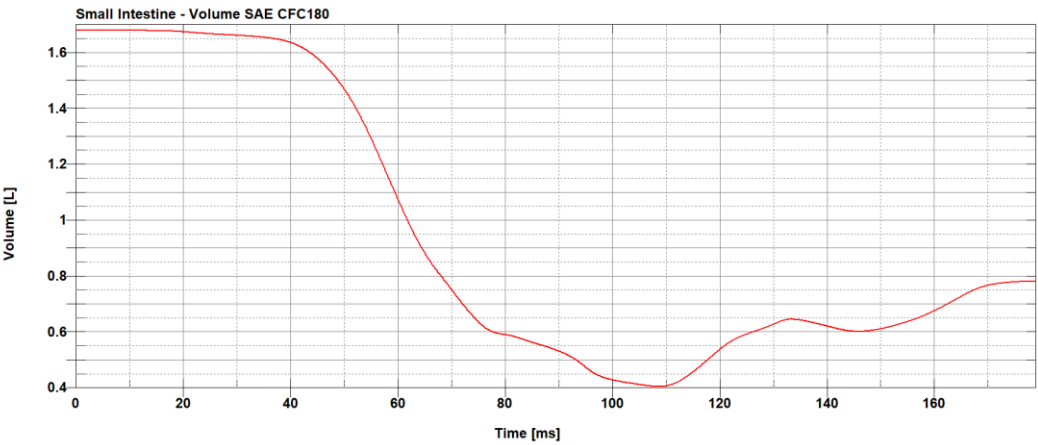
Appendix A 19: Small Intestine - Volume
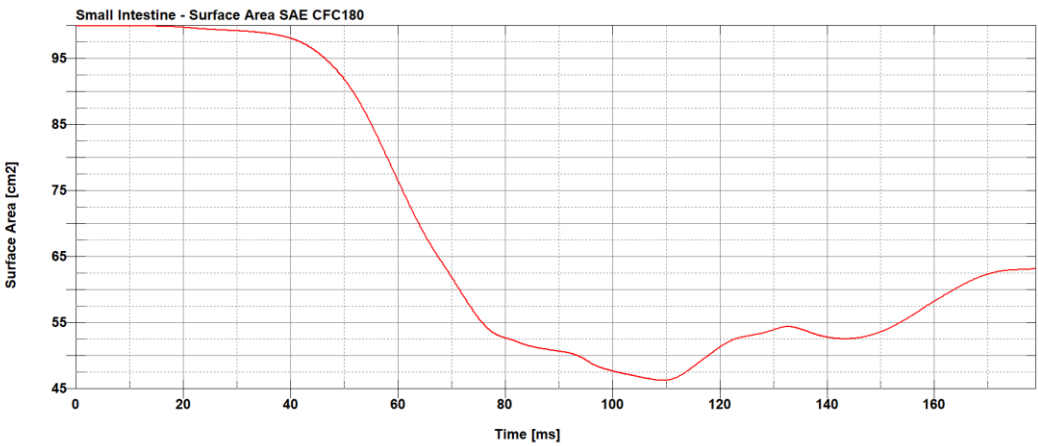
Appendix A 20: Small Intestine - Surface Area

ABDOMEN
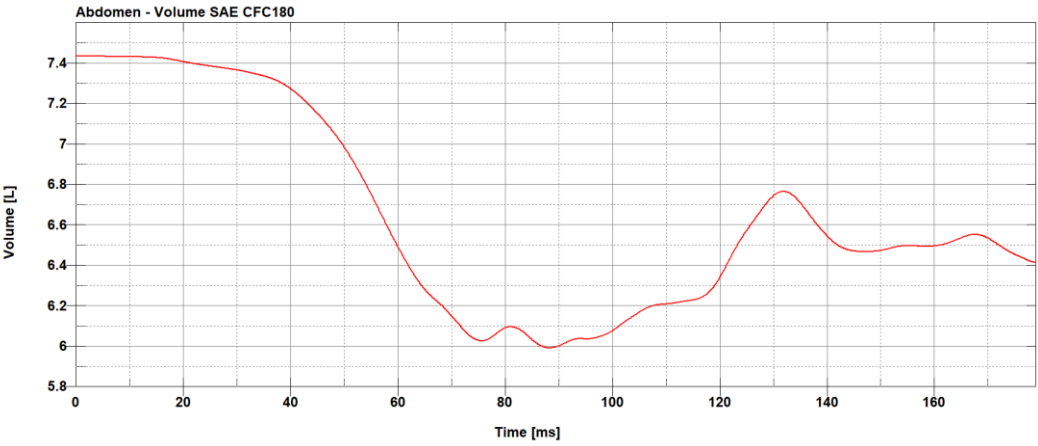
Appendix A 21: Abdomen - Volume
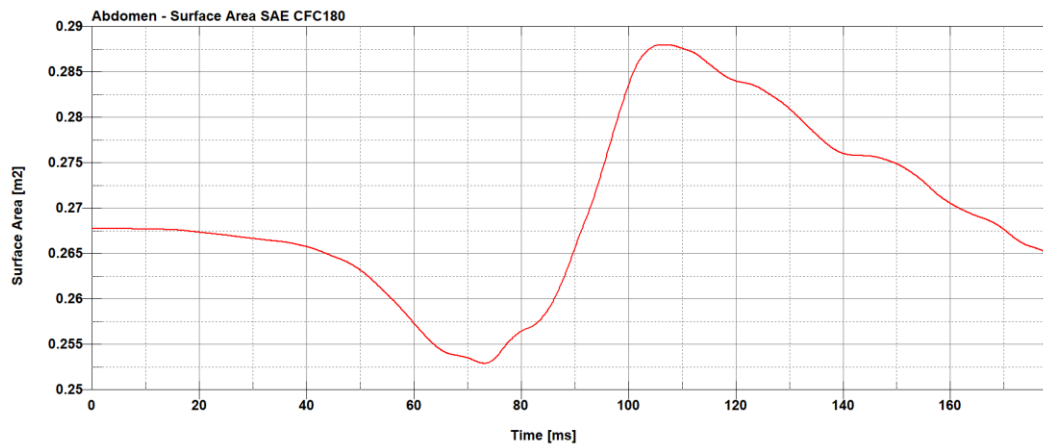
Appendix A 22: Abdomen - Surface Area

Appendix B
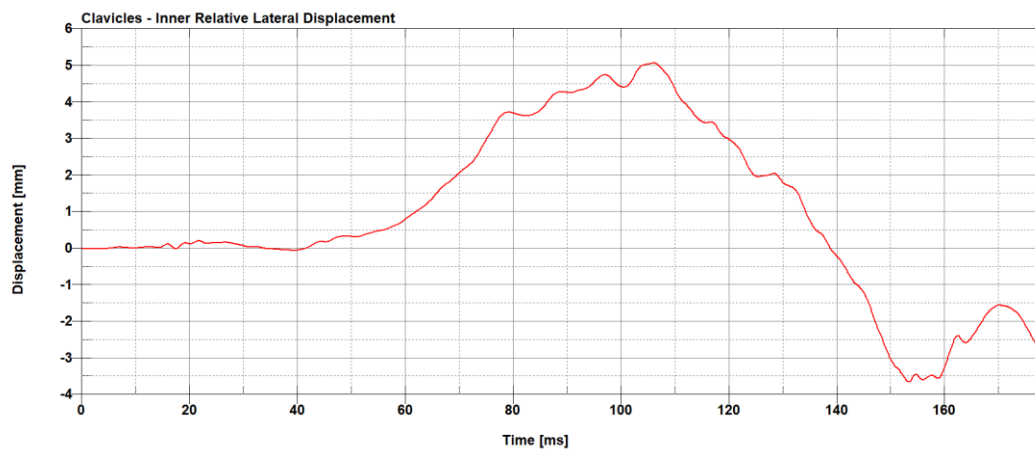
Appendix B 1: Clavilces – Inner Relative Displacement
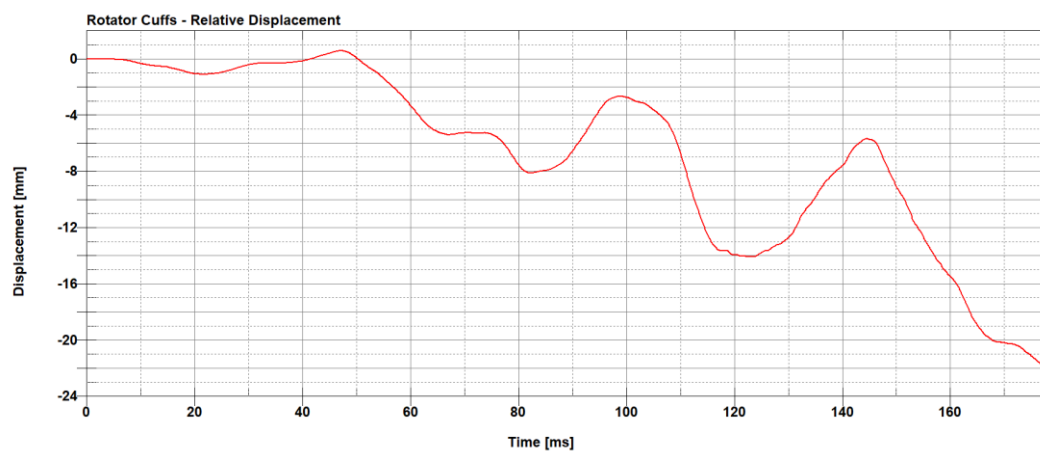
Appendix B 2 : Rotator Cuffs - Relative Dispalcement

Acknowledgments